Integration of microtubule-kinetochore attachment formation and spindle assembly checkpoint signalling



Christina H Y Barnard

Lincoln College

University of Oxford

A thesis submitted for the degree of

Doctor of Philosophy

Michaelmas 2018

Acknowledgments

I am so grateful and indebted to the many people who have helped and supported me over the last few years. Firstly to Ulli, who has managed my expectations and frustrations wonderfully and who has helped me stay the course and supported me in the tough times. I am so grateful for all your guidance and support over the past years. I am also grateful you hire well! I am deeply indebted to James, Dan, Renaud, Pelin and Flavia for all their scientific advice as well as their sense of humour. For all the occasions you have given your time and advice generously, it has been very much appreciated. I am very grateful to Zoe who epitomizes the best of what teamwork is and has been a pleasure to work alongside and enjoy all those conversations both scientific and non-scientific.

This work would not have been possible without the generous support of Shabaz Mohammed, for his training and advice. To Svenja in whom I have found a firm friend, thank you for all of your help over the last years, I would not be here without you.

I am grateful to Lincoln College and the Sir William Dunn School of Pathology for their support along the way. In particular Lucinda and Carmella who have always shared words of wisdom with me.

To my friends in Oxford Pro Musica, Oxford hockey club and Lincoln who have kept me sane (relatively), happy and well fed. Finally to my family, who have, as always, been amazing. Whether it is an unexpected phone call, cooking me dinner, keeping my spirits up or teaching me what a subordinate clause is (which I still don't understand). I am so grateful for all the love and support.

Table of Contents

Chapter 1: Introduction 1

1.1 The cell cycle 1

1.1.1 Outcomes of misregulation of the cell cycle 2

1.1.2 Mitosis 3

1.2 Structure of the kinetochore 6

1.2.1 The inner kinetochore 6

1.2.2 The outer kinetochore 8

1.3 The formation of attachments 17

1.3.1 The bipolar spindle 17

1.3.2 Methods of chromosome congression 18

1.3.3 How attachments form and persist 19

1.4 The role of kinases at the kinetochore 20

1.4.1 Plk1 20

1.4.2 Aurora B and its role in error correction 21

1.4.3 Mps1 is a master regulator of the Spindle Assembly Checkpoint 26

1.5 The dynamic kinetochore 31

Chapter 2: Materials and methods 34

2.1 Cell culture 34

2.1.1 Tissue culture 34

2.1.2 Optimising a synchronisation protocol 34

2.1.3 Cell cycle arrests 35

2.2 GFP-Astrin cell lines 35

2.2.1 Cloning 35
2.2.2 Production of stable cell lines 36
2.3 Transfection and rescue experiments 36
2.3.1 siRNA treatments 36
2.3.2 Rescue experiments 36
2.3.3 Transient transfection 37
2.4 Image processing and analysis 37
2.4.1 Imaging of fixed cells 37
2.4.2 Cytospin 38
2.4.3 Imaging of live cells 38
2.5 Analysis of the efficiency of endonucleases 39
2.5.1 Comparison of benzonase with micrococcal nuclease 39
2.5.2 Phenol extraction experiment 39
2.6 Biochemical assays 40
2.6.1 Kinase assay 40
2.6.2 Far western 40
2.6.3 Immunoprecipitation 41
2.6.4 Glycine/Urea elution 42
2.7 Mass spectrometry 42
2.7.1 In-gel 42
2.7.2 FASP 43
2.7.3 Di-methyl labelling 43
2.7.4 Titanium dioxide enrichment 44

2.7.5 Online nano-LC and tandem mass spectrometry 44

2.7.6 Mass spectrometry processing 45

Chapter 3: Optimising kinetochore pull-downs for analysis of in vivo phosphorylation events 48

3.1 Introduction 48

3.1.1 Aims 54

3.2 Results 55

3.2.1 Isolating the outer kinetochore for MS analysis 55

3.2.2 Improving kinetochore release from chromatin during lysis 58

3.2.3 MS Analysis of in-gel Knl1 IP 61

3.2.4 Adapting to an in-solution method 66

3.2.5 Introducing a phospho-enrichment step 72

3.2.6 Determining whether a labelling strategy was advantageous 75

3.2.7 Digestion by multiple enzymes increases phospho-peptide identifications 77

3.2.8 Testing our optimised protocol 83

3.2.9 Generating a prometaphase kinetochore phospho-site data set 90

3.3 Discussion 98

3.3.1 Summary 98

3.3.2 Discussion 98

Chapter 4: An unbiased analysis of the kinetochore in different k-MT attachment states .. 102

4.1 Introduction 102

4.1.1 Aims 103

4.2 Results 104

4.2.1 Analysis of synchronous cell cycle timings 104
4.2.2 Creating a release protocol 107
4.2.3 Optimising for large-scale releases 111
4.2.4 Confirming releases do recapitulate an attached state 113
4.2.5 Comparing kinetochore phospho-states depending on attachment status 115
4.2.6 Ndc80 pThr61/Ser62 and pSer69 show higher levels of phosphorylation upon MT attachment 122
4.2.7 Knl1 sites are lost upon MT attachment 124
4.3 Discussion 128
4.3.1 Summary 128
4.3.2 Discussion 128
Chapter 5: The phosphorylation of Astrin by Plk1 is critical to timely mitotic progression .. 131
5.1 Introduction 131
5.1.1 Aims 134
5.2 Results 135
5.2.1 Plk1 and Astrin interact during mitosis 135
5.2.2 Plk1 binds via its PBD through a PBD-binding motif on Astrin 138
5.2.3 Plk1 phosphorylates Astrin in vivo 143
5.2.4 Confirming phospho-sites found 152
5.2.5 The PBD mutant is unable to be phosphorylated by Plk1 but able to reform bipolar spindle 156
5.2.6 ST110/111AA Astrin exhibits a delayed congression and anaphase onset phenotype 161
5.3 Discussion 165

5.3.1 Summary 165

5.3.2 Discussion 165

Chapter 6: Concluding remarks 169

6.1.1 Observations from our study 170

6.1.2 Future directions for our MS methodology 172

6.1.3 Conclusion 175

Chapter 7: Bibliography 176

Table of Figures

Figure 1.1 The mitotic stages 5

Figure 1.2 The kinetochore-microtubule interface 16

Figure 1.3 Microtubules can attach to kinetochores to create a range of different geometries 25

Figure 1.4 The SAC works to prevent premature anaphase onset 28

2.1 For correct numbering!?! 45

Figure 3.1 Timeline of MS studies which identify kinetochore-related phosphorylation events 51

Figure 3.2 Both Ndc80 and Knl1 immunoprecipitations are capable of isolating the outer kinetochore 57

Figure 3.3 50U Micrococcal nuclease enhances kinetochore release 60

Figure 3.4: In-gel processing of Knl1 immunoprecipitation for mass spectrometry analysis 64

Figure 3.5 In-gel digestion of Knl1 immunoprecipitation is capable of isolating most direct interaction partners 66

Figure 3.6: Combining Glycine and Urea elution steps allow efficient release 70

Figure 3.7 Comparatively FASP represents an improvement over in-gel digestion 72

Figure 3.8: An enrichment strategy creates a large increase in kinetochore-related phospho-site 74

Figure 3.9: In silico analysis indicates trypsin is an unsuitable enzyme for analysing the N-terminus of Ndc80 81

Figure 3.10: V8 complements trypsin, the combination of the two out-performs trypsin alone 83

Figure 3.11 Confirmation of Ndc80-GFP and GFP-Zwint cell lines 88

Figure 3.12 Analysis of the initial MS experiment 89

Figure 3.13 Analysis of the experiment outcomes from the pro-metaphase data set .. 95

Figure 3.14 Identification of the novel sites found 96

Figure 4.1: Analysis of synchronous cell cycle timings. 107

Figure 4.2: Synchronisation protocol established 110

Figure 4.3: Synchronisation reoptimised for larger-scale 112

Figure 4.4: Immunoprecipitations are capable of identifying changes of attachment state. 114

Figure 4.5 MS pipeline 119

Figure 4.7 The majority of phospho-sites show reduced levels of phosphorylation upon MT attachment 121

Figure 4.8 Ndc80 phospho-sites increase in intensity post-attachment 124

Figure 4.9 Knl1 is phosphorylated on multiple MELT motifs 127

Figure 5.1: Plk1 and Astrin do interact during mitosis 137

Figure 5.2 Plk1 binds Astrin through ST110/11 140

Figure 5.3 Plk1 binds Astrin through its PBD site 142

Figure 5.4 Astrin is phosphorylated by Plk1 146

Figure 5.5 Plk1 phosphorylates Astrin at 4 residues 149

Figure 5.6 Reproducibility of Plk1-dependent phosphorylation sites 150

Figure 5.7 Fragmentation patterns for Plk1 dependent phosphorylation sites 151

Figure 5.8 Validation of phospho-antibodies 154

Figure 5.9 Phospho-antibodies are specific to Astrin 156

Figure 5.10 Generating GFP-Astrin cell lines 159

Figure 5.11 siRNA 3' UTR capable of efficiently depleting endogenous Astrin 161

Figure 5.12 Live cell imaging of GFP-Astrin variants 164

Abbreviations

3’ UTR	3’ Untranslated region
APC/C	Anaphase promoting complex/cyclosome
BUB1	Budding uninhibited by benzimidazoles 1
BUB3	Budding uninhibited by benzimidazoles 3
BUBR1	Budding uninhibited by benzimidazoles related 1
CAA	Chloroacetamide
CDK	Cyclin dependent kinase
CPC	Chromosomal passenger complex
CCAN	Constitutive centromere associated network
CH	Calponin homology domain
DMEM	Dulbecco’s modified eagle medium
DMSO	Dimethyl Sulfoxide
EGTA	Ethylene glycol tetraacetic acid
FASP	Filter-aided sample preparation
FRAP	Florescence recovery after photobleaching
GFP	Green florescence protein
HEC1	Highly expressed in cancer
IF	Immunofluorescence
IP	Immunoprecipitation

K-MT	Kinetochore- microtubule attachments
KMN	Knl1 Mis12 Ndc80 network
KNL1	Kinetochore scaffold 1
MAD1	Mitotic arrest defect 1
MAD2	Mitotic arrest defect 2
MAP	Microtubule associated protein
MCC	Mitotic checkpoint complex
MELT	Knl1 motifs which consist of Met-Glu-Leu-Thr
MIS12 complex	Complex of Mis12, Dsn1 Nfn1, Nsl1
MS	Mass Specttrometry
MT	Microtubule
NEB	Nuclear envelop breakdown
NDC80 complex	Complex of Ndc80 (Hec1 in humans), Nuf2, Spc24, Spc25
NUF2	Nuclear filament-related 2
PLK1	Polo like kinase 1
RT	Room temperature
RZZ	Complex of Rod-Zwilch-Zw10
SAC	Spindle assembly checkpoint
SKA	Spindle and Kinetochore associated network
SiRNA	Small interfering RiboNucleic acid
TiO_2	Titanium Dioxide enrichment

V8	GluC enzyme
WB	Western blot
WT	Wildtype

Abstract

This study focuses on mitosis and the regulation of microtubule-kinetochore attachment formation by phosphorylation. Kinetochores act as platforms for both the attachment of bi-polar spindle microtubules to chromosomes and the generation of the surveillance systems which regulate this process. Both the error-correction pathway and the spindle assembly checkpoint are activated in the presence of non-attached or non-tension bearing kinetochores. These mechanisms rely on dynamic phosphorylation and dephosphorylation for the transduction of signals allowing the regulation of protein:protein interactions.

Many kinetochore proteins have been found to be highly phosphorylated in mitosis, but less is known about the temporal regulation of these phospho-sites. In addition, only a small proportion of sites and their biological function have been investigated in detail.

Here, I have developed a mass spectrometry protocol combined with a synchronisation step to isolate the outer kinetochore and compare the phosphorylation state at unattached and attached kinetochore states. Our analysis showed that multiple phosphorylation sites on the outer kinetochore are dephosphorylated upon attachment. As key examples we identified the six active MELT motifs on Knl1, which regulate the recruitment of SAC proteins. Intriguingly, we also identified two Ndc80 phosphorylation sites, pThr61/Ser62 and pSer69, which are up-regulated upon kinetochore-microtubule attachment. This suggests that the regulation of microtubule attachment to the outer kinetochore by different kinases may be more complex than hitherto thought, as up-regulation upon attachment has so far not been reported.

As an example of a specific kinase-regulated protein complex involved in the generation of microtubule-kinetochore attachment formation we investigated the role of Plk1 associating with the Astrin-Kinastrin complex. Previous results in our lab showed depletion of Astrin or Kinastrin +results in delayed chromosome alignment and loss of

spindle bipolarity. In this study we demonstrate that Plk1 binds directly to Astrin via a Cdk1-phosphorylated sequence in the N-terminus of Astrin. Using mass spectrometry we identify four Plk1-dependent phosphorylation sites on Astrin at residues, pSer157, pSer159, pSer353 and pSer411 and demonstrate that phosphorylation of these sites is dependent on Plk1 activity in vivo. Interestingly, we can demonstrate that the interaction of the Astrin-Kinastrin complex with Plk1 is dispensable for bipolar spindle formation but does play a role in timely chromosome congression and anaphase onset, thus separating the different aspect of the Astrin/Kinastrin depletion phenotype.

Chapter 1: Introduction

1.1 The cell cycle

The importance of cell division has been known for well over a century ever since Virchow's statement "omnis cellula e cellula" in 1855 (all cells come from cells). It is evident therefore that the accuracy of this process is fundamental to the continuation of every lifeform or species. The cell cycle is broken into four stages: gap 1 (G1), DNA synthesis (S), gap 2 (G2) and mitosis (M). In G1 cells grow and prepare for entry into S-phase where the DNA is replicated, G2 is another growth phase also allowing any errors in DNA replication to be corrected before the onset of M-phase where the DNA is segregated into two daughter cells (Harashima et al. 2013). In the metazoan cell cycle stages occur sequentially whereas in archaea and bacteria the S and M phases are coupled and occur simultaneously, with DNA being segregated to the two ends of the cell as DNA replication occurs (Reyes-Lamothe et al. 2008).

The cell cycle is governed by the cyclin-dependent kinases (CDK) which in combination with their regulatory subunits, cyclins, drive the cell cycle by their oscillating actions. In the mammalian cell cycle, Cdk2, under the regulation of CycE and CycA, controls the entry and progression of S-phase before Cdk1 and its cyclins, CycA and CycB, lead to mitotic entry and progression. The sequential degradation of CycA and CycB inactivates Cdk1 leading to mitotic exit (Harashima et al. 2013).

During the cell cycle there are three checkpoints which survey the cell, halting progression if errors are present until such time as they are repaired, at which point the cell cycle will restart. They control the major decision points of the cell cycle: the entry into cell division, monitoring the success of DNA replication, and controlling correct

segregation of chromosomes (Hochegger et al. 2008). The first checkpoint occurs during late G1, and is known as the restriction point in mammals and START in *S. cerevisiae*. It acts to commit the cell to undergo cell division; once triggered, cells will proceed into S-phase in a non-reversible manner. The DNA damage checkpoint detects DNA damage, and effector kinases prevent cell cycle progression until it has been repaired (Wang et al. 2015). Finally, the spindle assembly checkpoint (SAC) ensures chromosomes segregation occurs with high fidelity. This will be covered in more detail in following sections.

1.1.1 Outcomes of misregulation of the cell cycle

Should any of these checkpoints fail, the results for the cell can be catastrophic. Errors in mitosis cause problems with the cells' ploidy, either causing aneuploidy, where cells gain or lose whole chromosomes, or polyploidy which is caused by a failure of the cells to undergo cell division following DNA replication, and leads to cells with a multiple of their haploid karyotype (Williams & Amon 2009). Polyploidy can be tolerated in many systems. However aneuploidy is much more serious (Storchova & Kuffer 2008). The gain or loss of a single chromosome causes a change in copy number of all the genes on the affected chromosomes, leading to imbalances in protein activity and protein stoichiometry (Torres et al. 2008). Aneuploidy is very common in cancer, occurring in 75% of hematopoietic cancers and over 90% of solid tumours (Weaver & Cleveland 2006).

1.1.2 Mitosis

Mitosis requires large-scale restructuring within the cell to achieve its purpose - the equal segregation of the duplicated genetic material into the two daughter cells. This process is subdivided into five stages (**Figure 1.1**): prophase, prometaphase, metaphase, anaphase and telophase. During prophase, the cytoskeleton undergoes widespread structural remodelling. The microtubule network is transformed by the duplicated microtubule organising centres (MTOCs), the centrosomes, creating microtubule asters. These radial arrays of microtubules move apart towards opposite poles in preparation for the formation of the mitotic spindle. Within the nucleus the duplicated sister chromatids condense into compact mitotic chromosomes through the actions of condensins. Sister chromatid cohesion that has been established during S-phase along the entire length of the chromosomes is largely lost during prophase through the actions of the prophase pathway, leaving only centromeric cohesion (Waizenegger et al. 2000; Sumara et al. 2002). At the end of prophase the nuclear envelope breaks down, resulting in the mixing of nucleoplasm and cytoplasm thus giving the spindle microtubules access to the condensed chromosomes.

During prometaphase the bipolar spindle forms. This MT-based array has three types of MT: astral, which makes links to the cortex holding spindle poles in position; inter-polar spindle microtubules which brace the spindle; and kinetochore fibres. These kinetochore microtubules are only referred to in this way following the microtubules binding to the kinetochore, the docking point on the chromosome. The microtubules grow from the microtubule organising centre (MTOC), and through a method of 'search and capture' (Kirschner & Mitchison 1986) bind kinetochores, leading to the stabilisation of microtubules.

Following the attachment of kinetochores to the bipolar spindle there is a period of chromosome congression. All metazoan cells create a metaphase plate where the

chromosomes group in a line on the cell equator in preparation for anaphase. As long as perfect alignment of the chromosomes has not been achieved the spindle assemble checkpoint (SAC) will be active and will prevent anaphase onset. Once all the chromosomes have been securely attached to microtubules and the SAC is silenced anaphase can be triggered through the activation of the anaphase promoting complex/ cyclosome (APC/C). The cohesin rings, which have up to this point prevented sister chromatid separation, are then destroyed by the protease separase. Once cohesion is lost, the tensile forces which the kinetochores experience from the pulling microtubules lead to the separation of chromosomes to the opposite poles of the cell. This an irreversible cell cycle transition, the so-called point of no return. Anaphase can be split into two sections, A and B, which are characterised by the separation of the chromosomes (A) and the movement of the spindle poles towards the cortex (B) to complete the segregation of DNA.

Telophase is characterised by the reformation of the nuclear envelope and the decondensation of the chromosomes. Also essential to a successful mitosis is cytokinesis, the physical separation of the two daughter cells. This relies on the actions of the microtubule-based midbody as well as the actin-myosin cytoskeleton and the membrane trafficking machinery to yield two separated cells.

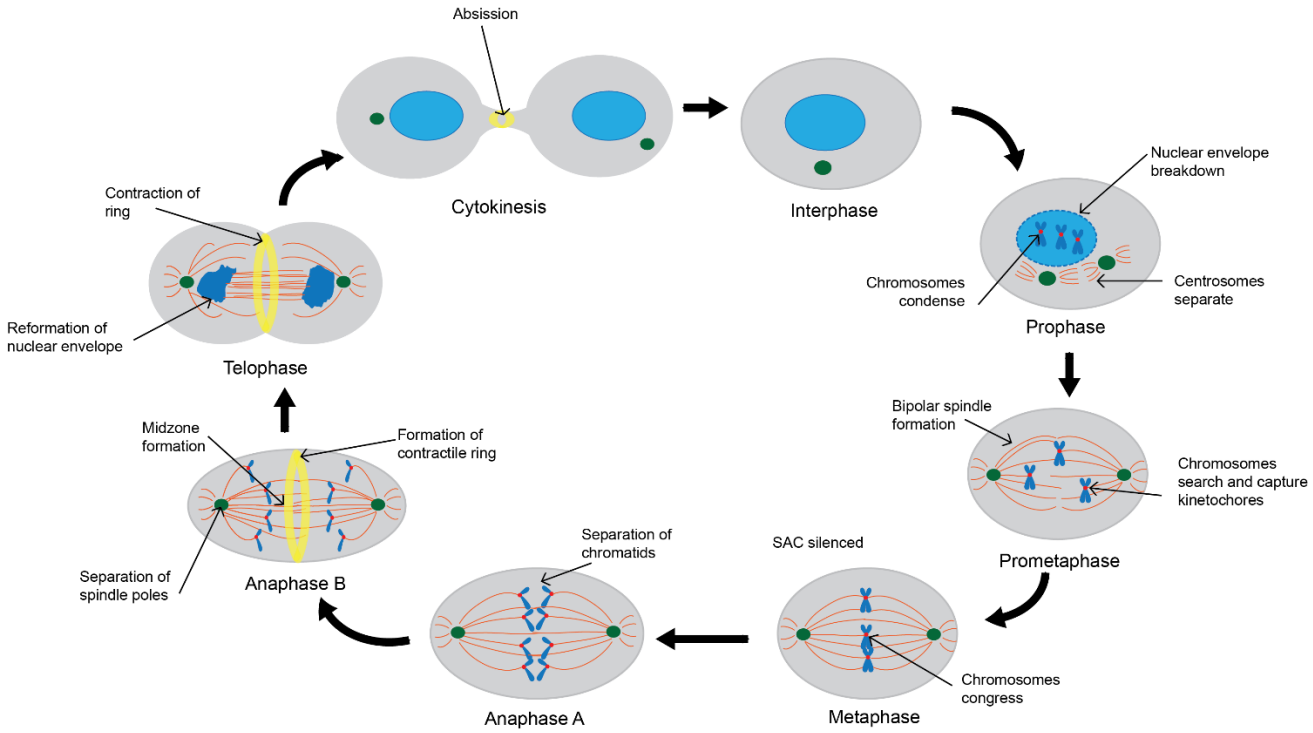


Figure 1.1 The mitotic stages

As cells advance through mitosis there are widespread structural changes. During prophase chromosomes condense and the nuclear envelope breaks down allowing chromosomes to attach to the bipolar spindle and congress to the metaphase plate. Once all chromosomes are successfully attached anaphase is triggered allowing the separation of chromatids to opposite poles. Nucleus and chromosomes are shown in blue, the kinetochore is indicated in red. The bipolar spindle is orange with the spindle poles in green. Finally the actin-myosin contractile ring is yellow.

1.2 Structure of the kinetochore

The kinetochore is a mega-dalton protein complex made up of ~100 proteins which ensures accurate distribution of genetic material (Hori & Fukagawa 2012). It is a highly dynamic platform which changes in composition and modification status as mitosis progresses (Musacchio 2015). It has two distinct functions. Firstly, it creates the physical load-bearing attachment between the chromosome and the bi-polar spindle. Secondly, it acts as the sensor for the attachment status at that individual chromosome. Owing to the vital importance of correct attachments, the cell has developed several mechanisms to assess and correct kineotochore-microtubule attachment state: the error correction pathway, and the SAC. These are both discussed in later sections. The kinetochore assembles on centromeric chromatin. Whilst the inner kinetochore is *in situ* throughout the cell cycle, the outer kinetochore is assembled in late S-phase and early mitosis (Musacchio & Desai 2017; Gascoigne & Cheeseman 2011). These different regions of the kinetochore have distinct roles. The inner kinetochore attaches the kinetochore to the centromere, and the outer kinetochore forms the site of MT-attachment and checkpoint regulation.

1.2.1 The inner kinetochore

The inner kinetochore provides the link between centromeric chromatin and the outer kinetochore. Made up of 16 proteins arranged in a series of sub-complexes, the inner kinetochore is all built off centromeric DNA (Foltz et al. 2006; Hori et al. 2008; Okada et al. 2006; Obuse et al. 2004). In humans, centromeric DNA is typically formed of tandem 171-bp repetitive sequences known as α-satellite domains (Musacchio &

Desai 2017). However, the major determining factor for where the kinetochore is built is CENP-A, with artificial targeting of CENP-A being sufficient to form a kinetochore (Hori et al. 2013; Guse et al. 2011). CENP-A is a histone H3 variant essential for the recruitment of other inner kinetochore components (Howman et al. 2000; Fachinetti et al. 2013). The constitutive centromere associated network (CCAN) is the collective term for the proteins making up the inner kinetochore; the majority of CCAN subunits localise to centromeres throughout the cell cycle (Cheeseman & Desai 2008; Hori et al. 2008). It is made up of four subcomplexes (**Figure 1.2**); CENP-CHIKM, CENP-TWSX, CENP-OPQRU and CENP-LN (Hori et al. 2008; Carroll et al. 2009; Carroll et al. 2010; Klare et al. 2015; Okada et al. 2006). Two of these proteins have been shown to interact directly with CENP-A; CENP-N and CENP-C.

CENP-N binds to CENP-A's centromere-targeting domain, the region with the highest sequence divergence from Histone H3 (Carroll et al. 2009). CENP-C instead binds through aromatic residues to CENP-A's C-terminal tail which is more hydrophobic than in Histone H3 (Kato et al. 2013). CENP-C also makes links to Histone H2A and H2B (Kato et al. 2013). *In vitro* CENP-C and CENP-N show a 5-10 fold selectivity for CENP-A over histone H3 (Weir et al. 2016; Carroll et al. 2010). The high level of selectivity that the CCAN shows for CENP-A may be conferred through multi-valency binding and interactions within the CCAN helping to increase the affinity for CENP-A over Histone H3 (Kato et al. 2013; Weir et al. 2016; Carroll et al. 2010).

The inner kinetochore has always been viewed as a bridge between the chromatin and outer kinetochore. Very recently, new evidence has come to light which shows CENP-OPQUR complex is also capable of directly binding microtubules through CENP-Q's basic, disordered N-terminal tail (Presenti et al. 2018). This suggests the division of labour between the inner and outer kinetochore is not quite so distinct as previously thought.

The CCAN interacts with the outer kinetochore via CENP-C and CENP-T. CENP-C binds Mis12 via its N-terminus, and phosphorylation of Dsn1, Ser100 and Ser109 by Aurora B increases CENP-C's interaction (Kim & Yu 2015; Rago et al. 2015; Welburn et al. 2010; Yang et al. 2008). CENP-C is therefore peculiar in binding both the innermost CCAN component, CENP-A, as well as the outer kinetochore. CENP-C is predicted to be largely unstructured, binding to Mis12 via its N-terminus (Screpanti et al. 2011), to CENP-A via its central region (residues 516-537) (Kato et al. 2013), and making multiple contacts with other CCAN proteins between these binding sites (Klare et al. 2015; McKinley et al. 2015; Pentakota et al. 2017). CENP-T meanwhile interacts with members of the Ndc80 complex (Schleiffer et al. 2012; Malvezzi et al. 2013). This interaction is enhanced by phosphorylation of CDK with CENP-T phospho-null mutants being unable to recruit KMN components (Rago et al. 2015).

1.2.2 The outer kinetochore

The outer kinetochore has two major roles: to link the inner kinetochore to the spindle microtubules, and to ensure this binding is regulated, such that attachment status is broadcast to the cellular environment and incorrect attachments can be identified and repaired. This is discussed in greater depth in **Section 1.4**. At its core it is comprised of the 9-subunit KMN network representing Knl1, Mis12 complex (which includes Mis12, Nnf1, Nsl1, Dsn1) and Ndc80 complex (Ndc80, Nuf2, Spc24, Spc25). It is essential for MT binding in eukaryotes (Cheeseman et al. 2006; Foley & Kapoor 2013; DeLuca & Musacchio 2012). The KMN network acts cooperatively, synergistically increasing the KMN network's ability to bind microtubules (Cheeseman et al. 2006). However, depletion experiments of KMN network components yield different phenotypes. Depletion of Ndc80 causes kinetochore-microtubule attachment defects and prevents the alignment of chromosomes, although some reports differ depending

on depletion efficiencies (DeLuca et al. 2002; Martin-Lluesma et al. 2002; Tooley et al. 2011). The loss of Mis12 and Knl1 leads to a partial chromosome alignment phenotype (Cheeseman & Desai 2008; Pagliuca et al. 2009; Kline et al. 2006). The loss of one KMN network component also affects the localisation of others, with Knl1 depletion reducing Dsn1 but not Hec1 in humans (Cheeseman & Desai 2008), whilst depletion of Hec1 decreases Knl1 levels by around 40% (Caldas et al. 2013).

1.2.2.1 The Ndc80 complex

The heterotetrameric Ndc80 complex is formed of: Ndc80 (Hec1 in humans), Nuf2, Spc24 and Spc25. It is the primary site of MT attachment, with the Spc24-25 head binding to the kinetochore, whilst the Ndc80-Nuf2 heads form load-bearing attachments to microtubules (Ciferri et al. 2008). Individual monomers interact via their coiled-coil domains to create an elongated, dumbbell-like structure of 57nm. Ndc80 contains a loop which interrupts the coiled-coil region and helps mediate protein:protein interactions.

The Ndc80-Nuf2 globular heads both contain calponin-homology (CH) domains which mediate microtubule binding (Ciferri et al. 2008). Structural work has revealed three microtubule-binding interfaces; the two CH domains of Nuf2 and Hec1, and the N-terminal tail of Hec1 (Alushin et al. 2010; Alushin et al. 2012). Hec1 binds both α- and β-tubulin monomers at the dimer interface via a small positively charged ‘toe’ region, which recognises a highly conserved, negatively charged ‘toe-print’ region on the tubulin monomers. By recognising both monomeric subunits, the Hec1 is able to bind every 4nm, enabling oligomerisation along a single microtubule protofilament. Also, the tubulin-dimer interface hinges, depending on whether microtubules are polymerising (where the protofilament is straight) or depolymerising (where the protofilaments bend). This bending could disrupt the toe-toeprint interaction, allowing

Hec1 to sense the state of the microtubules through the microtubule conformation and allow bias for straight, polymerising microtubules (Schmidt et al. 2012).

The N-terminal tail of Hec1 is unstructured and therefore has been impossible to crystallise. But, several studies have shown it is a high-affinity binding site for microtubules *in vitro* (Ciferri et al. 2008; Alushin et al. 2010). The N-terminal tail also allows oligomerisation of Ndc80 complexes in the presence of microtubules (Johnston et al. 2010; Lawrimore et al. 2011). Cryo-EM and biochemical analysis suggest it electrostatically interacts with the tubulin E-hooks (Alushin et al. 2010; Alushin et al. 2012). The Ndc80 N-terminal tail is phosphorylated by Aurora B, and this disrupts its ability to create these electrostatic interactions (this is discussed later in greater detail) (Welburn et al. 2010; Ciferri, et al. 2008; DeLuca et al. 2011).

1.2.2.2 Knl1

Knl1 (Kinetochore null-1) is a scaffold protein with a highly disordered structure; the only region which is largely ordered is the C-terminus, which contains binding domains for Mis12 via a tandem RWD motif and a coiled-coil domain which mediates an interaction with Zwint-1 (Petrovic et al. 2014; Petrovic et al. 2010). It binds microtubules via its N-terminus synergistically increasing the KMN microtubule-binding capacity *in vitro* (Cheeseman et al. 2006; Espeut et al. 2012). It also has numerous motifs which mediate protein:protein interactions.

There are RVSF and SILK motifs in the N-terminus of Knl1 which jointly mediates PP1 binding (Liu, et al. 2010). Knl1 contains multiple sites which allow the recruitment of Bub proteins: two KI motifs and nineteen methionine-glutamate-leucine-threonine (MELT) motifs. The MELT motifs are phosphorylated by the spindle checkpoint kinase Mps1, and in their phosphorylated form act as binding sites for the Bub proteins (Yamagishi et al. 2012; London et al. 2012; Shepperd et al. 2012; Primorac et al.

2013). KI1 and KI2 motifs in the N-terminus of Knl1 also interact with Bub1 and BubR1 respectively through the Bubs' TPR motifs (Bolanos-Garcia & Blundell 2011; Krenn et al. 2012). However these motifs are insufficient for high affinity binding, and the MELT motifs constitute the major docking site for the Bub proteins (Krenn et al. 2012; London et al. 2012; Primorac et al. 2013).

There are crystal structures of the Ndc80^{bonsai} complex and Mis12 complex, but due to Knl1's flexibility structural data on Knl1 is currently lacking. Only small fragments of Knl1 containing either the KI motifs or a region containing MELT motifs have been crystallised (Bolanos-Garcia & Blundell 2011; Krenn et al. 2012; Primorac et al. 2013). Whilst they appear, in complex with Bub1 or BubR1 to form short helices, circular dichroism experiments suggest this configuration is created upon binding; alone Knl1 has no secondary structure (Bolanos-Garcia & Blundell 2011).

1.2.2.3 The Mis12 complex

Of the three outer kinetochore complexes Mis12 is the only one that does not make direct links to microtubules but acts as a scaffold linking the KMN network to the chromatin (Cheeseman et al. 2006). It is made up of four subunits; Nsl1, Nnf1, Dsn1 and Mis12. They are all largely helical proteins which form pairs Nsl1:Dsn1 and Mis12:Nnf1 which create two separate head domains before all four proteins combine to create a central stalk (Petrovic et al. 2016; Dimitrova et al. 2016). Overall this creates a 22nm rod with the head domains forming the connections to CENP-C and CENP-T (Petrovic et al. 2010; Rago et al. 2015; Huisin'T Veld et al. 2016; Kim & Yu 2015). At the C-terminus, connections are made to the other KMN network components: Kn1, through Nsl1, and the Ndc80 complex components Spc24 and Spc25 via Nsl1 and Dsn1 (Petrovic et al. 2010; Petrovic et al. 2016; Dimitrova et al. 2016).

1.2.2.4 Other kinetochore associated factors

Whilst the Ndc80 complex is a major contributor in the kinetochore-microtubule interface, there are many others which contribute including: the Ska complex, Astrin/Kinastrin complex , EB proteins, Clip170, CLIP-associated proteins (CLASPs), mitotic centromere-associated kinesin (MCAK), CENP-E, CENP-F and Dynein (Foley & Kapoor 2013). Together these proteins help generate stable attachments to microtubules. This is especially important as the microtubules themselves are not static and in anaphase their depolymerisation leads to chromosome movement (Musacchio & Desai 2017), during which the kinetochore must remained bound to the disassembling microtubule.

1.2.2.4.1 The Ska complex

The Ska complex and its functional homologue in yeast, Dam1, both play important roles in coupling kinetochores to microtubules (Hofmann et al. 1998; Welburn et al. 2009; Gaitanos et al. 2009). The Ska complex is totally dissimilar in structure to Dam1, which generates a 10-subunit ring complex capable of encircling and moving along chromosomes (Westermann et al. 2005; Westermann et al. 2006). Instead, the Ska complex has three subunits; Ska1, Ska2 and Ska3 which form a W-shape upon trimerisation (Jeyaprakash et al. 2012). Depletions of Ska1 cause prolonged checkpoint-dependent mitotic arrests with misaligned chromosomes (Welburn et al. 2009; Hanisch et al. 2006). The Ska complex binds microtubules via a winged-helix domain which interacts with regions of tubulin monomers. These are accessible regardless of whether microtubules are depolymerising or polymerising, allowing Ska to track in both forms with equal efficiency (Abad et al. 2014). Ska is dependent on Ndc80 for its recruitment (Schmidt et al. 2012; Zhang et al. 2012), and it was recently suggested that Ndc80 clustering may play a role in Ska recruitment, with Ska binding lengthways along the microtubule protofilament (Janczyk et al. 2017).

1.2.2.4.2 The Astrin/Kinastrin complex

The Astrin/Kinastrin complex also shows depletion phenotypes, suggesting a role in the stabilisation of kinetochore-microtubule attachment. Depletion of Astrin has been shown to impair kinetochore-microtubule attachments, causing delayed chromosome alignment and loss of spindle bipolarity, as well as reducing CENP-E, CENP-F and CLASP1 recruitment to the kinetochore (Schmidt et al. 2010; Thein et al. 2007; Dunsch et al. 2011). Astrin was first characterised by Gruber et al. (2002) as a spindle-associated protein involved in mitotic progression. Together with Kinastrin, it makes up the core components of the Astrin/Kinastrin complex, which also has as sub-stochiometric components Dynein light chain 1 and Shugoshin-like2, Plk1 and MYCBP (Dunsch et al. 2011; Kern et al. 2017). The Astrin/Kinastrin complex is recruited to attached kinetochores and has been suggested by our group and others to help stabilised attachments. Until recently, it was not clear what Astrin's interacting kinetochore partner was. However there is now some evidence for an interaction with Ndc80 (Kern et al. 2017). Astrin will be discussed more deeply in **Chapter 5**, where it is our main focus.

1.2.2.4.3 Kinetochore phosphatases

PP1 and PP2A-B56 phosphatases are not often thought of as core kinetochore components, nevertheless they localise to and play a key role at the kinetochore over the course of mitosis. Both are members of the phospho-protein phosphatase (PPP) family of Ser/Thr phosphatases (Barr et al. 2011; Axton et al. 1990; Picard et al. 1989). Structurally both are holoenzymes, made up of the catalytic subunit (PP1 or PP2A) which then associate with a regulatory subunit and, in the case of PP2A, a scaffolding subunit (Barr et al. 2011).

Both PP1 and PP2A-B56 have roles in controlling kinetochore-microtubule attachments and silencing the SAC through antagonistic dephosphorylation. PP2A-B56 is recruited to the kinetochore via BubR1 through an LxxxIxE motif in the

kinetochore-attachment regulatory domain (KARD) on BubR1 (Hertz et al. 2016; Suijkerbuijk, van Dam, et al. 2012). Ser670 and Ser676 within the KARD domain can be phosphorylated by Cdk1 and Plk1 respectively, stimulating the interaction of PP2A-B56 with BubR1 (Kruse et al. 2013; Suijkerbuijk, Vleugel, et al. 2012). These phosphorylation events are exclusive to tension-less unattached kinetochores promoting the binding of PP2A-B56 to BubR1 in prometaphase (Elowe et al. 2010; Huang et al. 2008). PP2A-B56 counteracts the activity of Aurora B (Kruse et al. 2013; Suijkerbuijk, Vleugel, et al. 2012; Foley et al. 2011), Upon formation of attachments and the subsequent generation of tension, Aurora B activity at the outer kinetochore drops (Foley et al. 2011). PP2A-B56 is therefore then able to dephosphorylate Aurora B sites including phosphorylation of the RVSF and SILK motifs in Knl1 (Liu et al. 2010; Nijenhuis et al. 2014). PP2A-B56 also opposes the Mps1 kinase and has been shown to remove the phosphorylation of MELT motifs on Knl1, a MELT-like Mps1 phosphorylation on Bub1 and other Mps1 phosphorylation sites on the Ska proteins (Espert et al. 2014; Maciejowski et al. 2017; Qian et al. 2017).

PP1 binding to the RVSF motif in Knl1 is dependent on the absence of phosphorylation of the serine within the motif. Phosphorylation of this site by Aurora B has been suggested to inhibit PP1 binding until metaphase, when Aurora B is physically separated from its targets at the outer kinetochore by the development of tension across the kinetochore (Liu et al. 2010). This should then allow dephosphorylation of this site by PP2A-B56 and recruitment of PP1, and it has been suggested that PP1 can then dephosphorylate the MELT motifs on Knl1 (Nijenhuis et al. 2014). There is some debate about the relative contribution of PP2A-B56 and PP1 for the dephosphorylation of the MELT motifs, however, it is clear that together they collaborate to silence the checkpoint and stabilise kinetochore-microtubule attachments.

1.2.2.4.4 The RZZ complex

The RZZ complex, consisting of Rod, ZW10 and Zwilch, is only found in metazoans (Barisic & Geley 2011). It is a large ~800kDa complex which forms an anti-parallel dimer (Mosalaganti et al. 2017). Depletion of the RZZ leads to an increase in aberrant mitosis, characterised by issues in anaphase such as lagging chromosomes, chromatin bridges, and the formation of micronuclei (Kops et al. 2005). siRNA of ZW10 also causes a more than 10 fold reduction in Mad1: Mad2 recruitment (Kops et al. 2005). The RZZ localises to the kinetochore in prometaphase via Zwint-1 in an Aurora B regulated manner (Kasuboski et al. 2011; Kops et al. 2005). Following kinetochore-microtubule attachment formation, the levels of RZZ at the kinetochore drop, and the protein complex is translocated to the spindle pole. This is mediated through an interaction with Spindly, a cargo adaptor protein to the Dynein-Dynactin complex (Mosalaganti et al. 2017; Gassmann et al. 2010).

The RZZ complex is particularly interesting because it interacts with Mad1:Mad2 and Spindly, controlling Mad1:Mad2 localisation and thereby both promoting and silencing the SAC (Silió et al. 2015; Caldas et al. 2014). Silió et al. (2015) posited that having two separate mechanisms to recruit Mad2 to the kinetochore it may help its targeting in two different situations; unattached kinetochores (the RZZ complex) and misaligned kinetochores (the Bub1 binding pool). Upon microtubule binding Dynein (a minus end directed motor) with the help of Spindly to strip proteins from the kinetochore and 'walk' them towards the centrosomes, reducing the levels of Mad1: Mad2 at the kinetochore (Howell et al. 2001). Inhibition of either Dynein stripping or Spindly prevents the removal of Mad1/2 and the silencing of the SAC (Howell et al. 2001; Griffis et al. 2007; Gassmann et al. 2010; Barisic et al. 2010).

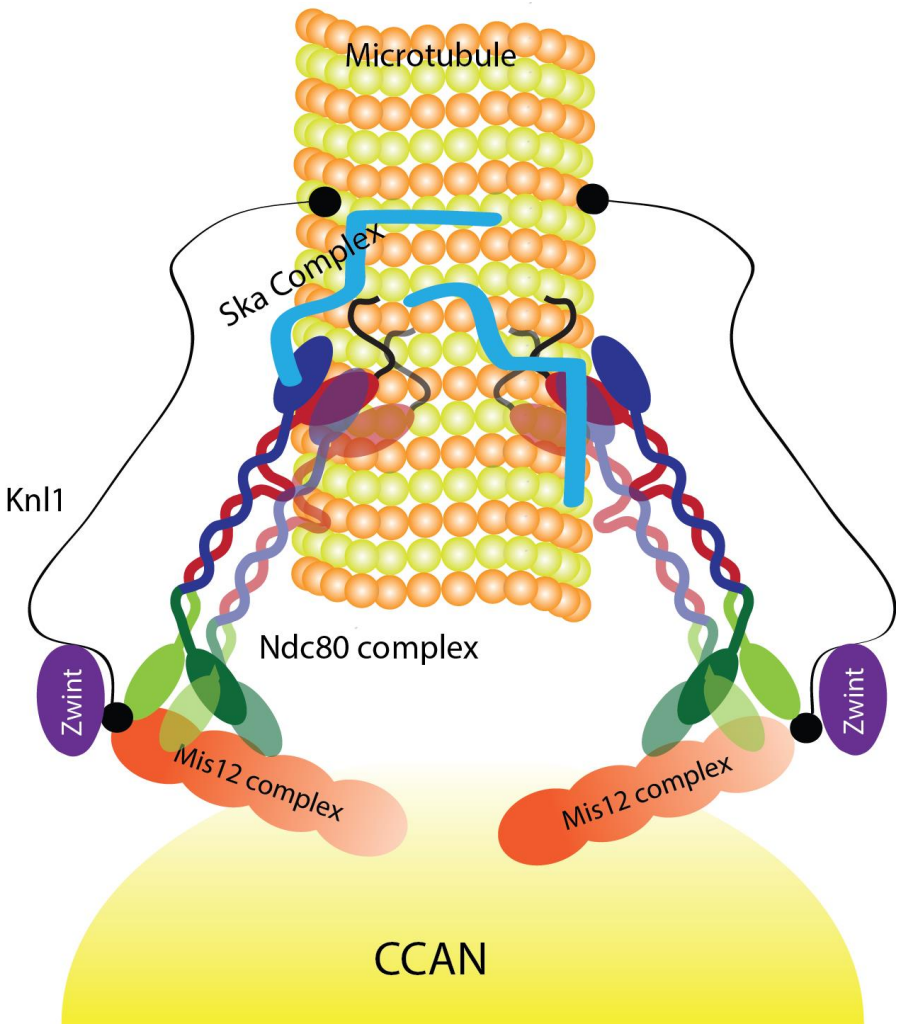


Figure 1.2 The kinetochore-microtubule interface

The outer kinetochore interacts with the microtubules via a number of different factors. The Ndc80 complex is the major microtubule binding site however this is supported by Knl1's ability to bind microtubules. The Ska complex helps stabilise microtubule kinetochore attachments possibly by helping Ndc80 to cluster on the chromosome and crosslinking different protofilaments within the microtubule. Together these interactions allow the kinetochore to remain attached to depolymerising microtubules

1.3 The formation of attachments

1.3.1 The bipolar spindle

A conserved feature of metazoan mitosis is the alignment of chromosomes on the metaphase plate. This requires the attachment of the kinetochores to the bipolar spindle. The spindle is made of microtubules which are highly dynamic, stochastically changing between rapid growth and shrinkage phases until they are stabilised by binding kinetochores. These cycles of polymerisation and depolymerisation allow microtubules to 'search' the cell for kinetochores, a process known as 'search and capture' (S&C) (Mitchison & Kirschner 1984).

Microtubules are made up of GTP-bound tubulin dimers which polymerise into long protofilaments arranged to form a cylindrical microtubule. The protofilaments are polarised, with α and β tubulin arranged head to tail, with the faster growing plus ends having β tubulin proximal to the tip. Dynamic instability exists as GTP-bound tubulin is hydrolysed following incorporation into microtubules, so that distal to the plus ends most β-tubulin is bound to GDP. Should the plus ends themselves hydrolyse the GTP bound to β-tubulin, the microtubules undergo a conformational change from straight to curved protofilaments. This causes the microtubules to 'unzip' themselves as they rapidly depolymerise. On rare occasions GTP-bound tubulin dimers rebind the tip and induces rescue, stabilising microtubules and allowing them to continue to polymerise (Mitchison & Kirschner 1984; Kumar & Wittmann 2012; Foley & Kapoor 2013). These stochastic dynamics of individual microtubules are the basis of the S&C mechanism. Microtubule associated proteins can regulate the frequency of catastrophe and rescue, biasing microtubule dynamics either for or against polymerisation (Kumar & Wittmann 2012)

Modelling suggests unbiased search and capture of kinetochores would take longer than the 30 minutes it takes to complete mitosis in human cells (Wollman et al. 2005; Magidson et al. 2011), but cellular organisation biases microtubule growth towards kinetochores thus speeding up the process. Following nuclear envelope breakdown, a chromatin-generated Ran-GTP gradient is formed, which acts to stabilise microtubules and create a spatial signal biasing growth towards the chromosomes (Clarke & Zhang 2008). Also, early in prometaphase the chromosomes rearrange themselves into a ring structure, with the chromokinesin KID acting to push the arms away from the forming spindle (Magidson et al. 2011). This precongression of chromosomes positions the kinetochores close to the forming spindle microtubules, in an optimal position for rapid biorientation.

1.3.2 Methods of chromosome congression

Should chromosomes not become biorientated initially, a number of motor proteins act to return them to the spindle equator allowing them to form bipolar attachments. Monoorientated chromosomes are initially dragged polewards by kinetochore-bound Dynein, a minus end directed motor. Current models suggest that this may help the conversion of initial lateral microtubule attachments to end-on attachments. This helps position the unattached kinetochore to face the distal pole enhancing the chance of microtubules binding (Kops et al. 2010). Another theory suggests that dynein-mediated movement facilitates the congression of monoorientated and syntelically attached chromosomes (which are often separated from the body of the spindle) dragging them polewards back towards the spindle (Li et al. 2007). There is no reason for these two theories to be mutually exclusive. But more work needs to be done to integrate theories about Dynein's activity because it is implicated in several mitotic processes including chromosome movement, k-MT attachment and SAC regulation (Bader & Vaughan 2010).

In order to increase the likelihood of biorientation, chromosomes need to be returned to the spindle equator. CENP-E is a plus end directed motor which is essential for congression of misaligned chromosomes (Kapoor et al. 2006). Kinetochore-bound CENP-E binds pre-existing k-fibres and helps slide chromosomes back to the metaphase plate. Chromokinesins also counteract Dynein's activity via polar ejection forces, however CENP-E is the dominant force (Barisic et al. 2014).

1.3.3 How attachments form and persist

Initially kinetochores usually bind to the side of microtubules (Magidson et al. 2011) because the probability of encountering the end of a MT is far lower than associating with the lateral surface of the microtubules. Little is known about the conversion process from lateral to end-on attachment although it is postulated to be a multi-step process (Shrestha & Draviam 2013). Lateral attachments appear to be largely immune to phosphorylation by Aurora B, allowing them to form without interference (Kalantzaki et al. 2015; Shrestha et al. 2017). Lateral attachments also appear unaffected by the deletion of the Ndc80 N-terminal tail. However these attachments then struggle to be converted to end-on attachments (Kalantzaki et al. 2015). It has been suggested that Astrin may play a late role in solidifying the conversion of microtubule attachment state (Shrestha et al. 2017).

1.4 The role of kinases at the kinetochore

Phosphorylation is used extensively at the kinetochore as a way of modulating activity and interactions at the kinetochore. Numerous kinases have activity at the kinetochore, including Cdk1, Plk1, Bub1, Aurora B and Mps1. Cdk1 has already been mentioned in its more global role, as the major cell-cycle driver. It is a proline-directed kinase with a minimal consensus motif of (S/T)-P but which can be expanded to (P/C/Xs)-X-(S/T)-P-X-(R/K)-K (Alexander et al. 2011).

1.4.1 Plk1

Plk1 is a member of the polo-like kinases (PLK), first discovered in *Drosophila* (Sunkel & Glover 1988). In humans there are five PLKs which have distinct roles; Plk1 and Plk4 are involved in cell division (K. S. Lee et al. 2014). PLKs are Ser/Thr kinases which have an N-terminal kinase domain, though in Plk5 this is non-functional. All variants of PLKs' C-terminal regions contain two polo box domains (PBD) with the exception of Plk4, which has a cryptic polo box which homodimerizes, and a third PBD (Slevin et al. 2012).

Plk1 is known to be of critical importance for successful mitotic progression. It has roles in multiple stages of mitosis including chromosome condensation and maturation, mitotic entry, regulation of cohesion and kinetochore fibres, as well as cytokinesis (Barr et al. 2004; Glover et al. 1998; Strebhardt & Ullrich 2006). It also has a role in the recruitment of SAC components and, via tension-sensitive phosphorylation of BubR1, kinetochore-microtubule stability (Elowe et al. 2007). Plk1's role at the kinetochore is interesting because it is required for efficient formation of attachments in prometaphase. However at metaphase it seems to prevent SAC silencing and

correction of merotelic attachments (Liu et al. 2012). Overexpression of Plk1 can cause the failure of checkpoints which can lead to aneuploidy and thus it is hardly surprising it has been linked to oncogenesis (Strebhardt & Ullrich 2006; Strebhardt 2010; Mundt et al. 1997).

Plk1 is activated by phosphorylation of the T-loop at Thr210, and inhibited by a C-terminal segment that acts as an autoinhibitory domain (Mundt 1997). The PBD targets Plk1 to its substrates, via recognition of phospho-Ser and phospho-Thr motifs (Andrew E H Elia et al. 2003a; Andrew E.H. Elia et al. 2003b). Thus the interaction of Plk1 with its substrates is dependent on the substrate being phosphorylated prior to Plk1 binding. This can be done by Plk1 itself (self-priming) or another kinase such as Cdk1 (Lee et al. 2008). Examples of both can be found in the literature and they could confer different outcomes based on the underlying biochemical differences (K. S. Lee et al. 2014). Park et al. (2011) found that self-priming reactions could form a positive feedback loop with rapid amplification of active Plk1 on a substrate surface, whilst non-self-priming reactions led to a linear amplification of active Plk1. Priming, which requires another kinase also naturally creates a sequence cascade, with Plk1 becoming active only after another kinase has acted to prime the PBD binding site. This is of high value in a system such as the cell cycle, where it is important that progression is unidirectional.

1.4.2 Aurora B and its role in error correction

Accurate chromosome segregation is dependent on kinetochore-microtubules creating the correct attachment geometry. A variety of incorrect geometries are frequently created during the initial stages of attachment (Santaguida & Musacchio 2009; Ye et al. 2017). Cells must be able to discriminate between attachments states selectively,

stabilising correct attachments whist destabilising incorrect states. Proper amphitelic attachments are defined as sister kinetochores, which are attached to microtubules emanating from opposite poles of the cell (ie biorientated). **Figure 1.3** shows the range of possible incorrect attachments. Initially cells often form monotelic attachments state where one kinetochore is attached but the other is unattached. Syntelic attachments are formed when both kinetochores are attached to a single spindle pole. In merotelic attachments, although biorientated, one kinetochore is attached to both poles. It has been suggested that the geometry of vertebrate kinetochores, with sister kinetochores facing away from each other in a back-to-back arrangement, helps to favours attachments to microtubules emanating from opposite spindle poles.

Cells have the capacity to correct initial attachment errors using the error correction pathway. Early experiments identified lack of tension as a key factor in destabilising incorrect attachments, with pulling forces, applied using a microneedle, capable of stabilising syntelic attachments (Nicklas & Koch 1969). Once amphitelic attachments are established, sufficient tension is created by opposing microtubule pulling forces to prevent destabilisation of attachments. Monotelic and syntelic attachments produce no tension, thus triggering error correction. How merotelic attachments, which do generate tension, are sensed and resolved is still not fully understood (Gregan et al. 2011).

This error correction pathway is mediated by Aurora B kinase, which is recruited as part of the chromosomal passenger complex (CPC) to the centromere. The CPC is made up of four components; Aurora B which contains the enzymatic activity, INCENP which acts as a scaffold, bridging to Borealin and Survivin which control its localisation (Jeyaprakash et al. 2007; Klein et al. 2006). The localisation of the CPC to the centromere is dependent on the phosphorylation of two histones. Phosphorylation of H3T3ph by Haspin kinase allows Survivin to bind directly (Yamagishi et al. 2010; Wang et al. 2010; Kelly et al. 2010; De Antoni et al. 2012). Phosphorylation of

H2AT120ph by Bub1 also helps localise the CPC to the centromere. Although the molecular mechanism is not fully understood, it is possibly that Sgo1 and Sgo2 act as an adapter between the phospho-site and CPC component Borealin (Yamagishi et al. 2010; Kawashima et al. 2010; Tsukahara et al. 2010).

Aurora B kinase was identified as a key regulator of microtubule-kinetochore attachments since its inhibition results in the stabilisation of syntelic and merotelic attachments (Lampson et al. 2004). If inhibition was released, cells were able to correct these attachment defects (Lampson et al. 2004; Bakhoum et al. 2009). Upon phosphorylation by Aurora B, the kinetochore's affinity for microtubules drops, leading to turnover of incorrect attachments and allowing further rounds of attempts to form correct attachments.

Aurora B acts on several members of the KMN network; phosphorylation of Dsn1, Knl1 and Ndc80 all contribute to weakened microtubule binding (Welburn et al. 2010). This response is graded depending on how many proteins are phosphorylated by Aurora B. The phospho-mimetics of Ndc80 reduce affinity for microtubule by almost half whilst phospho-mimetics of all three proteins resulted in no microtubule binding was measured at all (Welburn et al. 2010). Although Dsn1 does not directly bind microtubules, it was seen to sensitise kinetochores to additional phosphorylation sites on Ndc80 and Kn1. The phosphorylation sites identified on Knl1 were pSer24 and pSer60, both within the N-terminal microtubule-binding region of Knl1 (Welburn et al. 2010). Ndc80 is highly phosphorylated on its N-terminal tail by Aurora B (DeLuca et al. 2006; Ciferri et al. 2008; Guimaraes et al. 2008; DeLuca et al. 2011; Santamaria et al. 2011; Malik et al. 2009) . The addition of the negatively charged phosphate groups disrupts the ability of Ndc80 to form electrostatic interactions with tubulin's E-hooks (Alushin et al. 2012; Alushin et al. 2010). It also leads to increased binding of Mps1 kinase, which is the master regulator of the SAC (Saurin et al. 2011; Hiruma et al.

2015; Ji et al. 2015). Linking the error correction pathway with SAC signalling thus ensures a robust response to incorrect attachment states.

Aurora B also acts on microtubule depolymerizing kinesins, such as mitotic centromere-associated kinesin (MCAK). Phosphorylation of MCAK affects their depolymerising activities and their localisation (Lan et al. 2004; Zhang et al. 2007; Lampson & Cheeseman 2011). It has been suggested that regulation of MCAK might provide a mechanism for the rapid fine-tuning of microtubule dynamics (Ems-Mcclung et al. 2013). Several complexes which act to stabilise K-MT interactions are negatively regulated by Aurora B, therefore Aurora B prevents the premature stabilisation of incorrect attachments (Tien et al. 2010; Chan et al. 2012; Kalantzaki et al. 2015; Schmidt et al. 2010). In summary, Aurora B acts to decrease K-MT binding affinity, regulate MT dynamics and prevent the stabilisation of the K-MT interactions leading to a high turnover of microtubules and the destruction of erroneous connections.

One major hypothesis for how Aurora B is able to sense tension is known as the 'spatial separation' model. Upon attachment the physical distance between the CPC located at the inner centromere and its targets at the kinetochore increases (Liu et al. 2012; Wan et al. 2009). Maresca & Salmon (2009) measured the change in distance between CENP-A and Ndc80 in *Drosophila* S2 cells under tension (102nm) and in tension-less kinetochores (~65nm). Liu et al. (2009) found that the localisation of substrates affects Aurora B's ability to phosphorylate its targets. Reducing the distance between Aurora B and its substrates (they used a FRET biosensor which reported Aurora B phosphorylation) led to high levels of phosphorylated sensor regardless of tension. However, when the sensor was localised to the outer kinetochore via Mis12 it was phosphorylated at unaligned kinetochores and dephosphorylated upon alignment, when the resulting tension separates the outer kinetochore for the centromere.

Overall this Aurora B mediated pathway helps bias towards correct attachment states ensuring that only amphitelic attachments persist.

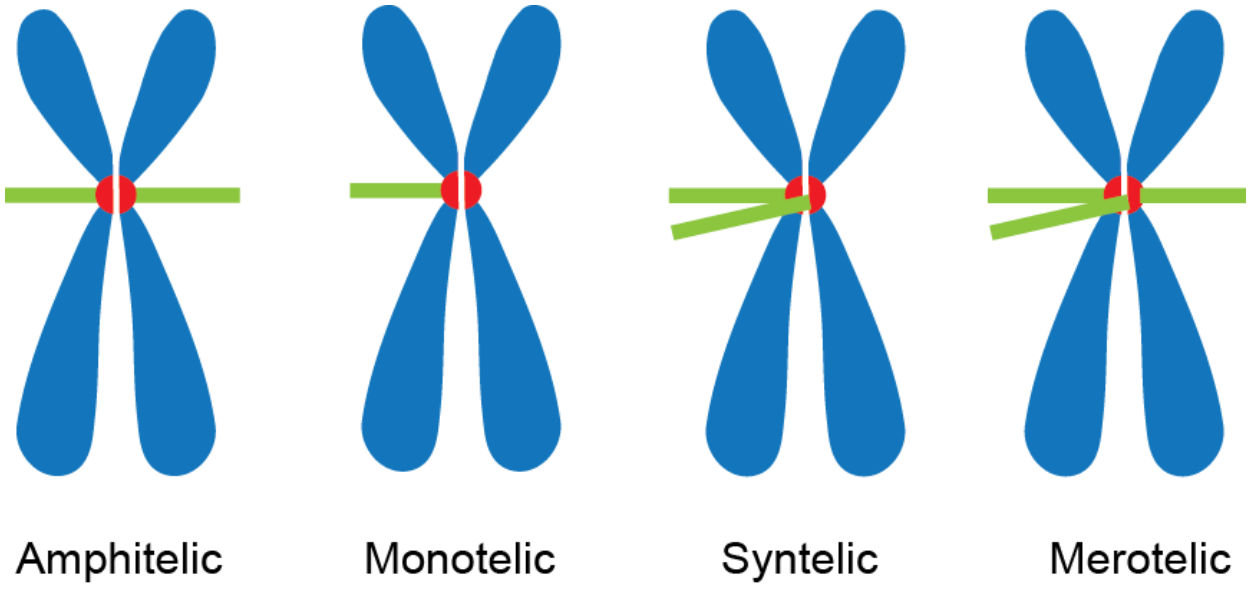


Figure 1.3 Microtubules can attach to kinetochores to create a range of different geometries

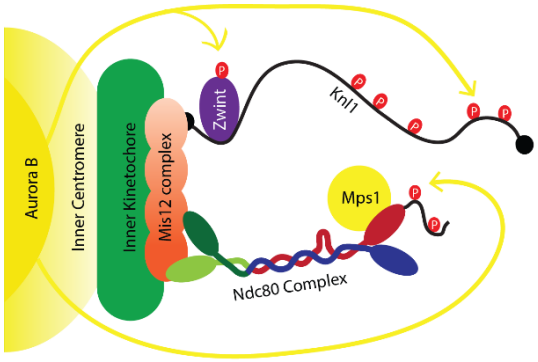
Sister kinetochore are attached to opposite poles in of the cell in amphitelic attachments. These correctly biorientated chromosomes have no error correction signalling due to tension. Both monotelic and syntelic attachments will generate an error correction signal due to the close proximity of Aurora B to the outer kinetochore. In the case of merotelic attachments one kinetochore makes links to both spindle poles. As yet the mechanism which recognises these errors is not well understood.

1.4.3 Mps1 is a master regulator of the Spindle Assembly Checkpoint

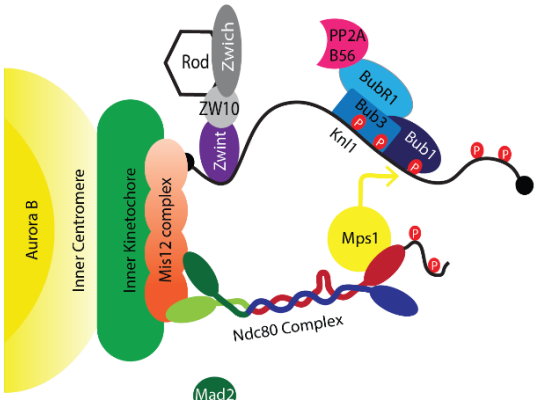
The SAC is a quality control mechanism which prevents progression into anaphase until all chromosomes are stably attached. Even the presence of a single unattached kinetochore is sufficient to halt anaphase onset (Rieder et al. 1995). The SAC generates a signal locally at unattached kinetochores which acts globally to prevent premature separation of chromatids and mitotic exit (Rieder et al. 1995; Li & Nicklas 1995; Kops & Shah 2012; Musacchio 2015).

In 1991, many of the proteins involved in generating the SAC signal were identified via genetic screens (Li & Murray 1991; Hoyt et al. 1991; Weiss & Winey 1996). In agreement with the idea that unattached kinetochores act as the source of the SAC signal (Rieder et al. 1995), all of the identified SAC proteins are recruited to the kinetochore during prometaphase and their levels generally drop as K-MT attachments form (Howell et al. 2004).

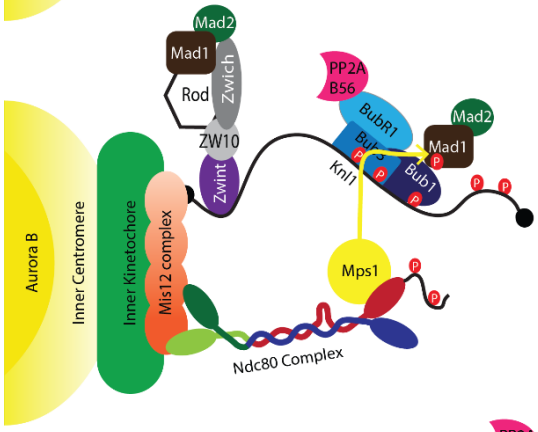
Just as in the error correction pathway, the spindle checkpoint system relies heavily on phosphorylation of targets to alter the activity, binding capability and localisation of system components (Hunter 2012; Cuijpers & Vertegaal 2018). Whereas in the error correction pathway Aurora B kinase is vital, in the SAC, Mps1 kinase acts as the key kinase responsible for generating and maintaining the checkpoint (Stucke et al. 2002; Musacchio 2015).



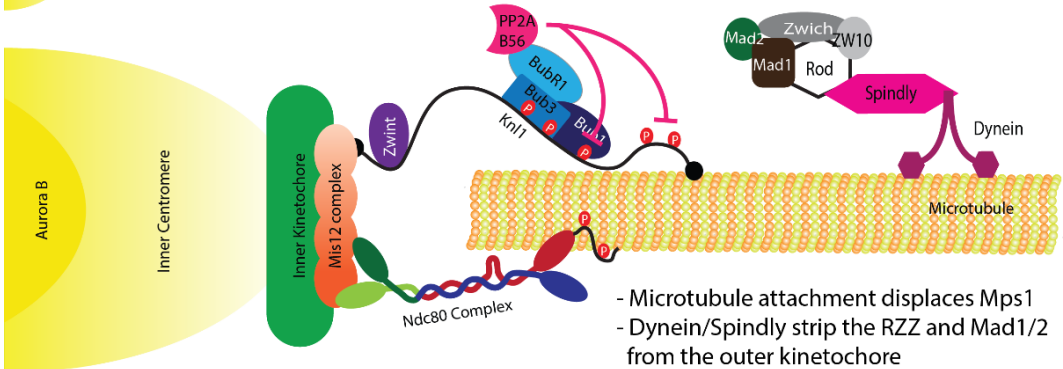
- Aurora B phosphorylates multiple residues at the outer kinetochore
- Mps1 is recruited to the Ndc80 complex



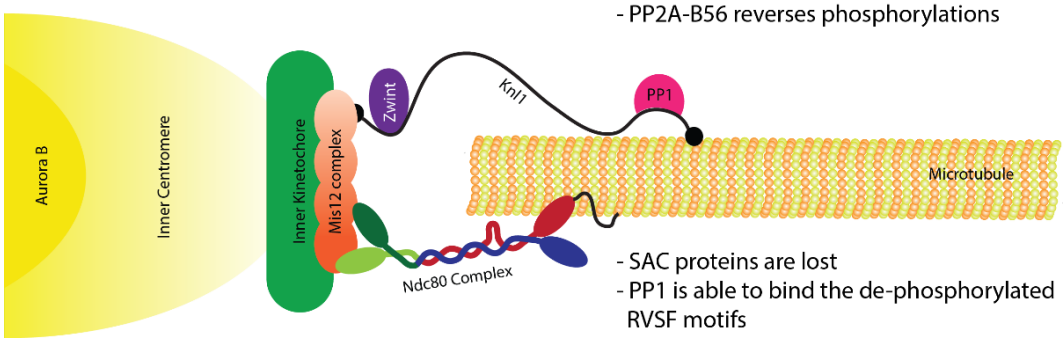
- Mps1 phosphorylates the MELT motifs
- The bub protiens are recruited to Knl1
- The RZZ is recruited to Zwint



- Mad1/2 is recruited
- MCC is formed



- Microtubule attachment displaces Mps1
- Dynein/Spindly strip the RZZ and Mad1/2 from the outer kinetochore
- Tension separates Aurora B from the outer kinetochore
- PP2A-B56 reverses phosphorylations



- SAC proteins are lost
- PP1 is able to bind the de-phosphorylated RVSF motifs

Figure 1.4 The SAC works to prevent premature anaphase onset

This figure represents the generation of the SAC response from an unattached kinetochore to a mature attachment state. How the core kinetochore is phosphorylated leading to the recruitment of the SAC proteins. Following binding of a microtubule the phospho-status changes and the SAC proteins are lost.

1.4.3.1 Mps1 recruitment and its phosphorylation of the MELT motifs

The recruitment of Mps1 to the kinetochore, via interactions with the calponin homology (CH) domain in Ndc80 and Nuf2's, is stimulated by the Aurora B mediated phosphorylation of the N-terminal tail of Ndc80 (Vleugel et al. 2013; Ji et al. 2015; Hiruma et al. 2015; Zhu et al. 2013). The phosphorylation of Ndc80 by Aurora B has a negative effect on the microtubule-binding affinity of Ndc80. This data has led to the suggestion that upon microtubule attachment, Mps1 is displaced from the kinetochore by direct competition with microtubules leading to checkpoint silencing (Ji et al. 2015; Hiruma et al. 2015). Whilst this is an appealing model, there is some evidence which shows Mps1 present at attached kinetochores, so it is likely this is not the full story (Aravamudhan et al. 2015).

Mps1 is a highly dynamic protein with a rapid turnover rate at the kinetochore (Howell et al. 2004; Jelluma et al. 2010). Upon recruitment to the kinetochore Mps1 dimerises, allowing trans-autophosphorylation leading to the active kinase (Jelluma et al. 2010; Kang et al. 2007; Mattison et al. 2007; Wang et al. 2009). Interestingly, Mps1 appears to negatively regulate its own binding, with kinase dead mutants or inhibited Mps1 leading to higher levels of kinetochore-associated Mps1 (Jelluma et al. 2010; Wang et al. 2014). This difference in residency time may give inactive Mps1 time to trans-

phosphorylate to form the active kinase. The switch to a more short-lived active form may help to create a responsive system which can be quickly silenced upon K-MT attachment (Pachis & Kops 2018). Once activated, Mps1 phosphorylates multiple targets at the kinetochore.

Knl1 acts as a scaffold for the generation of the SAC response with SAC components binding both directly (Bub proteins) and indirectly (Mad proteins). Phosphorylation of the MELT motifs by Mps1 is a prerequisite of Bub binding (Shepperd et al. 2012; London et al. 2012; Yamagishi et al. 2012). Human Knl1 contains 19 MELT motifs which show variable levels of conservation to the consensus (Vleugel et al. 2013). In line with this is the prediction that only a third or so of the MELTs are active (Zhang et al. 2014; Vleugel et al. 2015). The MELT motif is at its core a four amino acid sequence motif, the Thr residue of which is phosphorylated by Mps1. The motif itself extends on both sides of the core MELT, with an activity weighted consensus sequence generating: DKTΦΦΩS[ED]x$[ED]_{2\text{-}3}$xxM[DE]ΦTxSHTΦxΦ. Here Φ refers to hydrophobic residues, Ω to aromatic residues, and X can be any amino acid (Vleugel et al. 2013; Vleugel et al. 2015). Vleugel et al. (2015) observed that the downstream SHT motif can only be phosphorylated once the Thr residue in the upstream MELT has been phosphorylated. Hence they proposed a model whereby Mps1 phosphorylates the MELT motif, creating its own target site allowing a further phosphorylation of the downstream SHT motif.

Phosphorylated MELT motifs create a binding site for the Bub proteins, in patricular Bub3 and Bub1 which together interact with pMELT motifs. Bub3 is the major reader of the pMELT signal. It's 7-WD40 β-propeller forms a bipartite binding site; with three Arg residues coordinate the phospho-Thr whilst the hydrophobic residues of the MELT fit into a hydrophobic pocket (Primorac et al. 2013). Bub1, which forms a complex with Bub3, also contributes an Arg residue which helps to coordinate the phosphorylated residue. Together this explains the necessity of the MELT phosphorylation for

Bub3:Bub1 binding. Later work by Vleugel et al. (2015) on the pSHT motif hypothesised that the acidic pSHT binds to basic residues on Bub3, and their experimental data shows that the pSHT motif directly contributes to Bub3 binding.

1.4.3.2 The formation of the MCC

Mad1 and Mad 2 can form a stable complex which is recruited to the kinetochore via Bub1 (Zhang et al. 2017). The Mad2 protein is able to adopt two distinct topologies; open (O-Mad2) and closed Mad2 (C-Mad2) (Luo & Yu 2008). Initially cytosolic Mad2 is in the O-Mad2 conformation, which upon binding to Mad1 and its other interactions undergoes a conformational switch to C-Mad2 (De Antoni et al. 2005). The core MCC is formed of BubR1, Bub3, C-Mad2 and Cdc20. BubR1 is recruited to the kinetochore in a Bub3-dependent manner, through a 'pseudo-symmetric' interaction with Bub1 (Zhang et al. 2015; Overlack et al. 2015). Mad1/C-Mad2 bind the kinetochore and recruit O-Mad2 through Mad2 heterodimerisation (De Antoni et al. 2005). The O-Mad2 is then converted to C-Mad2. Upon conformational change the newly formed C-Mad2 interacts with Cdc20 via the Mad2-interaction-motif (MIM) (Sironi et al. 2002). The crystal structure of the APC/C bound to MCC in fission yeast (Chao et al. 2012) has suggested that BubR1, Cdc20 and Mad2 bind cooperatively to the APC/C with each protein aiding the binding of the other two subunits, creating a stable core MCC.

The formation of MCC prevents anaphase onset via several mechanisms. Firstly, MCC sequesters Cdc20. Cdc20 is a co-activator of the APC/C, acting to present substrates to the APC/C (Primorac et al. 2013). MCC not only sequesters one Cdc20 molecule within the MCC and thereby prevents it from activating the APC/C, but is also capable of binding a second Cdc20 molecule (to form MCC^{2Cdc20}), via the D-box and KEN2 box of BubR1 (Primorac et al. 2013; Izawa & Pines 2015). These two Cdc20 molecules are bound via different interactions. Importantly this second subunit can already be bound to APC/C thus allowing the MCC to directly inhibit active APC/C.

The MCC inhibits the APC/C by acting as a pseudo-substrate (Izawa & Pines 2015; Ji et al. 2017), through the action of BubR1. BubR1 precludes the E2 enzyme: APC/C association, ensuring no ubiquitination can occur (Alfieri et al. 2016). Once formed the MCC can diffuse away from the kinetochore and is thus able to inhibit APC/C at a distance.

1.5 The dynamic kinetochore

Over the course of mitosis the kinetochore adopts two fundamentally different states, differentiated by their microtubule-attachment status. These states differ in both their composition and post translational modification (PTM) state. Prior to the formation of under-tension kinetochore-microtubule attachments, the kinetochore is dominated by kinase activity with both Aurora B and Mps1 adding phospho-groups to multiple proteins. This leads to the formation of the SAC signal as SAC proteins recognise their phospho-binding sites.

As end-on load-bearing microtubule attachments form, tension is generated lowering the ability of Aurora B to phosphorylate the outer kinetochore. Whether microtubules actively displace Mps1, or are indirectly responsible for its removal from the kinetochore, is as yet not entirely clear (Ji et al. 2015; Hiruma et al. 2015; Aravamudhan et al. 2015). However, Mps1 is lost from the kinetochore upon attachment (Jelluma et al. 2010). PP2A-B56 localises to unattached kinetochores during prometaphase, via the KARD domain of BubR1. BubR1 interacts with the PP2A regulatory subunit, B56 (Hertz et al. 2016; Suijkerbuijk, Vleugel, et al. 2012).

Prior to attachment, PP2A-B56 is insufficient to silence the checkpoint and remove Aurora B's phosphorylations due to the high level of kinase activity. As attachments form and the level of kinase activity drops, it biases the state of equilibrium in favour of

PP2A-B56. PP2A-B56 decreases Aurora B, Plk1 and Mps1 phosphorylations resulting in the loss of its own binding sites, and helps to recruit PP1 through dephosphorylation of the Knl1-RVSF motif (Foley et al. 2011; Espert et al. 2014; Nijenhuis et al. 2014; Maciejowski et al. 2017; Qian et al. 2017) (Foley et al. 2011; Espert et al. 2014). PP1's recruitment is inversely proportional to Aurora B activity, as phosphorylation of Knl1 by Aurora B prevents PP1's localisation (Liu et al. 2010). The kinetochore will therefore move from a PP2A-B56 dominated state during prometaphase to a PP1-associated state in metaphase.

This interplay between kinases and phosphatases often creates feedback loops allowing reversible regulation of MT-attachment stability (Nijenhuis et al. 2014; Espert et al. 2014; Funabiki & Wynne 2014). Dephosphorylation is critical for the stabilisation of attachments and the downregulation of SAC components (Foley et al. 2011; Espert et al. 2014; Nijenhuis et al. 2014; Maciejowski et al. 2017; Ji et al. 2017). Depletion of phosphatases can prevent kinetochores forming load-bearing attachments and increase the number of misaligned chromosomes (Espeut et al. 2015). Upon the formation of load-bearing kinetochore attachments, the SAC must be rapidly silenced to allow mitosis to proceed in a timely manner. There are a number of mechanisms which actively help to prevent further MCC formation: the removal of SAC proteins by Dynein-mediated stripping; prevention of further C-Mad2 formation by $p31^{comet}$; the active removal of phosphorylation sites preventing further recruitment of SAC proteins. All of these steps will lead to a situation where the kinetochore will change from a state dominated by accumulated SAC proteins to a status where SAC proteins will be replaced by other proteins necessary to finalise microtubule kinetochore attachments.

In conclusion, the kinetochore is a highly dynamic protein structure that adapts during the course of the cell cycle to fulfil its different functionalities. These changes affect both the protein composition of the kinetochore as well as the post-translational modifications, particularly phosphorylations that are found on kinetochore proteins.

The aim of my thesis was to characterise the differences that distinguish distinct kinetochore states using both unbiased and targeted strategies.

Chapter 2: Materials and methods

2.1 Cell culture

2.1.1 Tissue culture

HeLa S3 cells were cultured with DMEM supplemented with 10% foetal bovine serum (FBS) at 37ºC with 5% CO_2. Flp-In cell lines expressing Hec1-GFP, GFP-Zwint and GFP-Astrin were cultured in medium supplemented with 200µg/ml Hygromycin B (Invivogen) and 4µg/ml Blasticidin (Invivogen).

2.1.2 Optimising a synchronisation protocol

On-dish release

GFP-Mad2 cells were seeded on coverslips in 6-well plates and arrested with 150µM Monastrol, 10µM STLC, 300nM Nocodazole and 100nM GSK923925 for 12hrs. Overnight treatment led to about 60-70% mitotic index. The cells were washed in pre-warmed media, 2xPBS; 3xDMEM and released into 20µM MG132. At 2hr and 3hr time points coverslips were fixed and stained for Tubulin, Astrin and DAPI (as described in **Section 2.4.1**).

In-solution release

In order to create a metaphase population HeLa S3 cells were grown to 70% confluency. Cells were arrested for 14hrs with 10µM STLC (Sigma) . Mitotic cells were collected via shake-off and cells were pelleted at 600g. Cells were washed with pre-warmed 4xPBS and 4xDMEM with 10% FBS. Three 15cm dishes were combined in a single 50ml Falcon. Each wash used 50ml media and samples were mixed well to

ensure the pellets were fully resuspended to aid STLC release. Following each resuspension stage, cells were incubated for 3mins at 37ºC followed by a 2min centrifugation step (at 600g). After the final wash cells were plated into a single large 15cm dish with 50ml medium. 20mins later 20 µM MG132 was added. Cells were left at 37ºC for a further 3hrs.

2.1.3 Cell cycle arrests

Chapter 3: Prior to Hec1-GFP and GFP-Zwint immunoprecipitations, cells were induced using 1ug/ml Doxycycline for 20hrs. Cells were arrested for 14hrs with 330nM Nocodazole (Merck). Samples were then processed for immunoprecipitation (see below sections).

Chapter 4: See above **In-solution release**

Chapter 5: In the case of GFP-Astrin cell lines, cells were grown to 70% confluency before being arrested for 14hrs with 10µM STLC. 1µM BI2536 (Cambridge Bioscience) or DMSO was added for 1hr prior to cell collection by mitotic shake-off.

2.2 GFP-Astrin cell lines

2.2.1 Cloning

GFP-Astrin WT and GFP-Astrin PBD binding mutants had been created by previous members of the lab; site-directed mutagenesis was performed using the QuickChange methodology (Agilent Technologies). Following confirmation of the mutagenesis by sequencing, samples were sub-cloned into a pcDNA5/FRT/TO N-terminal GFP vector (Invitrogen).

2.2.2 Production of stable cell lines

HeLa S3 parental cells containing the Flp-in TREx system (a kind gift from Stephen Taylor, Manchester) were transfected with 100ng of GFP-Astrin constructs and 900ng of POG44 plasmid using Mirus LT1 (Mirus Bio LL) according to manufacturer's instructions. After 24 hours cells were transferred to a 15cm dish and a further 24 hrs later selected using 200µg/ml Hygromycin (Invitrogen) and 4µg/ml Blasticidin (Invitrogen). Colonies were grown for 2 weeks before picking using cloning discs (Thermo-Fisher). Both immunofluorescence and western blots were used to screen for successful, homogeneous clones. These were then checked in a doxycycline negative background to confirm there was no leaky expression. Hec1-GFP, GFP-Zwint and GFP-Mad2 cells had been produced by other members of the laboratory.

2.3 Transfection and rescue experiments

2.3.1 siRNA treatments

Cells were seeded at 30,000 cells/ 2cm well for HeLa S3 cells or 80,000 cells/ 2cm well for GFP-Astrin Flp-in cells. 6hrs prior to transfection, cells were induced using 1ug/ml Doxycycline and then transfected with Oligofectamine (Invitrogen) and 20nM of Astrin targeted using 5′-TCCCGACAACTCACAGAGAAA -3′ (QIAGEN) for a total of 60hrs (according to manufacturers instructions).

2.3.2 Rescue experiments

GFP-Astrin WT and ST110/111AA cells were seeded at 80,000 cells per well. 24hrs after seeding cells were induced and treated with RNAi as in **Section 2.3.1**. Following 60hrs of RNAi treatment cells were fixed in PTEMF.

2.3.3 Transient transfection

Flag-Astrin constructs where the candidate PBD binding sites had been mutated to a double alanine (created by previous members of the lab) were transiently transfected into HEK293T cells using TransIT-LT1 transfection reagent (Mirus Bio) according to the manufacturer's protocol. 24hrs post-transfection cells were arrested with 330nM Nocodazole for 14hrs overnight. Cells were collected via a mitotic shake-off and a Flag-immunoprecipitation was performed (See **Section 2.6.3**).

2.4 Image processing and analysis

2.4.1 Imaging of fixed cells

Media was removed and replaced with PTEMF fixation buffer (20mM Pipes-KOH, pH 6.8, 0.2% Triton X-100, 1mM MgCl2, 10mM EGTA and 4% formaldehyde) for 12mins at room temperature (RT). Coverslips were washed 3xPBS before transfer into blocking solution (PBS with 2% BSA) and blocking proceeded for 30mins. Primary and secondary antibody incubations were performed in blocking solution for 1hr and 30mins respectively (antibodies used in this study appear in **Table2.1**). DNA was stained in the secondary antibody incubation with 1µg/ml DAPI. Coverslips were washed 3xPBS after each incubation. Coverslips were dried and mounted in moviol on microscope slides.

Slides were imaged using a BX61 Olympus microscope with a 60x 1.35 NA oil immersion objective lens. The microscope was fitted with filter sets for DAPI, Alexa Fluor 488, Alexa Fluor 555 and Alexa Fluor 647 along with a CoolSnap HQ2 camera (Roper Scientific) in conjunction with MetaMorph software. Each image is compiled of 12 Z-stacks with a 0.2um separation between stacks. Stacks were Z-projected with maximum intensity and analysed in ImageJ. Figures were made using Adobe Illustrator CS6.

2.4.2 Cytospin

Cells were counted using a haemocytometer. In order to create a monolayer on the slide a suspension of 20,000 cells in at least 150ul liquid was created; if needs be cells were diluted in DMEM with 10%FBS. Cells were spun at 2000RPM for 5mins using a Shandon Cytospin 3 machine. Samples were left to dry for 1min so cells could adhere to the microscope slide before proceeding with the immunofluorescence as before (see Error! Reference source not found. **Fixed imaging**).

2.4.3 Imaging of live cells

GFP-Astrin WT and ST110/111AA cells were seeded at 40,000/ well in a 2-well dish with coverglass bottoms (World Precision Instruments). Cells were depleted of Astrin by siRNA using the same protocol as in **Section 2.1.3**. Following 36hrs Thymidine was added. After 16hrs cells were released from Thymidine using 3x media washes. The media was replaced with media which included Doxycycline (1ug/ml) and SiR-DNA. 9hrs post-Thymidine release cells were imaged.

A Deltavision Elite microscope system using filter sets for DAPI and Alexa Fluor's 488, 555 and 647, and a Photometrics Evolve 512 Delta EMCCD camera along with a heated 60xNa 1.4 oil immersion lens, was used. An environmental chamber (Imaging Solutions) at 37ºC with 5% CO_2 was used. SoftWoRx software was used to image 8-9 fields of view per condition for 10hrs with time points at every 2 minutes. A FITC-mCh-Cy5 filter set was used. Exposure times were as follows: FITC - 5% laser light, 0.05ms exposure; Cy5 - 5% laser light, 0.01ms exposure; Pol - 32% laser light, 0.5ms exposure for a single Z point. 12 Z-stacks were taken at 1um distances and SoftWoRx software was used to deconvolve the images using 8 rounds conservative setting. ImageJ was used to create maximum intensity projections and measure timings. Stills

were imported into Adobe Illustrator. Data analysis was performed using Microsoft Excel and Graphpad Prism.

2.5 Analysis of the efficiency of endonucleases

2.5.1 Comparison of benzonase with micrococcal nuclease

HeLa S3 cells were grown until 70% confluent in 7x15cm dishes and arrested overnight with Nocodazole. Cells were collected via mitotic shake-off and lysed using 250µl lysis buffer (50mM HEPES pH8, 100mM KCl, 1%IGEPAL, 0.25% Triton X-100, 1mM DTT, 1:250 Protease Inhibitor cocktail (Sigma), 1:100 Phosphatase Inhibitor cocktail 3 (Sigma), 50mM EDTA, 1mM PMSF for 30mins at 4ºC with varying amounts of benzonase and micrococcal nuclease (10U, 50U, 100U per ml); a control with no inhibitor was also used. Following lysis 100µl was taken for western blots.. For this fraction cells were centrifuged to clarify the lysate at 4ºC (15mins at 14,000 RPM). The supernatant and pellet were both suspended in Laemmli buffer and denatured. For the remaining 150µl of lysate a phenol:chloroform extraction was performed to analyse the state of DNA digestion.

2.5.2 Phenol extraction experiment

The 150µl of lysate was diluted with a further 150ul lysis buffer (without benzonase or micrococcal nuclease. 12.5mM EGTA (for micrococcal nuclease) or EDTA (for benzonase) was added to inactivate the enzymes. 10µg RNase was added and incubated for 2hrs at 37ºC, 20µg Proteinase K was incubated overnight. The following day 300µl of 1:1 phenol:chloroform (pH8) was added, then mixing samples were centrifuged (10mins, 4ºC, 12,000 RPM). To the aqueous phase Isopropanol and 3M NaOAc pH5 was added (1 volume and 1/10 volume respectively). Samples were centrifuged as before. The supernatant was removed and 700µl 70% Ethanol 4ºC

was added and samples were votexed before centrifugation (5mins, 4ºC, 7,500 RPM). Supernatant was discarded and pellets were air-dried before being resuspended in 30µl TE buffer. Samples were nanodropped and 1µg was run on a 2% agarose gel. Samples were western blotted for the presence of Knl1, Histone H3 and Tubulin.

2.6 Biochemical assays

2.6.1 Kinase assay

His-tagged N-terminal Astrin constructs containing WT or ST110/111AA mutations were used (prepared by previous members of the lab). 1µg of each construct was incubated with 10µl 2x MEB (100mM Tris-HCl pH7.4, 100mM KCl, 20mM $MgCl_2$, 40mM Sodium beta-glycerolphosphate, 30mM EGTA), 1µl of 10x ATP/DTT mix (10mM ATP, 100mM DTT), 100ng Cdk1/cycB1 (abcam) and made up to 20µl in water. Reactions were incubated for 60mins at 30ºC. Samples were denatured in Laemmli buffer (5mins at 95ºC)

2.6.2 Far western

5µl of Kinase assay samples were run on a 10% SDS-PAGE gel and transferred onto nitrocellulose membrane. The membrane was incubated overnight in blocking (50mM Tris-HCl pH7.5, 137mM NaCl, 0.1% Tween, 4% milk powder). Samples were incubated with 1µg/ ml His-GST-tagged Plk1-PBD constructs (either WT or HKAA mutants) for 8hrs at RT. The membrane was then washed 3x in blocking and incubated overnight with anti-GST Rabbit antibody before 3x washes (PBS+0.1% Tween). The secondary antibody (Donkey anti-rabbit HRP) was incubated for 1hr before the wash steps were repeated.

2.6.3 Immunoprecipitation

Cells were grown in 15cm dishes (the number of dishes varied depending on the size of the immunoprecipitation). Cells were harvested via a mitotic shake-off. Here a synchronisation step might be incorporated (if so an immunofluorescence step would be performed alongside the immunoprecipitation to confirm the success of release into MG132). Cells were pelleted at 500G for 3mins at RT and washed with PBS and spun down again (same settings). If a Calyculin A treatment was performed cell pellet was resuspended in PBS with 100uM Calyculin (Tocris, Bio-Techne) for 1min prior to cell pelleting. Pellets were lysed (50mM HEPES pH8, 100mM KCl, 1%IGEPAL, 0.25% Triton X-100, 1mM DTT, 1:250 Protease Inhibitor Cocktail (Sigma), 1:100 Phosphatase Inhibitor cocktail 3 (Sigma), 50mM EDTA, 1mM PMSF, 50U micrococcal nuclease) for 30mins at 4ºC before being clarified (14,000RPM for 15mins). Per 1mg of lysate 1µg of the appropriate antibody (homemade Sheep anti-Knl1, commercial Mouse anti-Ndc80, homemade Sheep anti-GFP, commercial Rabbit anti-FLAG) was added. As a negative control pre-immune serum was used for the homemade antibodies and commercial Mouse anti-Myc was used to control the Ndc80 immunoprecipitations in order to identify non-specific interactors. Ndc80 and Knl1 immunoprecipitations were performed using Protein-G Dynabeads (Invitrogen), GFP and FLAG immunoprecipitations were performed using Protein-G Sepharose beads (Sigma). All beads were washed 3x in lysis buffer prior to use. Immunoprecipitations were performed at 4ºC for 2hrs. Six washes were performed 3x lysis buffer and 3x wash buffer (50mM HEPES pH8, 100mM KCl) with incubations of 2mins per wash step. Protein-G Dynabeads were separated from flow-through using a magnet, Protein-G Sepharose beads were spun down (8000RPM for 3mins). If samples were for western blot analysis 1x Laemmli buffer was added and samples denatured at 100ºC for 5mins.

2.6.4 Glycine/Urea elution

Dynabeads were resuspended in 50µl HEPES wash buffer (from immunoprecipitation protocol above) and 5µl were taken for western blot as the before-elution fraction. The remaining buffer was removed and replaced by 50µl 0.1 Glycine pH2.6 and left with vigorous shaking (1500 RPM) at RT for 10mins. This was repeated three times, 5µl of eluate was collected each time for western blot analysis, the remainder was pooled. Each pool was neutralised with equal vol/vol 1M Tris pH8.5. The beads were washed with pre-urea wash buffer (50mM Tris pH8.5, 1mM EGTA, 75mM KCl) for 10mins, the wash was discarded and 3 x 50µl Urea elution buffer (50mM Tris pH8.5, 8M Urea) was added for 30mins at RT (the last elution was left eluting overnight). Again 5µl of eluate was collected for western blot analysis per wash with the remainder pooled together with the glycine pooled eluate. The pooled fraction was snap frozen in liquid nitrogen. Before proceeding to FASP, western blot samples were run to confirm a successful immunoprecipitation and elution.

2.7 Mass spectrometry

2.7.1 In-gel

Immunoprecipitation samples were loaded onto a 6-15% gradient gel and run at 180V for 65mins. Gel was stained using colloidal coomassie. Gel lanes were separated into seven slices each put into a LoBind Eppendorf tube. The gel plugs were destained for 15mins at RT in 100µl 50mM Ambic/50% ACN. Samples were spun down and destain liquid was discarded and replaced for a second wash (done as before). Samples were reduced using 200µl 10mM DTT (Fluka) in 100mM Ambic for 30mins at RT followed by alkylation using 200µl 55mM chloroacetamide in 100mM Ambic in the dark for 30mins. Dehydration was performed by addition of 100µl 100% ACN for 15mins. Before each of these steps the samples were spun rapidly and previous solution discarded.

Proteins were digested using 200µl of 0.2µg trypsin in 50mM Ambic per gel plug. Trypsin was added in twice, 100µl each time 1hr apart and left overnight. The following morning formic acid was added to a final concentration of 250mM and all supernatant was collected in a fresh LoBind Eppendorf tube. Samples were spun to dryness using a SpeedVac.

2.7.2 FASP

FASP columns (Vivicon 500, 10,000Da cut off columns from Satorius) were calibrated by spinning through 200µl 50% ACN/ 0.1%TFA, all centrifugation steps were performed for 30mins at 10,000 RPM. Immunoprecipitation eluate was loaded onto FASP columns and reduced using 200µl reducing buffer (8M Urea, 100mM TEAB, 10mM TCEP) for 30min before spinning. 200µl alkylation buffer (8M Murea, 100mM TEAB 20mM CAA) was added for 30mins in the dark then spun through. Samples were then washed twice with wash buffer (1M Urea, 50mM TEAB (pH8)). 1µg trypsin (Promega)/ 100µl Wash buffer is added for 1hr at 37ºC before an additional 0.5µg trypsin (Promega)/ 100µl wash buffer is added on top (no centrifugation performed between these steps). After an overnight incubation samples were switched to a fresh FASP tube, centrifuged and washed with first 200µl 0.1% TFA then 200µl 50% ACN/ 0.1% TFA. 10% of the eluate was put into a fresh LoBind Eppendorf and concentrated using a Thermo Scientific SpeedVac Concentrator centrifuge for proteome analysis.

2.7.3 Di-methyl labelling

Tryptic peptides were bound to SepPak reverse-phase C18 (Walters). Sep-Pak columns were washed 3x with 2ml ACN and 2x 2ml with Solvent A (0.6% [vol/vol] acetic acid). Samples were loaded onto separate Sep-Pak columns and washed with

2ml Solvent A. Columns were flushed with either heavy or light labelling reagent (4.5ml 50mM sodium phosphoate buffer pH7.5, 250µl 0.6M cyanoborohydride in water, 250µl of 4% [vol/vol] formaldehyde (CH_2O or CD_2O) 5 x 1 ml of respective labelling reagent with a maximal flow speed of 5ml/ 10mins (ie a drop every 6secs). Columns were washed 2x with Solvent A and eluted into a single LoBind Eppendorf tube with 500µl/ column Solvent B (0.6% [vol/vol] acetic acid and 80% [vol/vol] ACN).

2.7.4 Titanium dioxide enrichment

Titanium dioxide micro-spin columns (TopTip, Glygen) were spun at 200 RPM for 30sec to ensure tight packing of the columns. Column tips were stripped with 50µl elution buffer (5% Ammonia solution) and equilibrated with 3 x 65µl wash buffer (80% ACN/ 0.2% TFA), each centrifugation step was performed at 1000 RPM for 2mins. The sample to be enriched was diluted 1:1 using loading buffer (10% TFA/ 2M Glycolic acid/ 80% ACN). Samples were loaded 60µl at a time with spin speeds of 500 RPM/ 5mins. Following loading of sample columns were washed 2 x with 5% TFA/ 1M Glycolic acid/ 80% ACN, 2 x with wash buffer and 1 x with 20% ACN. All washes were performed at 1000 RPM for 2mins. Columns were spun at 2000 RPM to remove residual liquid and placed into a fresh LoBind Eppendorf tube containing 20µl 5% formic acid. Samples were washed 2x 10µl of elution buffer 750 RPM for 2mins. Samples were spun at 2000 RPM to collect residual buffer.

2.7.5 Online nano-LC and tandem mass spectrometry

Samples were resuspended in 50µl 5% DMSO/ 5% formic acid. 3µl of sample was loaded onto an LTQ-XL system to ensure no contamination of samples. Samples were loaded onto an EASY-nano-LC 1000 system (Proxeon). Peptides were loaded onto a trap column (75µm internal diameter guard column packed with Reprosil-Gold

120 C18, 3µm 120Å pores) using Solvent A (0.1% [vol/vol] formic acid in water) at 500bar. Separation was performed by an EASY-Spray column (50cm x 75µm ID, PepMap RSLC C18, 2µm; Thermo Fischer Scientific). Gradients used were 30mins (per phospho-peptide or in-gel sample) and 1hr (per kinetochore immunoprecipitation proteome sample). The gradient was a linear 8-30% [vol/vol] acetonitrile gradient at a flow rate of 200nl/ min. EASY-Spray nano-electrospray ion source was used to introduce peptides into a Q-exactive hybrid quadrupole-Orbitrap mass spectrometer (Thermo Fisher Scientific). Spectra were acquired with an m/z range of 350-1500. The 20 most abundant peaks were fragmented using CID.

2.7.6 Mass spectrometry processing

Data analysis was performed using MaxQuant. With mass tolerances for MS of 20ppm. Up to two missed cleavages were allowed. Oxidized-methionine and STY phosphorylation were searched for as variable modifications and carbamidomethyl cysteine as a fixed modification. Peptides were identified by searching MS/MS spectra against the *H. Sapiens* protein database. Samples were processed with and without matching between runs.

RawMeat was used to analyse the quality of tryptic digestions and the comparable chromatography between sample runs. Perceus was used to analyse the mass spectrometry data sets. Samples were filtered for contaminants and reverse peptides. Histogram and Pearson correlations were performed to compare repeats. Samples were grouped and t-tests performed to generate statistical significance values. Perceus was also used to generate the Pearson correlation and volcano plot visuals.

Table2.1 Antibodies used in this study

Target	Species	Supplier
Primary Antibodies		
Actin-HRP	Mouse	Abcam
Bub1	Mouse	Abcam
BubR1	Rabbit	Bethyl
Bub3	Rabbit	Abcam
CREST	Human	Millipore
CENP-A	Mouse	Abcam
Dsn1	Goat	Santa-Cruz
FLAG	Rabbit	Pierce
GFP	Sheep	Homemade
GST	Sheep	Homemade
Histone H3	Rabbit	Abcam
IgG pre-immune	Sheep	Homemade
Kinastrin	Sheep	Homemade
Knl1	Sheep	Homemade
Mad2	Rabbit	Cell signalling
Mis12	Sheep	Homemade
Myc	Mouse	Santa-Cruz
Mps1	Mouse	Millipore
Ndc80	Mouse	Genetex
Plk1	Goat	Santa-Cruz
Tubulin (DM1A)	Mouse	Abcam
Zwint	Rabbit	Bethyl

Target	Species	Supplier
Secondary Antibodies		
Donkey anti-sheep Alexa Fluors	Donkey	ImmunoResearch Laboratories
Donkey anti-mouse Alexa Fluors	Donkey	ImmunoResearch Laboratories
Donkey anti-rabbit Alexa Fluors	Donkey	ImmunoResearch Laboratories
Donkey anti-human Alexa Fluor 647	Donkey	ImmunoResearch Laboratories
Donkey anti-mouse HRP	Donkey	Jackson laboratories
Donkey anti-rabbit HRP	Donkey	Jackson laboratories
Donkey anti-sheep HRP	Donkey	Jackson laboratories

2.7.6.1 Production of phospho-specific antibodies

Phospho-specific antibodies for Astrin pSer157/pSer159 and pSer353 were raised against KLH-coupled phosphopeptides CMAETNSISLNGP and CKGVNTSVMLEN respectively. The antibodies had been affinity purified against the immunising peptide by a former postdoc in the lab, Dr Pelin Uluocak.

Chapter 3: Optimising kinetochore pull-downs for analysis of in vivo phosphorylation events

3.1 Introduction

During mitosis, the kinetochore acts as the central point in the surveillance mechanisms which allow mitosis to proceed in a coordinated and timely manner. In order to achieve this functionality the kinetochore is very dynamic. The addition and loss of post-translational modifications (PTMs) allows the kinetochore to be highly responsive to changes in state, making this mechanism an effective way of regulating mitosis. Transcriptional regulation would be less effective, as transcriptional activity in mitosis only occurs at a low level (Palozola et al. 2017).

The gain or loss of modifications can have a range of effects on its target leading to changes in a proteins localisation, conformation, activity or its ability to interact with other proteins (Cuijpers & Vertegaal 2018). There is a vast array of PTMs which have been categorised (over 600) ranging from protein cleavage events to the reversible additions of small chemical groups (Cuijpers & Vertegaal 2018). Phosphorylation is the PTM of choice for many signalling networks within the cell, owing to its versatility, chemical properties and its ability to be reversed easily (Hunter 2012). This makes it an effective choice for kinetochore regulation with many kinetochore components undergoing phospho-regulation (see **Introduction**).

A great deal of work has been done to elucidate the role at kinetochores of phosphorylation events. These studies generally fall into one of two categories: large-scale mass spectrometry (MS) based techniques designed to find changes in cells phospho-proteome under different conditions, or targeted approaches to investigate

individual or groups of phosphorylation and their specific effects. In 2003 the number of phospho-sites studied by the latter method was 2616, compared with just over 100 sites found using high-throughput methodologies like MS (Hornbeck et al. 2015). Since then, owing to technological advances, MS has far outstripped the classic low-throughput methods and now accounts for 95.5% of the large number of sites (more than 330, 000 sites) now collated by phosphositeplus (Hornbeck et al. 2015). Both methods have pros and cons. Low-throughput methods have the advantage of rigour with papers focusing on a few phospho-sites. These use a variety of methods including phospho-specific antibodies and site-directed mutagenesis in order to investigate biological consequences of the PTMs identified. High-throughput methods can identify thousands of novel sites with no prior knowledge required beforehand. However, the data does need to be assessed carefully; all sites found by MS based methods are probabilistic by nature and unless otherwise verified, must be assessed with a degree of caution. Understanding the methodology of MS is vital to assessing the quality of site assignments.

Both approaches have informed our understanding of the kinetochore, how it is regulated and which kinases are responsible for individual phosphorylation events. For some phospho-sites, their mechanisms of action is understood in detail. In contrast the majority of kinetochore phosphorylation sites identified have been as a result of a series of large-scale MS studies which observe but do not explain the biological mechanisms involved (**Figure 3.1**). Each of these studies had a different objective. They can be grouped into three broad categories (although there is some overlap):

- Looking for spindle-associated proteins
- Looking for kinases responsible for certain phosphorylation sites
- Looking at different cell cycle stages

Nousiainen et al. (2006) were the first to identify many kinetochore phosphorylation sites. Their study expanded on their group's previous proteome study (Sauer et al. 2005), isolating taxol-stabilised spindles and enriching for phospho-peptides using Fe^{3+}-IMAC. They found 312 phosphorylation sites on spindle proteins, 279 of which were novel. Included in these were approximately 100 phosphorylation events of kinetochore proteins. This was the first time a large-scale study of kinetochore phosphorylation sites had been carried out. Malik et al. (2009) built on this work, looking again at spindle associated-phosphorylation sites but adding in a temporal element. Using Noscapine releases they isolated roughly synchronised prometaphase, metaphase and post-metaphase populations which were each SILAC labelled and phospho-enriched using TiO_2 columns. They found many phosphorylation events (particularly Cdk1 phosphorylation events) are downregulated after metaphase. There was also a clear correlation with phospho-threonine residues being preferentially dephosphorylated compared with phospho-serines.

Two years after Nousiainen's work, Dephoure et al. (2008) produced a significant study; they used a lysate based approach to identify 14,000 phosphorylation events which occurred as cells enter mitosis, of which many were on kinetochore-associated proteins. As enrichment and MS methods develop, the depth and quality of data continues to improve. Olsen et al. (2010) expanded the Dephoure paper, finding 20, 443 unique phosphorylation events (60% of which had previously been identified by Dephoure). In addtion, Olsen also attempted to assign stochiometry to these sites based on the relative differences in SILAC labelling.

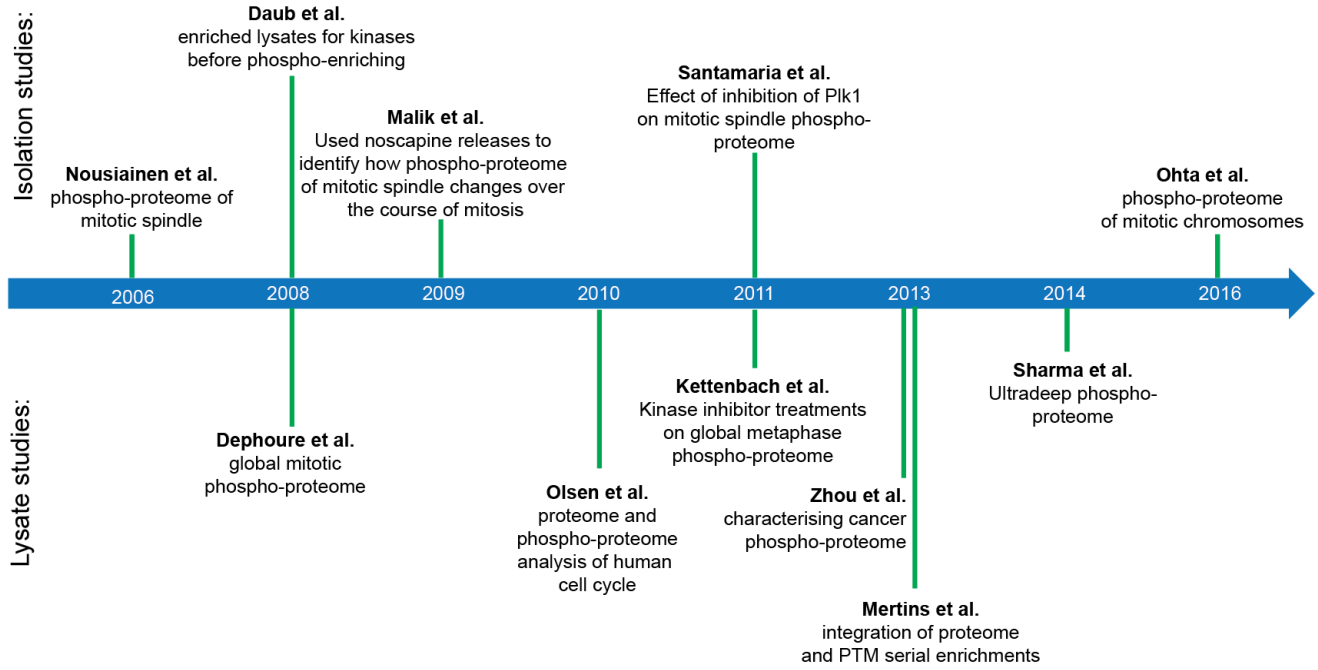


Figure 3.1 Timeline of MS studies which identify kinetochore-related phosphorylation events

Many groups have identified kinetochore or centromere phospho-proteins over the course of their work. This timeline provides an overview of how each study has improved on prior work. These studies been separated into those which used isolation techniques prior to MS (above the timeline) and those which have investigated the entire cellular phospho-proteome (those below the timeline). (Daub et al., 2008; Dephoure et al., 2008; Kettenbach et al., 2011; Malik et al., 2009; Nousiainen, Silljé, Sauer, Nigg, & Körner, 2006; Ohta, Kimura, Takagi, Toramoto, & Ishihama, 2016; Olsen et al., 2010; Santamaria et al., 2011; Sharma et al., 2014; Zhou et al., 2013; Mertins et al. 2013)

Kinase inhibitors have been used to try and assign phosphorylation sites to a kinase. Kettenbach et al. (2011) used small molecule inhibitors of Plk1, AurA and AurB to identify substrates of each kinases. Metaphase-arrested SILAC sample were treated with either MG132 or MG132+inhibitors and analysed after TiO_2 enrichment. The same year Santamaria et al. (2011) inhibited Plk1 and isolated the mitotic spindle. These types of approaches allow a greater understanding of the consensus sequences of kinases, an important tool in assessing novel un-assigned phosphorylation events and the role they may have.

However Kettenbach's paper (2011) highlighted the need for care in interpretation of MS data. They identified four phosphorylation sites on Ndc80; Thr31, Thr49/Ser50, Ser55 and Ser69. Of these Thr31 and Ser69 were identified in only one to two times out of the eight samples and the phosphorylation on Thr49/Ser50 the data is not good enough quality to identify conclusively which residue is phosphorylated.

They report Ndc80 as being phosphorylated solely by Aurora A. This does not concur with past literature which has previously shown several of these phosphorylation sites are dependent on Aurora B (DeLuca et al. 2006; Ciferri et al. 2008). However, a recent paper by Deluca et al. (2018), building on work done by Ye et al (2015), suggests that Aurora A acts on one Ndc80 site, phosphorylating pSer69 during metaphase. Aurora A and B have very similar primary sequences and relocalisation of Aurora A to the kinetochore is sufficient to act on Aurora B substrates (Fu et al. 2009; Hans et al. 2009). Indeed they do have similar consensus sequences with a requirement of downstream arginine and lysine residues (Kettenbach et al. 2011). These considerations emphasise the importance of rigorous examination of the MS data output, and ensuring conclusions are supported by further biochemical or biological experiments.

The overarching objective of these studies was the identification of novel phosphorylation events. However, it is somewhat difficult to amalgamate this data as

the studies were carried out using a variety of different approaches, methods and MS setups. Many kinetochore proteins have several distinct pools, for example members of the MCC associate with the kinetochore but also form the distinct MCC (Musacchio 2015; Chao et al. 2012). Studies which use a lysate-based approach, are unable to distinguish between differently modified pools of the same protein. Therefore caution must be taken in interpreting the role of the phosphorylation.

Many phosphorylation sites have previously been identified on kinetochore components. Our objective was to build on this work, creating a protocol which bridged the gap between these large-scale and small-scale targeted based approaches to phosphorylation events, and investigate whether, by specifically isolating the outer kinetochore we would be able to:

a) confirm the previously published results as a baseline for future work, which would then allow us to systematically perturb the system and investigate the changes in phosphorylation;
b) identify novel phosphorylation events whose functionality could then be investigated using conventional cellular and molecular approaches; and
c) make links between phosphorylation sites which had the same dynamics or were associated with the presence or absence of other proteins, possibly indicating that the phosphorylation sites were causing changes in protein binding

The generation of a more complete database would allow me to check the reproducibility of the previously published data, and act as a baseline for further investigation of how the phospho-status changes in response to systematic changes to the kinetochore.

3.1.1 Aims

- Optimise immunoprecipitation procedure for an efficient pull-down of the outer kinetochore
- Establish the MS based tools required to identify phosphorylation events
- Use this method to isolate the phospho-proteome of the outer kinetochore in a prometaphase-like state

3.2 Results

3.2.1 Isolating the outer kinetochore for MS analysis

Previous studies have isolated the outer kinetochore as a complex both in yeast and human cells (Welburn et al. 2010; Akiyoshi et al. 2010; Overlack et al. 2015). These studies used key KMN network components (Dsn1 and Knl1) to immunoprecipitate the outer kinetochore as an entity using tagged cell lines.

The long-term goal was to study how phosphorylation sites are established and removed as K-MT attachments are formed and stabilised. A compelling case for using Knl1 and Ndc80 as bait could be made; both these proteins make physical links to the microtubules and are known to be phospho-regulated. Owing to Knl1's size (over 2300 amino acids) creating a fully functional tagged protein has so far proved technically challenging; the advent of CRISPR promises to side-step those challenges.

Thus for the initial experiments antibodies against the endogenous proteins were used; a well characterised commercially available mouse monoclonal antibody (9G3) recognising amino acids 200-215 of Ndc80 (Chen et al. 1997; DeLuca et al. 2006) and a home-made sheep-anti-Knl1 antibody, raised against bacterially expressed Knl1 amino acid 728-1200.

HeLa S3 cells were arrested overnight, using either Nocodazole or STLC to create two different prometaphase populations. Nocodazole promotes microtubule depolymerisation, leading to the destruction of the bipolar spindle and creating a prometaphase-like state with all kinetochores unattached. STLC is an Eg5 inhibitor which prevents separation of the spindle poles, leading to a single microtubule organising centre (Skoufias et al. 2006). Microtubules polymerising from this single

point form a star-shaped spindle to which kinetochores can bind, creating monotelic attachments.

Immunoprecipitations of Ndc80 and Knl1 were performed using Ndc80 9G3 Mouse monoclonal antibody and Knl1 Sheep homemade polyclonal antibodies, with mCherry Mouse and pre-immune Sheep antibodies used as negative controls. Samples were western blotted for the presence of components of each of the KMN network subcomplexes (Knl1, Mis12 and Ndc80) (**Figure 3.2**). Interactors of Knl1 were also blotted for, with both immunoprecipitations capable of isolating Zwint and all of the Bub proteins. The more transient interaction of Mps1 with outer kinetochore proteins was not seen by western blot. This is consistent with past literature which has not reported interactions between endogenous Mps1 and outer kinetochore proteins, previous publications have instead used *in vitro* studies to identify Mps1's interaction with Hec1 (Ji et al. 2015; Hiruma et al. 2015).

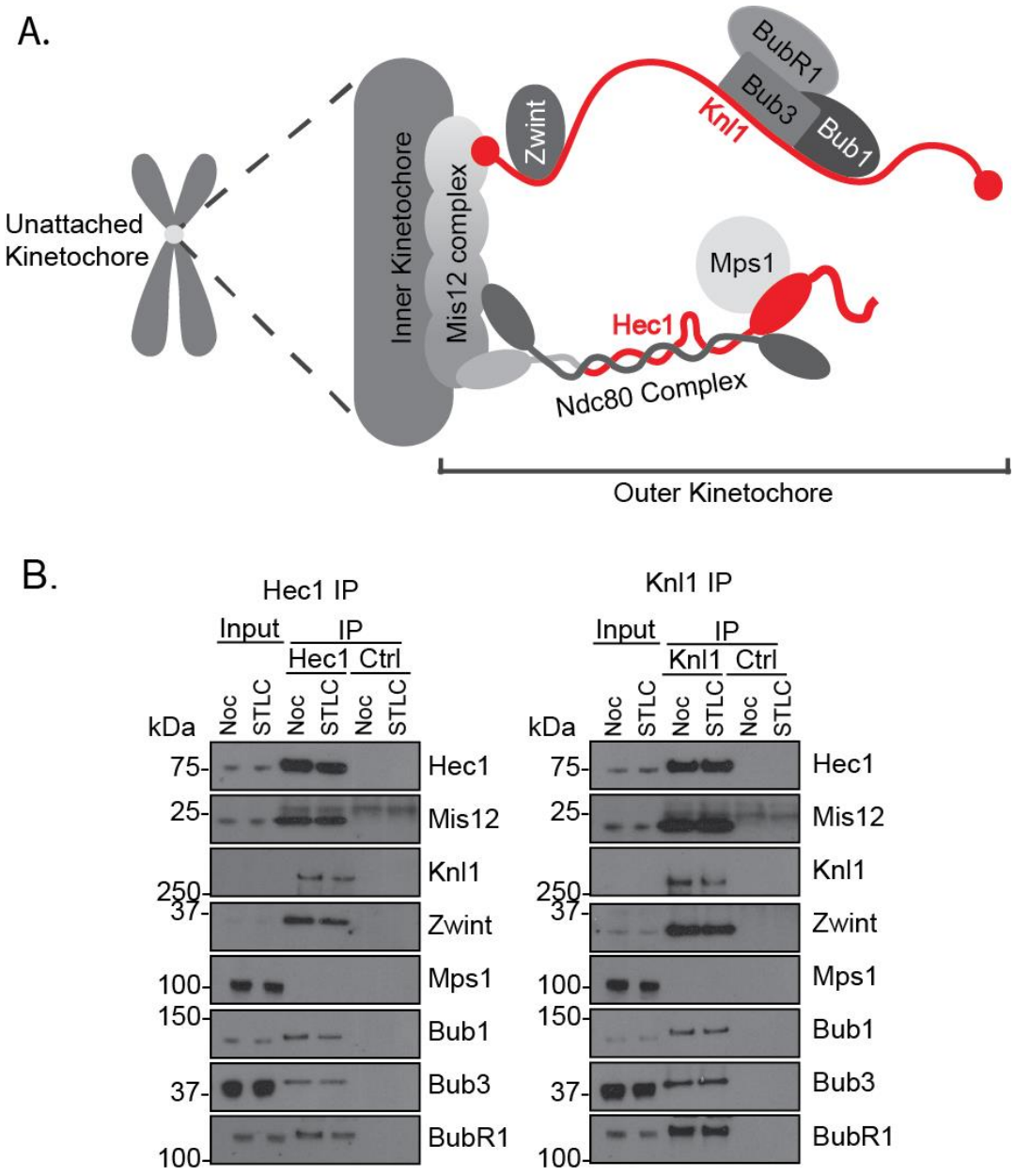


Figure 3.2 Both Ndc80 and Knl1 immunoprecipitations are capable of isolating the outer kinetochore

A) HeLa cells arrested in mitosis with nocodazole and STLC for 14 hrs were collected by mitotic shake-off. Ndc80 and Knl1 were immunoprecipitated (IP) with mouse Hec1 9G3.1 and homemade sheep Knl1 antibodies, anti-mCherry and pre-immune IgG used as negative controls in each case. Coprecipitating proteins were analysed by western blot.

3.2.2 Improving kinetochore release from chromatin during lysis

One of the great advantages of MS is its large dynamic range, allowing identification of transient or sub-stochiometric interactors of isolated complexes. To maximise the chances of isolating lesser interactors it is necessary to start the immunoprecipitation with a large amount of material. In the course of our immunoprecipitation procedure we clarified the lysate by centrifugation removing un-lysed cells, DNA and other particulates. Because the outer kinetochore is in complex with the inner kinetochore, which is bound to chromatin via CENPA, it is important to consider losses when pelleting the DNA (Musacchio & Desai 2017). **Figure 3.3A** demonstrates that in our initial lysis conditions only 50% of the outer kinetochore was released into the supernatant.

We investigated two different endo-nucleases, Benzonase and Micrococcal nuclease (MN) and assessed their ability to improve the release of the kinetochores. Both enzymes are commonly used endo-nucleases. The lysis buffer was tailored slightly with the inclusion of Ca^{2+} or Mg^{2+} ions (in the form of $CaCl_2$ or $MgCl_2$). Both enzymes work best at 37ºC. However, an experimental temperature of 4ºC was required.

HeLa samples were arrested overnight with Nocodazole and a mitotic shake-off was performed. Cells were lysed in lysis buffer with varying amounts of Benzonase and MN for 30 minutes at 4ºC. Samples were then clarified and the supernatant was separated from the pellet. Half the sample was denatured in Laemmli buffer for western blots to compare the release of Knl1 (**Figure 3.3A**). The remaining sample was taken for DNA extraction to analyse the endonuclease's efficiency (**Figure 3.3B**).

MN was chosen for further studies because it is capable of working with a low level of efficiency at 4ºC marginally increasing the release of kinetochores during lysis; in contrast Benzonase showed ug. Our data showed that addition of 50U of MN/ml was

sufficient to bias Knl1 release from 50% to nearer 80%. Longer lysate times or an increase in temperature could have been trialled, but there was a significant risk of an increase in dephosphorylation rate.

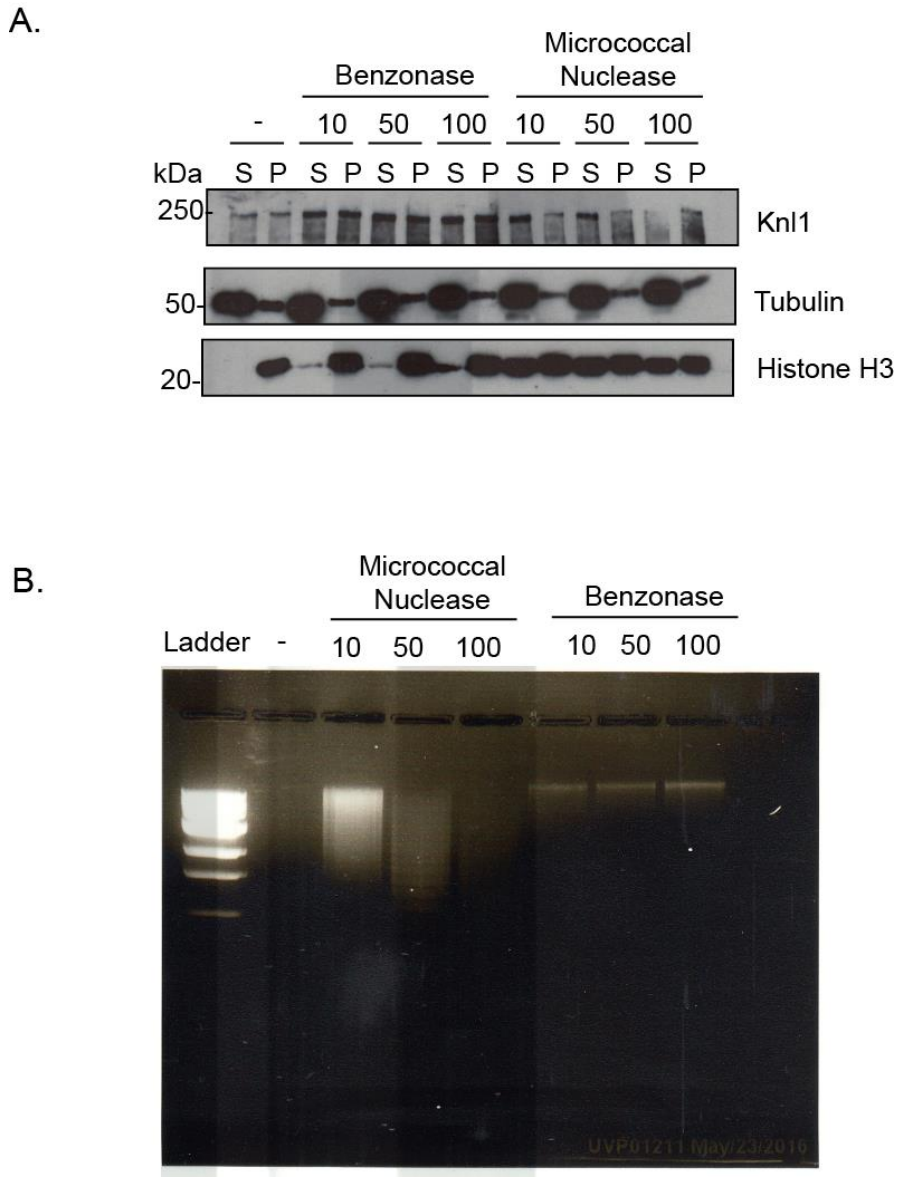


Figure 3.3 50U Micrococcal nuclease enhances kinetochore release

A) HeLa cells arrested in mitosis with Nocodazole for 14hrs were collected by mitotic shake-off. Cells were lysed for 30mins at 4ºC in the presence of varying levels of Benzonase and Micrococcal Nuclease (10U, 50U and 100U per millilitre of lysis buffer) or with no inhibitor (-). Samples were western blotted for Knl1, Tubulin and Histone H3. B) DNA was extracted via phenol extraction and 1µg was run on 2% agarose gel to compare the state of DNA Digestion. Two independent repeats were performed, data shown depicts representative images.

3.2.3 MS Analysis of in-gel Knl1 IP

HeLa S3 cells were grown to 60% confluency and arrested overnight in Nocodazole. A 5mg Knl1 immunoprecipitation was performed and eluted using Laemmli buffer containing 3% SDS. The efficiency of the immunoprecipitation was assessed by western blot to confirm that Kn1 and Ndc80 had been pulled down (**Figure 3.4B**). Owing to the low levels of Knl1 in the cell lysate and its size, it was not possible, to see Knl1 in the input despite loading 30µg in the input. However, this does emphasis the level of enrichment which was achieved in the immunoprecipitation.

The sample was processed for MS using in-gel digestion. The gel was sectioned so as to avoid the IgG bands, and individual segments were diced (**Figure 3.4A**). Samples were then de-stained and disulphide bonds irreversibly reduced using a two-step process of reduction and alkylation. 0.2µg of Trypsin per sample was added to cleave proteins into short peptides which can be easily identified by mass spectrometry (**Figure 3.4C**). Each segment was run on a 30 minute gradient on a QEX machine.

The quality of digestion was analysed by an analysis package RawMeat (developed by vastscientific), which allows analysis of the charge state of the peptides. Complete digestion of a protein with Trypsin should typically yield peptides carrying a 2+ charge at the C-terminal tryptic cleavage site of an Arg/Lys amino acid and the N-terminus. Samples with a large fraction of highly positive peptides would suggest incomplete digestion by Trypsin. **Figure 3.5A** shows the Trypsin digestion was inefficient, with a high number of 4+ and higher charged peptides identifying multiple missed cleavages. If peptides are too long they would not be eluted successfully from the C18 column of the liquid chromatography system. Therefore they would be missed by MS leading to poor protein sequence coverage. In order to prevent such poor digestion again and

increase reproducibility fresh sequencing grade Trypsin was bought from Promega (Burkhart et al. 2012).

The MS data show large difference in intensities and number of peptides between Knl1 and the other interactors, with Knl1 being 10-100 fold more abundant (**Figure 3.5B-C**). This difference is not nearly as marked when looking at sequence coverage, as Knl1 is the largest kinetochore component, and several peptides can cover the same region. One of the key reasons to run this experiment was to investigate whether we were isolating the entire kinetochore or only a subsection of it. The results indicate that each sub-complex of the KMN network was successfully isolated along with some direct interactors of Knl1. No inner-centromere proteins or other kinetochore proteins such as Mad1, Mad2 or RZZ components were seen. The results agree with the western blot data in **Figure 3.2B i**n that the same components were seen.

As the protocol suggested, the gel bands containing the IgG used for the immunprecipitation were excluded from the analysis to prevent them being the dominant protein, and wasting MS run time on sequencing IgG peptides. However, this severely affected the number of KMN network components we were able to see. Mis12, Pmf1, Spc24 and Spc25 all have molecular weights of about 25kDa (24, 23, 22 and 26kDa respectively), similar to the light chain, whilst Nuf2 runs at the height of the heavy chain with a molecular weight of 54kDa. It would be logical to conclude that these components were present but not processed for MS, because Ndc80, the most distant component of the KMN network was seen. This strongly suggests that the more proximal proteins, Spc24 and 25, must have been present.

Because an abundant protein will be sequenced in preference to those which are less plentiful in an MS analysis it is important for the protein of interest to be the dominant component in the sample with low levels of contaminating proteins. With in-gel digestion the risk of contaminants is high, owing to the amount of sample handling. This is compounded by the extraction of in-gel proteins being relatively inefficient.

Reports estimate losses between 15-50% (Granvogl et al. 2007). As the gel bands are diced, the risk of contamination is high and the yield of the true interactors can be poor.

In these samples Knl1 was only the second most abundant protein, behind Keratin (Krt1) which was a magnitude higher, with an average intensity of 4.5E11 per sample compared to 2.4E10 for Knl1. Some negative impact on the number of peptides of true interactors sequenced is possible for these reasons, but was considered unlikely to be a limiting factor to identifying proteins. As each gel band was run on a 30 minute gradient, the samples were individually relatively simple, and using the liquid chromatography column there was sufficient separation to ensure sequencing of all peptides present.

Overall this experiment made clear the need for further optimisation:

a) the tryptic digestion was relatively poor
b) we were unable to identify 5 out of 9 KMN network components
c) those we were able to identify had relatively low peptide numbers and sequence coverage which would be likely to severely impact our chances of seeing many phospho-peptides
d) the run time was long and expensive. A new methodology had to be considered in order to make more effective use of the research budget.

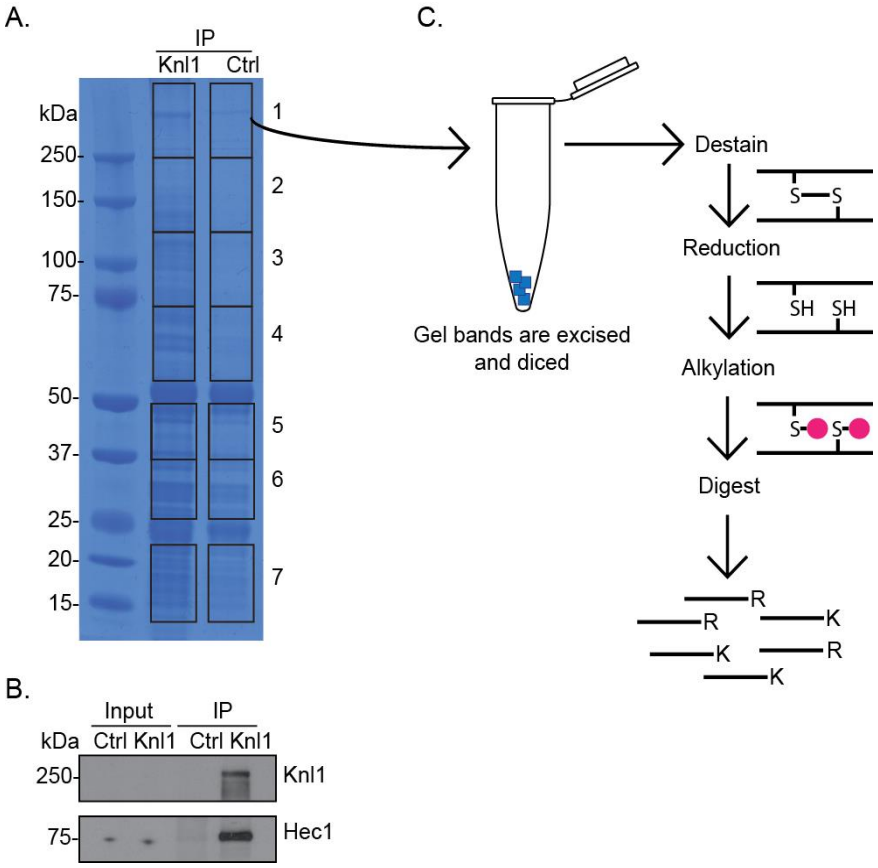
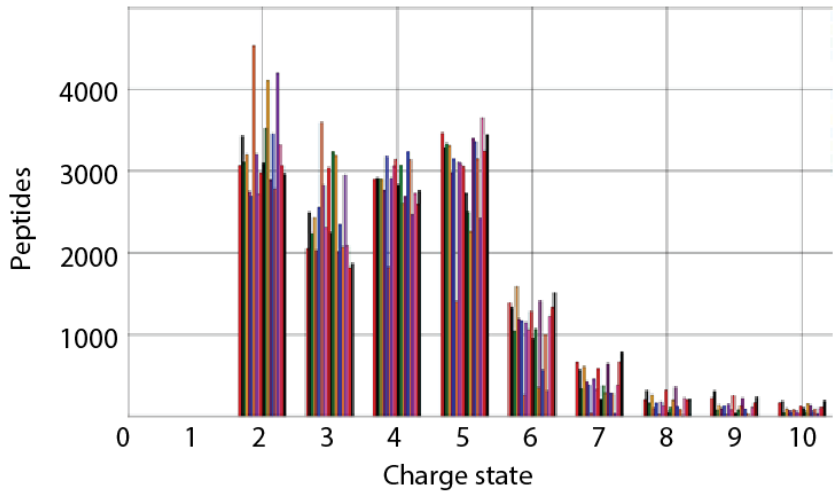


Figure 3.4: In-gel processing of Knl1 immunoprecipitation for mass spectrometry analysis

A) HeLa cells were arrested in mitosis for 14hrs using Nocodazole. A 5mg Knl1 immunoprecipitation was performed using homemade sheep Knl1 antibody, the sheep pre-immune antibody was used as a negative control. Samples were eluted using lammeli buffer with 3% SDS. 90% of the immunoprecipitation was run on a coomassie gel. The gel was sectioned in order to avoid the heavy and light chain bands. B) Western blots on the remaining 10% of immunoprecipitation confirmed the Knl1 immunoprecipitation had been successful in isolating Knl1 and analysed for Ndc80. C) Schematic showing the in-gel digestion procedure to prepare samples for MS. Gel bands are diced and destained before peptides are reduced and alkylated to destroy and prevent reformation of di-sulphide bridges. Gel bands were then digested with 0.2µg of Trypsin per sample.

A.



B.

Protein	Intensity	Peptide number	Sequence coverage (%)
NDC80	1.05E+08	3	7.35
BUB1	5.32E+08	5	10.25
BUB3	8.18E+08	8.5	31.7
BUBR1	1.24E+09	12.5	20.85
ZWINT	2.8E+08	5.5	24.9
KNL1	4.92E+10	135.5	64.95
NSL1	1.8E+08	3.5	16
DSN1	2.82E+08	6	20.65

C.

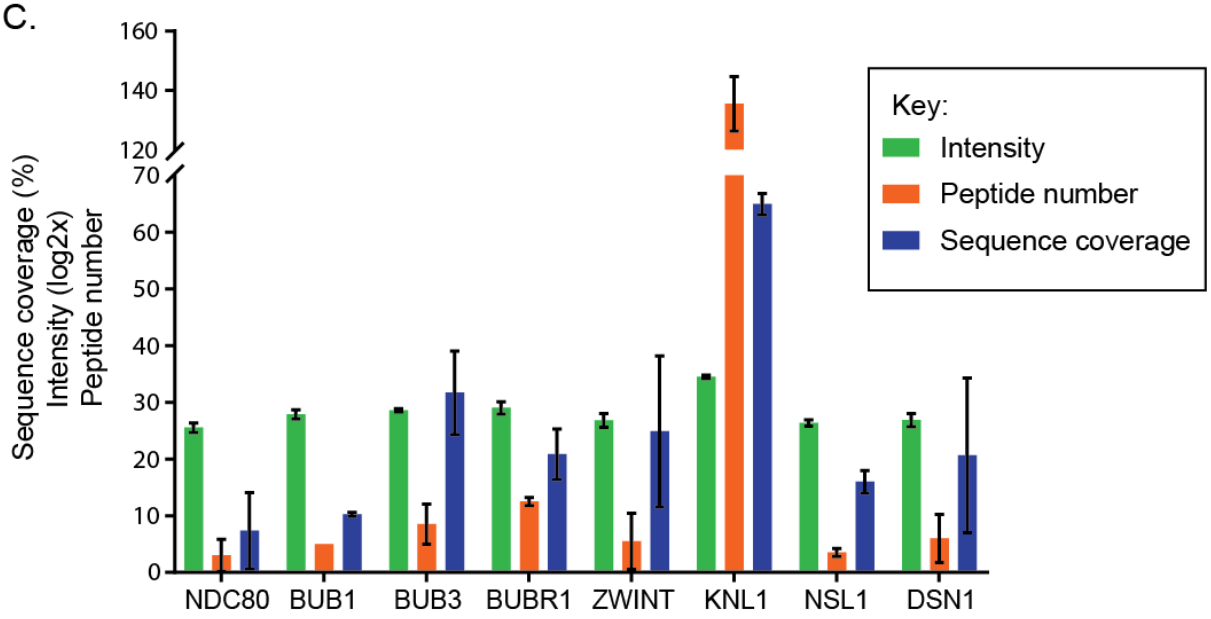


Figure 3.5 In-gel digestion of Knl1 immunoprecipitation is capable of isolating most direct interaction partners

A) Each gel band was run on a 30 minute gradient on a LC-QEX Mass spectrometry machine. Their peptide charge status was analysed via the RawMeat software package. Graph represents the distribution of peptide charge states, with peptide number on the y-axis and charge state on the x-axis. Each colour represents a gel band from either the control or Knl1 IP.and shows all have the same pattern with a high level of 4+ and 5+ charge states B) MS analysis shows the data output from all Knl1 IP gel bands which were combined in silico via the MaxQuant software package. The table shows the data available for all kinetochore proteins identified. C) Graphical representation of data in B (with standard error generated from two independent experiments).

3.2.4 Adapting to an in-solution method

Sample processing can be approached either using an in-gel or an in-solution methodology. As a potentially more effective approach we investigated using an in-solution system. Compared with in-gel, in-solution is simpler with lower sample loss and lower protein contamination risk from keratins as there is less sample handling involved. However contaminants such as detergents, lipids and genomic DNA would still need to be removed. Detergents can prevent enzymatic digestion, and also irreversibly damage chromatography columns. Other contaminants can interfere with the liquid chromatography systems effectively damping the signal and reducing the clarity of the spectrum and thus making the protein identification more tricky (Feist &

Hummon 2015). Historically this required protein precipitation and re-dissolving steps to be incorporated, which causes loss of material.

The invention of FASP (Filter-Aided Sample Preparation) has markedly improved on previous in-solution methods (Manza et al. 2005; Wiśniewski et al. 2009). FASP utilises a molecular weight cut-off filter system. Ultra-centrifugation is used to remove low-molecular weight components and detergents from samples; the proteins remain bound to the membrane. The cut-off used can either be 3kDa or 10kDa, although these numbers refer to folded protein size as opposed to denatured proteins. The same steps of reduction, acetylation and digestion are followed, each buffer is removed by ultracentrifugation. Following enzymatic digestion, the peptides are small enough to pass through the filter and are thus eluted, leaving behind any high-molecular weight contaminants, including any contaminating DNA. Estimates of sample loss in FASP have varied in different reports (Liebler & Ham 2009; Wiśniewski et al. 2009). However, this elegant protocol has been demonstrated to outperform both in-gel and previous in-solution digestion techniques (Feist & Hummon 2015).

Although the sample remains on a single filter, (in order to reduce losses) it can be time-consuming to remove detergents. A sample initially containing 3% SDS may need more than fifteen 30 minute washes to remove it, extending the protocol by a day. In an effort to shorten the timeline, different immunoprecipitation elution buffers which were compatible with MS were investigated. Both a pH2.6 Glycine elution and an 8M Urea elution was tested for their ability to elute Knl1 from Protein-G Dynabeads. Three sequential elutions were performed, and fractions run on western blots to assess their success (**Figure 3.6A**). Although both methods were capable of releasing some Knl1, the release was incomplete. We also noticed that the glycine elutions produced diminishing results in the second and third collection.

We decided to combine elution methods so that when all possible material had been eluted in a glycine-dependent manner, the urea elution might elute the remainder. Following rounds of optimisation the final protocol had numerous changes;

a) the volume of glycine and urea used was doubled
b) rather than being left to incubate on the laboratory bench, samples were vigorously agitated
c) elution time was extended, to 10 minutes per glycine elution and 30 minutes per urea elution

This improved protocol proved highly efficient with the majority of Knl1 and Ndc80 immunoprecipitations being eluted with very little material being seen in the after-elution fraction (**Figure 3.6B-C**). Indeed only using very long western blot exposures was it possible to see Knl1 in the after-elution fraction and in lanes other than Glycine elution 1 (**Figure 3.6B**).

It is common for a fractionation step to follow in-solution digestion. Samples are more complex than those resulting from in-gel digestion which are often separated into multiple gel plugs. After consideration, we decided fractionation should be unnecessary as our immunoprecipitation procedure should act as a separation technique; it should give a relatively simple sample (by MS standards) which would be sufficiently separated using the high-performance liquid chromatography. This was backed up by our initial experiments which identified only 393 proteins in the entire repeated experiment. This is well within the mass spectrometer's capacity to analyse in a single hour. This allows us to run an immunoprecipitation sample on an hour gradient. By cutting the running costs down to about £70 per sample, compared with £500 per sample for the earlier in-gel samples, the chosen protocol allowed much more efficient use of resources, and capacity to run significantly more tests in this investigation.

In order to test our Glycine/Urea elution and the FASP protocol a Knl1 immunoprecipitation was performed using the same immunoprecipitation protocol as in **Section 3.2.3**. The immunoprecipitation efficiency was checked using western blots and samples were processed for MS using FASP, 1.5µg of Trypsin were used for digestion. Samples were run on a one hour gradient on a QEX machine. RawMeat showed the tryptic digestion was far more successful (**Figure 3.7A**). Analysis of this experiment revealed all KMN network components were identified in this experiment. The peptide number and sequence coverage was better in all cases except Knl1, Bub1 and Zwint. The experiment also yielded a number of other interactors at low levels such as CENPC1.

This represents a major step forward in terms of data yield and so all subsequent experiments used the FASP protocol.

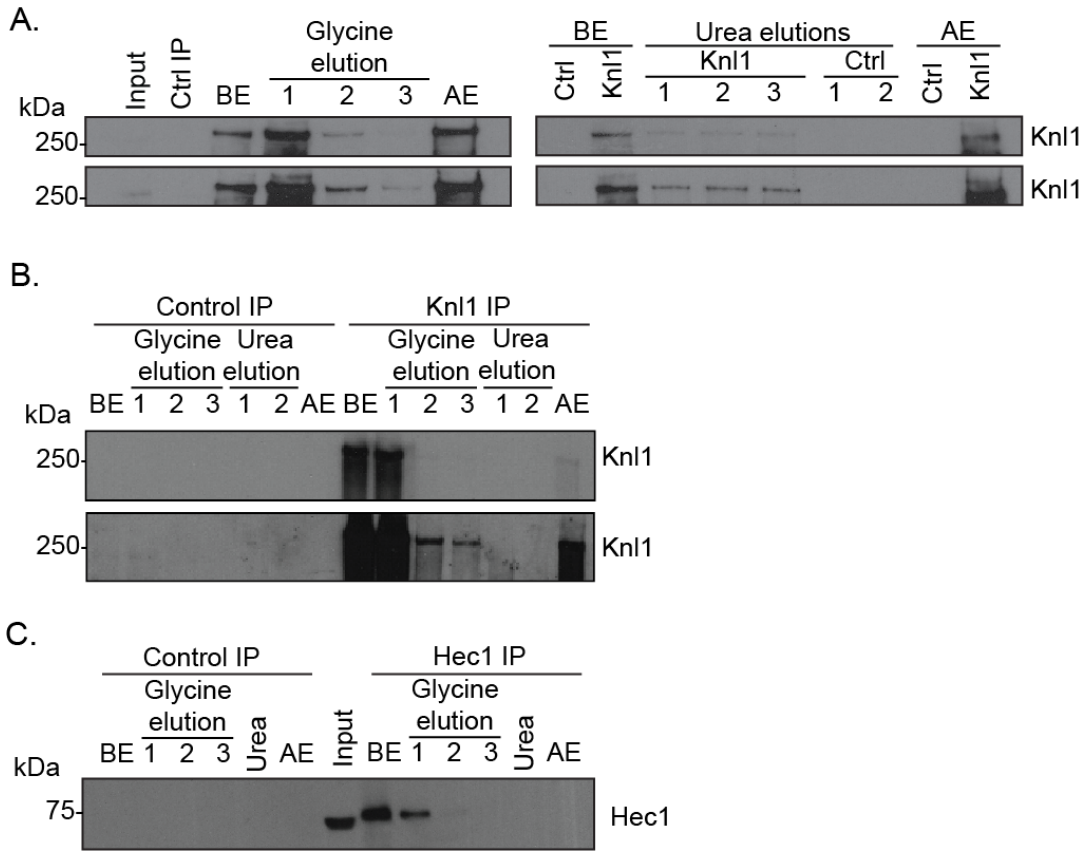
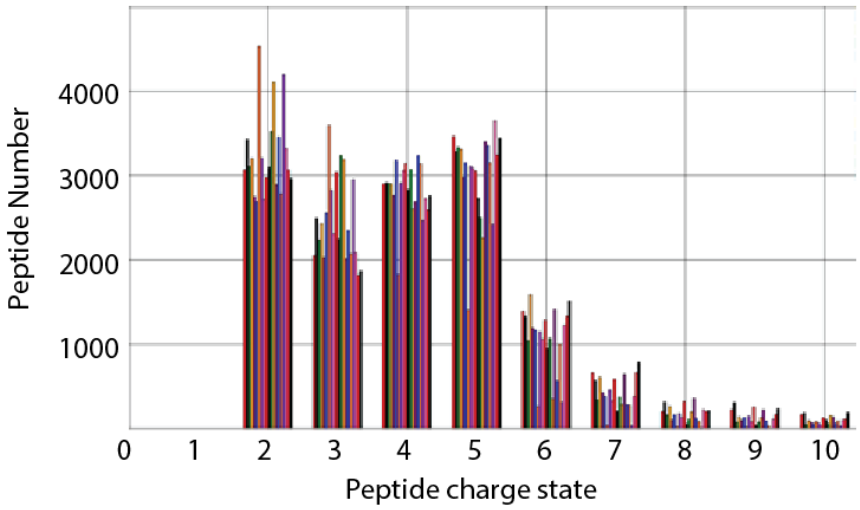


Figure 3.6: Combining Glycine and Urea elution steps allow efficient release

A) HeLa cells were arrested in mitosis using Nocodazole for 14hrs and a 2mg Knl1 IP was performed in duplicate. 10% of beads were taken and boiled with lammeli buffer as a before-elution fraction (BE). Samples were then either eluted by Glycine or Urea. In the case of Glycine, Protein-G Dynabead Knl1 IP's were mixed with 50µl 0.2M pH2.6 Glycine for 5 minutes three times. For Urea Protein-G Dynabead Knl1 IP's were mixed with 50µl 8M Urea for 30 minutes three times. Post-elution 5ul of beads were taken and boiled with lammeli buffer as an after-elution fraction (AE). Western blots were run and immunoblotted for Knl1 to compare the success of each elution method. B) Subsequent optimisation showed by increasing the volume of Glycine or Urea from 50ul to 100ul; doubling washing time; incorporating shaking and combining both elution methods together gave a highly efficiency release for both Knl1 and C) Ndc80 immunoprecipitiations. BE= Before elution, AE= After elution

A.



B.

Protein	Intensity	Peptide number	Sequence coverage (%)
NDC80	1.05E+08	3	7.35
BUB1	5.32E+08	5	10.25
BUB3	8.18E+08	8.5	31.7
BUBR1	1.24E+09	12.5	20.85
ZWINT	2.8E+08	5.5	24.9
KNL1	4.92E+10	135.5	64.95
NSL1	1.8E+08	3.5	16
DSN1	2.82E+08	6	20.65

C.

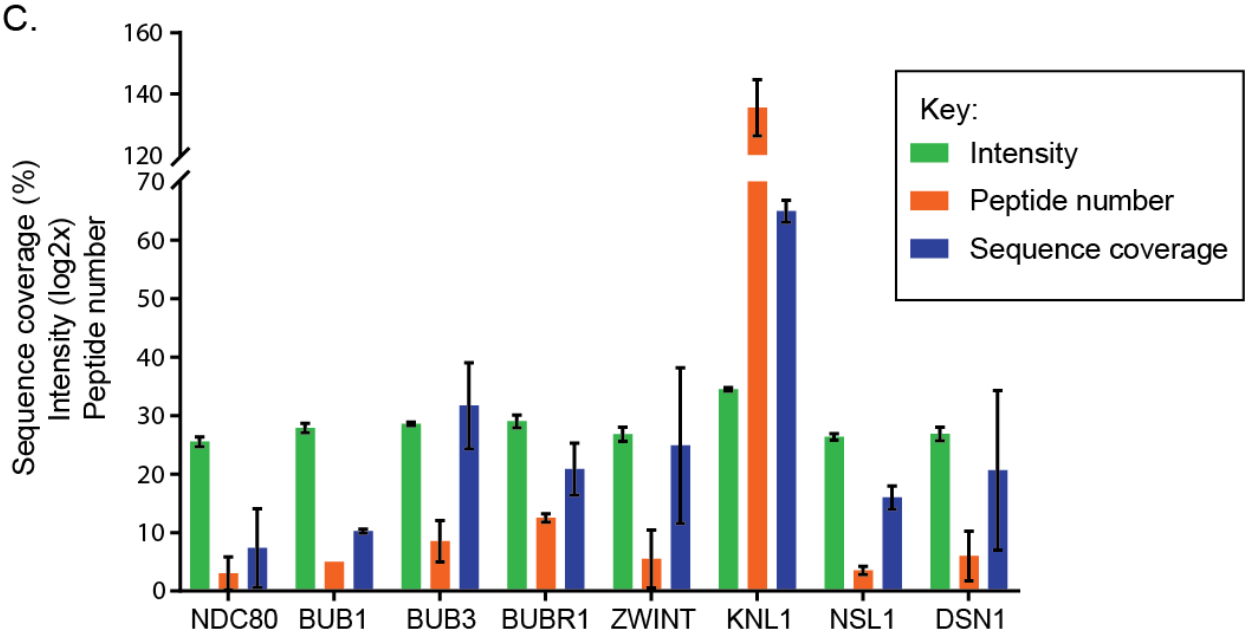


Figure 3.7 Comparatively FASP represents an improvement over in-gel digestion

A) HeLa cells were arrested in mitosis using Nocodazole for 14hrs and a 4mg Knl1 IP was performed and processed using glycine-urea elution followed by FASP. Each IP sample was run on a 1hr gradient on a LC-QEX Mass spectrometry machine. Their peptide charge status was analysed via the RawMeat software package. Graph represents the distribution of peptide charge states, with peptide number on the y-axis and peptide charge state on the x-axis. Each colour represents a FASP sample from either the control (red) or Knl1 IP (black) and shows samples were well digested. B) Data from FASP experiment shows the protein intensities and sequence coverage for kinetochore proteins. C) and D) compares this data with that generated by in-gel digestion. Samples are compared for both their C) peptide number and their D) sequence coverage.

3.2.5 Introducing a phospho-enrichment step

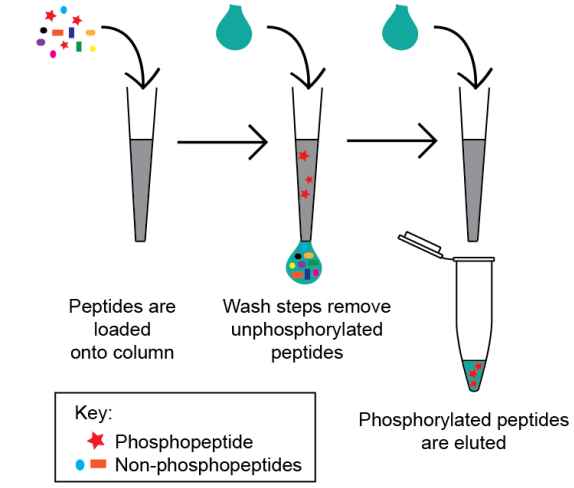
The phospho-data generated by both the in-gel and FASP experiments were extremely limited. Only 9 and 7 kinetochore sites were seen respectively in the entire series of experiments. This is not an unexpected result, because the presence of unphosphorylated peptides can suppress the signal of phospho-peptides, and specific phosphorylation events can be substochiometric - occupancy levels can vary widely from less than 1% to over 90% (Macek et al. 2009).

In order to identify phospho-sites by MS efficiently, an enrichment step is required. There are two main enrichment methods used were IMAC (Immobilized Metal Affinity Chromatography), developed by Andersson & Porath (1986) and Titanium Dioxide (TiO_2) enrichment, developed by Pinkse et al. (2004). Both use the same principle; an immobilised metal ion coordinating phosphate groups with high-affinity. Whilst IMAC

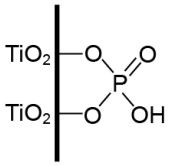
columns are relatively expensive, TiO_2 enrichment is simple and less expensive with disposable titanium dioxide columns available. A comparison of the two methods abilities to isolate phospho-peptides revealed similar levels of enrichment although IMAC was better at identifying multi-phospho-peptides (Yue et al. 2016). IMAC had a lower affinity for phospho-peptides, and therefore requires more bead volume, leading to a need for more sample volume and a lower throughput. This was considered to be a drawback. Given our inclusion of a preceding immunoprecipitation protocol, material is limited (compared with a lysate approach), therefore this is a significant draw back. The columns are also more costly. Therefore TiO_2 was chosen as the enrichment strategy.

Both Ndc80 and Knl1 immunoprecipitations were run with and without enrichment and the total number of phosphorylation events along with the number of kinetochore-related phosphorylation events was identified. This showed that the use of enrichment had a significant impact on the success of identifications (**Figure 3.8C-D**).

A.



B.



C.

	Control IP				Kinetochore IP			
	Proteome		TiO2 enriched		Proteome		TiO2 enriched	
	Hec1	Knl1	Hec1	Knl1	Hec1	Knl1	Hec1	Knl1
Total phosphorylations	6	52	50	113	66	100	455	602
Kinetochore-associated phosphorylations	0	1	1	5	11	8	56	94

D.

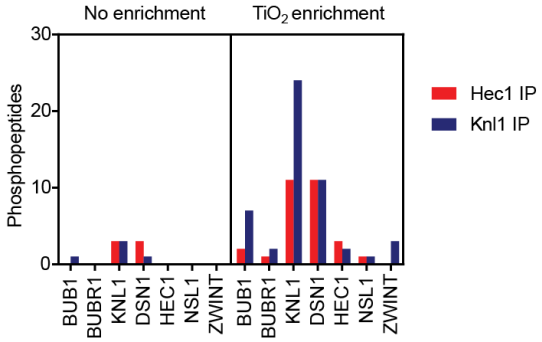


Figure 3.8: An enrichment strategy creates a large increase in kinetochore-related phospho-site

A) Schematic of titanium dioxide enrichment strategy. Phospho-peptides bind with high affinity to the column whilst unphosphorylated peptides are washed through and thus depleted from the sample. B) Shows how the phosphorylation coordinate with the bidentate ion. C) Table of Knl1 and Hec1 IPs prepared by FASP compare between pre and post- enrichment stages. D) Data from C) shown graphically

3.2.6 Determining whether a labelling strategy was advantageous

This section considers whether there is a case for labelling, what type of labelling could be used, and reviews the evidence for different options.

Samples can be labelled prior to MS and then combined and run simultaneously on the mass spectrometer. The intensity of signal will be directly proportional to their concentration in each sample. Therefore labelled samples can be directly compared and quantitative data generated (Macek et al. 2009). The chemical and physical properties of the tags must be identical so they do not affect the ionisation efficiency but are different in some way observable by MS.

There are two main ways of labelling; metabolic labelling or chemical labelling. Metabolic labelling relies on culturing cells in medium, with either light or heavy stable isotopes. Owing to their difference in mass there will be distinct m/z peaks in the mass spectrometer. Of the methods developed the most commonly used is SILAC (stable isotope labelling by amino acids in cell culture) developed by the Mann group (Ong et al. 2002). By labelling prior to any other processes, errors which can be introduced by performing procedures in parallel are minimised. Chemical labelling on the other hand is performed at either the protein or peptide level. It can be applied to a wider variety of samples, for example, where culturing cells is not possible, and allows multiplexing of tags rather than single side-by-side comparisons. Two methods are iTRAQ (Wiese et al. 2007) or Di-methyl labelling (Boersema et al. 2009). Di-methyl labelling was chosen because it is easy to use and reagents and expertise were available the department.

Together with Davinderpreet Mangat in the lab, we tested the relative benefits of an experiments with and without labelling. An Mps1 immunoprecipitation was performed (by Davinderpreet Mangat) with and without a 2μM AZ3146 (an inhibitor of Mps1) in

the presence of MG132 (to prevent anaphase onset) to create conditions which mimic a SAC on and SAC off checkpoint. These samples were processed by FASP and then were either di-methyl labelled (according to protocol of Boersema et al., 2009) or left unlabelled prior, to both being TiO_2 enrichment.

A direct comparison of dimethyl labelled and non-labelled experiments showed 19 and 41 Mps1 phosphorylation sites respectively. Three criteria were used for filtering the data set; on the basis of a localisation score of over 75%; a MaxQuant score of over 50 and a measurable intensity reading in at least one sample. Following filtering the number of phospho-sites seen by di-methyl labelling was 12 compared to 36 in the unlabelled samples.

The negative impact of di-methyl labelling appeared to be the result of sample loss. With every processing step protein is lost, particularly likely in low concentration samples where proteins are more likely to adsorb to surfaces. The immunoprecipitation protocol limits the amount of starting material. For every increase in the number of MS procedures, there are associated losses from additional handling steps and more time for adsorption to occur. Our data shows the di-methyl labelling step had a negative impact on phospho-peptide retention and identification. It was concluded the costs outweighed the benefits.

Published work has reported that good results could be achieved without labelling. As label-free methods have improved, the relative benefit may be small. Patel et al. (2009) actually reported that a label-free methodology outperformed iTRAQ in terms of proteins identified an sequence coverage, even with a 10^{th} of the MS running time. Both label-free and iTRAQ methods generated relative quantification data sets which were well correlated with each other. Montoya et al. (2011) performed a label-free TiO_2 experiment and showed over 90% of phospho-peptides could be quantified with accuracy derivation of less than 30% once outliers were removed and robust normalisation strategies applied. This result seemed compatible with our experimental

set-up as we are primarily interested in phosphorylation sites which show dramatic changes between states.

As a result it was decided that the case for labelling was not strong, and similarly good quality data should be achieved without it.

3.2.7 Digestion by multiple enzymes increases phospho-peptide identifications

Although the inclusion of a phospho-peptide enrichment step had a considerable impact on the number of phosphorylation events seen, the number of sites on Ndc80 was somewhat disappointing. Ndc80 has been intensively studied and numerous sites on the N-terminal tail have been implicated in regulating k-MT attachment. Several studies put forward evidence of many Aurora B phosphorylation sites which, acting together, disrupt Ndc80's ability to create electrostatic interactions with microtubules (DeLuca et al. 2011; DeLuca et al. 2006; Ciferri et al. 2008; Guimaraes et al. 2008). Much of this work was done using a 9A-Ndc80 phospho-mimetic mutant based on the work of Ciferri et al. (2008) and DeLuca et al (2010). Ciferri et al. (2008) identified Ser5, Ser8, Ser15, Ser44, Thr49, Ser55, Ser62 and Ser69 as Aurora B phospho-sites, as well as Ser4, which they were unable to assigned categorically to Aurora B. We only saw four phospho-sites on Ndc80 of which only one was in the N-terminal tail, Ser69 (the other sites we identified were S76, S616 and S620). Ser69 is one of the most commonly identified site on Ndc80 within the literature (Hornbeck et al. 2015).

Disappointingly, our protocol was thus unable to identify well established phosphorylation sites on one of the most intensively studied phospho-regulated kinetochore proteins. We judged good coverage of the N-terminal region of Ndc80 a prerequisite to a successful MS based K-MT attachment study. We wondered if our

methodology was precluding us identifying other phosphorylation sites on Ndc80. Possible explanations we considered were:

a) That our method was less able to maintain phosphorylation status over the course of cell-collection and the immunoprecipitation
b) That some bias introduced by the processing for MS, such as;
    i. Under-digestion by Trypsin
    ii. Triptic digestion leading to peptides which are inappropriate for MS
    iii. Poor MS responses or inadequate fragmentation of peptides.

Trypsin is the most commonly used enzyme because it cleaves highly specifically at lysine and arginine residues creating a C-terminal basic residue which aids sequencing using CID fragmentation (Sakurai et al. 1999; Huang et al. 2005). So, the size of tryptic peptides is based on:

a) whether Trypsin is acting with maximal efficiency, cleaving at every lysine and arginine in the amino acid sequence and
b) the number of lysine and arginine residues within the sequence and their proximity to each other.

Peptides have to have certain properties to be successfully injected into a MS machine. They have to be capable of binding to, and being eluted from, the liquid chromatography C18 column, and have an m/z of 300-1500 for electrospray ionisation to be efficient.

Although peptides differ in terms of their ability to bind the C18, or be ionised based on chemical make-up, the chances of a peptide being sequenced by the mass spectrometer drops if it is shorter than 8aa or longer than 22aa. Using $8 \leq n \leq 22$ as a working bounds, I investigated what was the best sequence coverage achievable using Trypsin (**Figure 3.9A**) and compared it to our experimental data. This showed that on average Kn1 and Ndc80 complex components were 13% lower than *in silico*

and components of the Mis12 complex were 33% lower than *in silico*. Analysis of the charge state of the peptides present shows the efficiency of tryptic digestion.

During the course of the *in silico* analysis it was noted that the nature of the peptides derived from the N-terminus of Ndc80 was negatively affected by the triptic digestion. Owing to the large number of lysines, and arginines in this domain of the protein, Trypsin digestion results in the shredding of the N-terminal tail to peptides too small to be sequenced (**Figure 3.9B**). In order to get better coverage of this underrepresented region other potential proteolytic enzymes were investigated (Gupta et al. 2010; Mohammed et al. 2007). Few have the properties required: highly-specific, capable of generating generate peptides of the right length for mass spectrometry, covering regions underrepresented by Trypsin (specifically the Ndc80 N-terminus). Using the same *in silico* digestion approach, we found V8/GluC was most compatible with these criteria. V8 cleaves at the C-terminus of aspartic or glutamic acid residues. The enzyme can be biased so it preferentially cleaves glutamic acid residues using ammonium acetate, pH4, in the reaction buffer. When V8/GluC was analysed *in silico* alongside Trypsin it generated slightly lower coverage of the KMN complex but in combination with Trypsin it showed increased overall coverage (**Figure 3.9C**). Mohammed et al. (2007) found in a multi-protease study, that V8 showed the highest number of phospho-peptides out of the proteases tested.

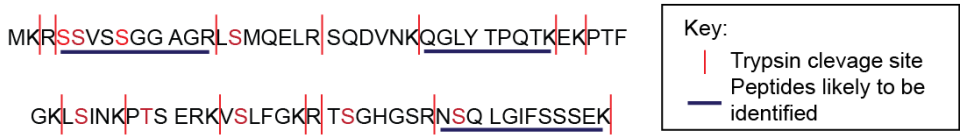
Based on this evidence we decided to test V8 alongside trypsin. An Ndc80 immunoprecipitation was performed in duplicate. One sample was digested with V8 and the other with trypsin; the only differences in protocol were the wash steps and digestion steps of the FASP. V8 has less than 3% activity in 2M Urea so samples were washed twice in 25mM ammonium acetate to remove residual urea. For digestion, 1.5 µg of V8 suspended in 25mM ammonium acetate was used. 1.5 µg of Trypsin was used suspended in wash buffer II. Samples were analysed on a half hour gradient on a QEX machine.

Full coverage of the N-terminal sequence of Ndc80 was achieved in the V8 sample. When the V8 and trypsin sample data was combined post-MS, sequence coverage increased by an average of 35% compared with Trypsin alone (**Figure 3.10D**). V8 gave higher protein intensities compared with Trypsin, with a best fit line gradient of 1.12. (**Figure 3.10B**). However, Trypsin gave better sequence coverage (**Figure 3.10C**). Digestion with two enzymes allows regions of interest to be covered in both Trypsin and V8 samples increasing the chance of identifying PTMs if they are present. Overall it was found that using a complementary enzyme to Trypsin should increase the number of phospho-sites identified in our kinetochore immunoprecipitations.

A.

Protein	Length (aa)	Total # peptides btwn 8-22aa in length	In silico coverage [%]	Actual coverage [%]
Hec1	642	476	74.14	63.2
Knl1	2342	1255	53.59	41.2
Nuf2	464	299	64.44	51.7
Spc25	224	145	64.73	47.3
Mis12	205	168	81.95	41.5
Nsl1	281	183	65.12	38.4
Dsn1	356	282	79.21	47.8

B.



C.

Protein	Uniprot code	Length (aa)	Trypsin digestion #peptides btwn 8-22	V8 digestion #peptides btwn 8-22	Trypsin in silico digestion (% coverage)	V8 in silico digestion (% coverage)
Hec1	O14777	642	476	371	74.14	57.79
Knl1	Q8NG31	2342	1255	1149	53.59	49.06
Nuf2	Q9BZD4	464	299	322	64.44	69.40
Spc25	Q9HBM1	224	145	133	64.73	59.38
Mis12	Q9H081	205	168	122	81.95	59.22
Nsl1	Q96IY1	281	183	178	65.12	63.35
Dsn1	Q9H410	356	282	277	79.21	77.81

Figure 3.9: *In silico* analysis indicates trypsin is an unsuitable enzyme for analysing the N-terminus of Ndc80

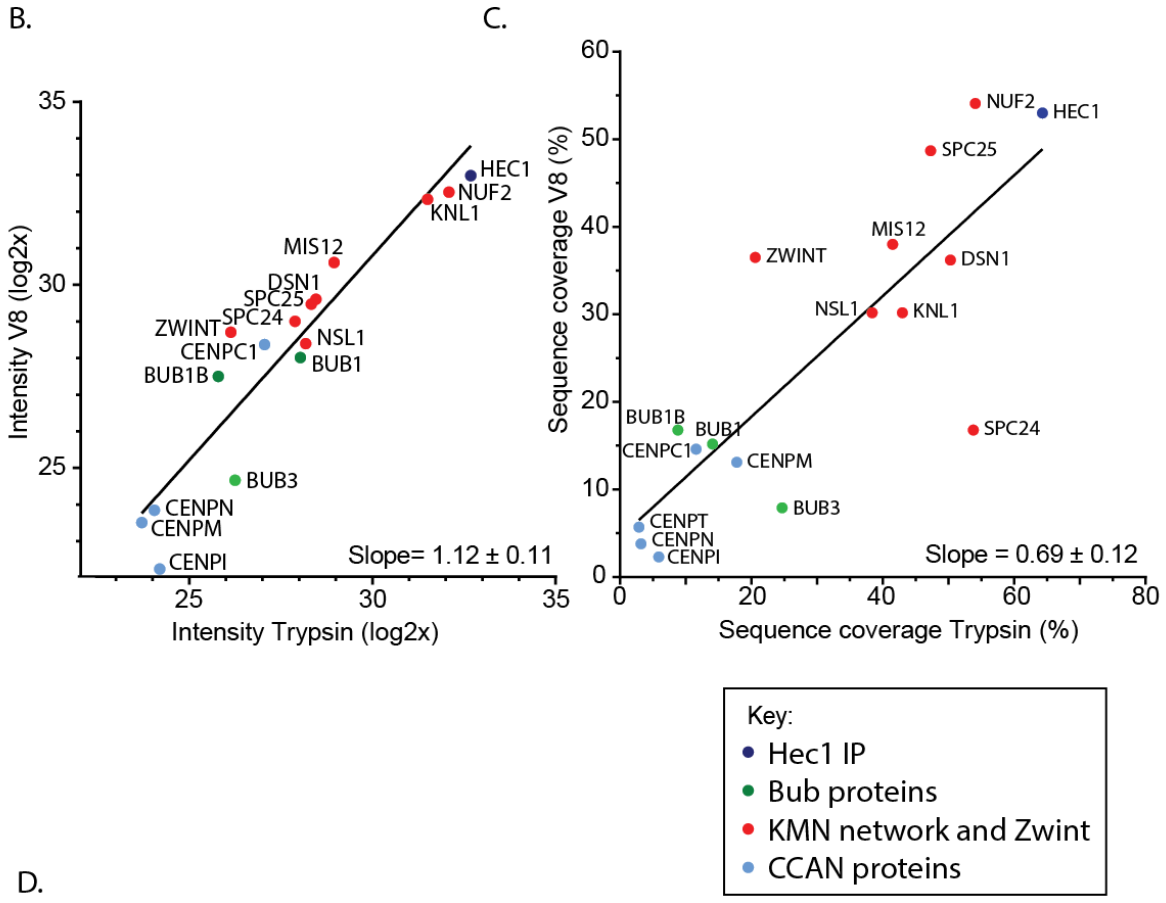
A) An *in silico* analysis compares trypsin's ability to create peptides of suitable size for MS. Table shows the length of proteins in amino acids; the number which fall within the range of 8≤n≤22 amino acids; the sequence coverage this would represent and then the average actual coverage experimental data achieves. B) The N-terminus of Ndc80 is shown with the trypsin cleavage sites (red lines) highlighting the 3 peptides we would expect to see reproducibly (underlined in blue). C) Compares Trypsin and GluC/ V8 digestions using the same analysis as in A.

A.

V8 allows complete coverage of the N-terminus of Hec1:

MKRSSVSSGGAGRLSMQELRSQDVNKQGLYTPQTKEKPTFGKLSINKPTSERKVSLFGKRTSGHGSRNSQLGIFSSSEK

| = V8 cleavage site



D.

Protein	Uniprot code	Length (aa)	Trypsin digestion #peptides btwn 8-22	V8 digestion #peptides btwn 8-22	Trypsin in silico digestion (% seq coverage)	V8 in silico digestion (% seq coverage)	Sequence coverage Tryp EXPT35 [%]	Sequence coverage V8 EXPT35 [%]	Sequence coverage [%]	% increase in total coverage	As an absolute (over trypsin)
Hec1	O14777	642	476	371	74.14	57.79	63.2	48.3	77.3	22.31	14.1
Knl1	Q8NG31	2342	1255	1149	53.59	49.06	41.2	28.4	55.8	35.43	14.6
Nuf2	Q9BZD4	464	299	322	64.44	69.40	51.7	45.3	74.8	44.68	23.1
Spc25	Q9HBM1	224	145	133	64.73	59.38	47.3	36.2	67.9	43.55	20.6
Mis12	Q9H081	205	168	122	81.95	59.22	41.5	37.1	57.6	38.79	16.1
Nsl1	Q96IY1	281	183	178	65.12	63.35	38.4	30.2	50.9	32.55	12.5
Dsn1	Q9H410	356	282	277	79.21	77.81	47.8	36.2	64	33.89	16.2

Figure 3.10: V8 complements trypsin, the combination of the two out-performs trypsin alone

A) The N-terminus of Ndc80 is shown along with the cut sites a V8 digestion of the N-terminus of Hec1 achieves (red lines). All peptides are of a suitable length to be identified by our MS set-up. B) and C) HeLa cells were arrested in mitosis using Nocodazole for 14hrs and after a mitotic shake-off a Knl1 IP was performed in duplicate and eluted using a sequential glycine-urea elution. Samples were prepared for MS using FASP, one of the samples was digested by 1.5µg V8 and one by 1.5µg Trypsin. Experiments are labelled either V8 or Trypsin depending on the digestion method. The graphs compare the intensity values and sequence coverage data for individual proteins digested either by V8 or trypsin. D) Compares the *in silico* data with experimentally generated data and calculates the increase in digestion efficiency overall

3.2.8 Testing our optimised protocol

Following multiple rounds of optimisation, the aim was to build a database of phosphorylation sites found in prometaphase arrested cells. The cell culture and immunoprecipitations itself was performed by Annabel Killen, a Part II medical student, under my direct supervision. The MS processing was performed by me. For these experiments HeLa Flp-in Ndc80-GFP cells were used as the commercial Ndc80 antibody previously used for pull-downs was no longer functional as a result of manufacturing errors. HeLa Flp-in GFP-Zwint cells were used in order that GFP pull-downs could be performed. Zwint is a direct interactor of Knl1, able to isolate Knl1 effectively, and has been shown to co-purify with the KMN network (Lin et al. 2006;

Pagliuca et al. 2009). Our initial experiment confirmed GFP-Zwint pull-downs were effective in isolating Knl1, with both Zwint and Knl1 isolated with similar efficiencies (**Figure 3.112C**).

HeLa cells containing the Flp-In TREx system were used (a kind gift of Professor Stephen Taylor, Manchester). The Flp-In TREx system allows different GFP-tagged constructs to be inducibly expressed under the same promoter leading to comparable expression levels. Ndc80-GFP and GFP-Zwint cells in IF showed correct localisation and 24hr doxycycline induction produced physiologically relevant levels of protein (**Figure 3.11A-B**). Cells were induced for 24hrs and arrested in Nocodazole overnight for 14hrs.

GFP immunoprecipitations were performed with antibodies against mCherry used as a negative control. Elutions were run on western blots to confirm both proteins were pulled down and eluted successfully, before samples were processed for MS (**Figure 3.11C**). FASPs were performed and V8 used to digest the Ndc80-GFP samples, while Trypsin was used to digest the GFP-Zwint samples. The reason for using two different proteins and digestion methods was to increase overall coverage of the outer kinetochore. Samples were separated; 10% was taken for proteome analysis and 90% was phospho-enriched using TiO_2. Each sample was run on a QEX system with an hour gradient for proteome samples and 30 minute gradient for phospho-enriched samples.

Analysis of the preliminary experiment yielded little usable data. The immunoprecipitation itself was successful based on the elution blots, and the proteomic analysis revealed components of each of the sub-complexes within the KMN network at intensities in the E9 range. However relatively few phosphorylation sites were seen (**Figure 3.12C**). RawMeat analysis showed a good digestion of all samples with the majority of peptides being +2/+3 charged (**Figure 3.12B**). The low level of sequence coverage and peptides identified is slightly misleading. The

proteome samples were far more complex than the phospho-proteome samples with the result that there was only incomplete sequencing of each individual protein. This is demonstrated by BUB1 which was not seen in the proteome samples, but was identified clearly in the Zwint-GFP phospho-proteome samples (**Figure 3.12C**).

In order to increase the quality and quantity of data, two areas of improvement were considered; improving the quantity of material isolated in the pull-down, and identifying ways of increasing the number of phospho-sites seen. The initial experimental immunoprecipitations were performed with 2.5mg of protein and used 1 µg of GFP antibody with 20ul of Protein-G sepaharose slurry. We altered three aspects of the pull-down procedure:

1) The amount of lysate used was doubled
2) For every 1mg lysate, 1 µg GFP antibody was used, and we also increase the amount of Protein G sepaharose to 30ul of slurry. Both changes were because in the initial experiment the amount of GFP antibody and Protein-G sepaharose was not sufficient to completely deplete the flow-through of GFP-protein (**Figure 3.12A**)
3) an overnight urea elution was added to achieve a more complete elution, as a result of the incomplete elution of bait protein from the beads (**Figure 3.12A**)

In the course of the experiment 52 kinetochore related phosphorylation sites were identified. The number of sites seen was on average only 15 per sample. The results ranged between 9 phospho-sites in Ndc80-GFP immunoprecipitations to maximally 27 in GFP-Zwint immunoprecipitations. This was considerably below the initial TiO_2 enriched Ndc80 and Knl1 samples which yielded over 50 each suggesting loss of phospho-sites during the procedure (**Figure 3.8C**).

We considered two possible explanations for the loss of phospho-signals. Either they were lost during the TiO_2 enrichment or they were not maintained during the collection

and immunoprecipitation stage. A protmix control was always run during TiO_2 enrichment procedures. This mix of BSA and α and β Casein acted as a positive control, with the un-phosphorylated BSA being depleted during enrichment. As the sample was of known concentration it would be expected to have a known base peak intensity reading on the MS (this reading is dependent on the gradient and MS used). That should confirm the enrichment procedure had not led to large scale loss of material. More importantly, a successful TiO_2 enrichment, would have depleted peptides associated with BSA, and retained Casein phospho-peptides. This control procedure suggested the TiO_2 enrichment was not the factor responsible for the poor yield of phospho-sites.

We therefore considered losses incurred at earlier stages. Great care had been taken to limit losses during MS preparation stages by using low-bind tubes and limiting transfer of material between tubes. We saw phosphatase proteins in our MS analysis at low levels. They cannot operate in 8M Urea so will have no effect on phospho-sites present after elution. During the immunoprecipitation stages the lysate contains a high-concentrations of phosphatase inhibitors which should prevent any phosphatase activity. It seemed most likely therefore, that any losses were occurring at the very start of the procedure.

Phosphorylations are known to be highly labile, particularly at the kinetochore where both the kinases and opposing phosphatases are present leading to a highly poised system. Kinases and phosphatases are inhibited by a reduction in temperature to 4ºC, and by the addition of inhibitors. Cells were put on ice immediately after the mitotic shake-off and washed in cold PBS prior to lysis; it was possible this was inadvertently affecting the natural equilibrium of the cells. These procedures took 15-30 minutes depending on the number of samples, ample time to manipulate the natural equilibrium of the cells' phospho-state. In this larger scale experiment, with an increased number

of samples the time delay was longer, potentially leading to a reduction in the number of phospho-peptides maintained.

Kinases require two substrates; MgATP and proteins, and following catalysis they produce MgADP and a phosphoprotein (Taylor & Kornev 2011; Wang & Cole 2014). By contrast, phosphatases react on a single substrate in a thermodynamically favourable reaction and are catalytically proficient enzymes (Hengge 2013; Lassila et al. 2012). In our experiment, decreasing the temperature prior to inhibition of enzymes was potentially biasing towards phosphatase activity thus leading to the loss of phospho-groups prior to addition of phosphatase inhibitors.

Further, during the first few minutes of lysis, where total inhibition has yet to be fully established, kinases could suffer more from the drop in relative concentrations of substrate and enzyme as the cell membrane broke down. In order to prevent loss of phosphorylation we adapted our protocol in two ways. Firstly, following mitotic shake-off cells were maintained at 37ºC until cold lysis buffer was added. Secondly calyculin A, a cell-permeable phosphatase inhibitor, was added in the final PBS wash prior to lysis, to ensure phosphatase inhibition was halted effectively. This three minute pre-treatment with calyculin A was designed to maintain the cells' phosphorylation equilibrium, while being too brief a timescale to create significantly bias towards the kinase.

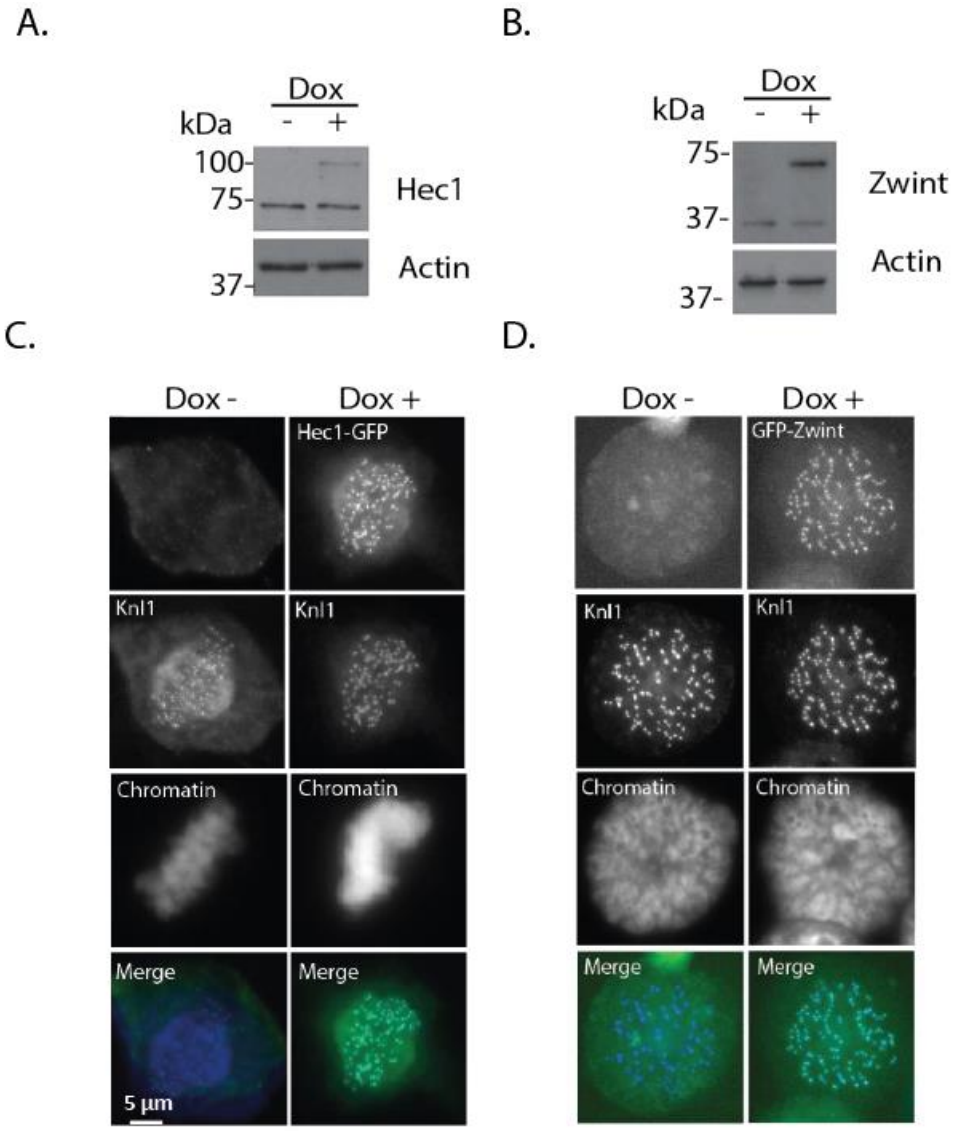
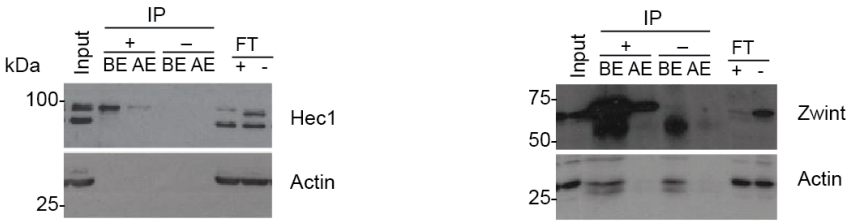


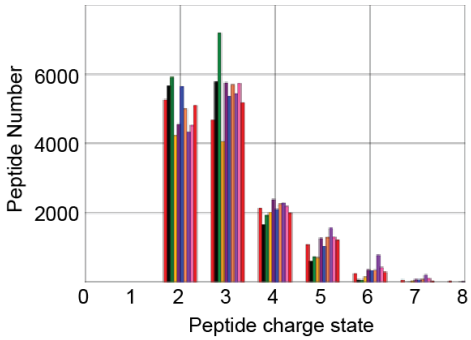
Figure 3.11 Confirmation of Ndc80-GFP and GFP-Zwint cell lines

A) HeLa Flp-in/TREx Ndc80-GFP and B) GFP-Zwint cells were induced for 24hrs with Doxycycline. Cells were collected via PBS +1mM EDTA and lysed. Samples were analysed by western blot to confirm protein levels relative to endogenous. C) and D) HeLa Flp-in/TREx Ndc80-GFP and GFP-Zwint cells were induced for 24hrs, samples were fixed and stained for Knl1 as a kinetochore marker, and DAPI. Both cell lines shows GFP-proteins localising correctly to the kinetochore in the presence of doxycycline.

A.



B.



C.

Protein	Intensity	Sequence coverage (%)	Peptide number	Number of phosphorylations seen
ZWINT	1.26E9	21.3	4	0
CASC5	1.24E9	3.8	6	10
NDC80	1.23E9	14.3	5	2
SPC25	3.26E9	21	5	1
SPC24	6.79E9	20.3	3	0
NUF2	1.25E9	8.4	6	1
NSL1	3.74E8	7.8	2	1
DSN1	1.25E9	8.4	2	9
PMF1	6.2E8	17.1	2	1
BUB1	-	-	-	4

Figure 3.12 Analysis of the initial MS experiment

A) HeLa Flp-in/TREx Ndc80-GFP and GFP-Zwint cells were induced for 24hrs with Doxycycline before the addition of Nocodazole for 14hrs. Samples were collected by mitotic shake-off and lysed. GFP-IP's were performed with mCherry antibodies used as a negative control. Samples eluted via a sequential glycine-urea elution protocol. Following immunoprecipitation samples were blotted before (BE) and after

elution (AE). To confirm the efficiency of the elution. The flow-through (FT) of the samples was also run. Samples were western blotted for the bait protein and actin (as a negative control). Ndc80 samples were digested with 1.5µg V8 and 1.5µg Zwint samples with Trypsin. B) Each FASP sample was run on a 30 minute gradient on a LC-QEX Mass spectrometry machine. Their peptide charge status was analysed via the RawMeat software package. Graph represents the distribution of peptide charge states, with peptide number on the y-axis and charge state on the x-axis. Each colour represents a sample from either the control or GFP-IP. The high trend of 2+ and 3+ charge states denotes a good digestion by both V8 and Trypsin. C) Analysis of proteins isolated in the initial experiment.

3.2.9 Generating a prometaphase kinetochore phospho-site data set

Using the experimental procedure with the adaptations described above, GFP immunoprecipitation using the Ndc80-GFP and GFP-Zwint cells were performed in triplicate with both Annabel and myself performing the procedures. The data was combined *in silico* with the initial experimental data set to create a master data set. A total of 5503 phosphorylation sites were found, of which 275 were on kinetochore components. Comparisons of data generated by Ndc80-V8 experiments were compared with Zwint-Trypsin experiments, and showed the Zwint-Trypsin experiments generated more phospho-site data than the Ndc80-V8 combination (**Figure3.13A-B**). Of the kinetochore phosphorylation sites found, 43 were only identified in Ndc80-V8 samples which demonstrates the usefulness of V8 to augment Trypsin's coverage (**Figure3.13C**). One noticeable result was the limited overlap between the Ndc80-V8 and Zwint-trypsin experiments. Only 49 phospho-sites were identified by both. Zwint-trypsin identified the largest number of phospho-sites at 183. It appears the database separates depending on digestion method into two semi-separate data sets.

In total 31 samples were run, of which eight were negative controls. Phosphorylation sites were assessed for their reproducibility between samples (**Figure3.13D**). There was a substantial number of missing values. As mentioned above the method of digestion seems to largely separate the database into two somewhat overlapping categories reducing the number of samples we would expect a phosphorylation to be seen in. Nevertheless, it still showed a suboptimal level of reproducibility less than half of the phospho-sites seen in at least six samples.

Post-filtering created a list of 184 phosphorylation sites on kinetochore-associated factors. Of these 36 were novel which are found mainly on Bub1, BubR1 and Knl1 (**Figure 3.14A-B**). Our data set showed eight Ndc80 phosphorylation sites - Ser5, Ser15, Ser44, Ser55, Ser62 and Ser69 – that were identified previously by Ciferri et al. (2008). We were also able to identified Thr31 and Ser50, both of which have been identified by other MS studies (Kettenbach et al. 2011; Santamaria et al. 2011; Sharma et al. 2014; Zhou et al. 2013).

These results validate the optimisation work done earlier in the chapter. Initially our procedure was unable to identify many well know sites, the developments to the protocol significantly increased its performance, yielding previously unseen phospho-sites along with many well-established sites.

Ndc80-Thr31 does not appear to be an Aurora B site based on its primary sequence (VNKQGLYpTPQTKEKP). Aurora B sites normally have positively charged residues just downstream, with most confirmed sites conforming to $(R/K)_{1-3}$-X-(S/T), where X is any amino acid (Meraldi et al. 2004; Kim et al. 2010). In fact the presence of a proline directly after the phosphorylated residue would indicate that it is being a Cdk1 site. Ser50 does have some characteristics of an Aurora B site, with positively charged residues either side of the phosphorylation (SINKPTpSERKVSLF). In our data set the phosphorylation was assigned to Ser50 rather than Thr49, with a 95% localisation probability. Previously DeLuca published that Thr49 was an Aurora B site. Because

both phosphorylatable residues are adjacent to each other, there is a chance that the phosphorylation could be mis-assigned to an amino acid based on the post-processing algorithms which interpret the raw data. Without access to the raw data it is difficult assess whether this is the case in DeLuca's work. However there are two pieces of evidence that support the phosphorylation of pSer50 rather than pThr49. Firstly, Ciferri et al. (2008), who also phosphorylated Ndc80 *in vitro* and analysed it by MS were able to identify other putative Aurora B sites but were unable to identify Thr49. Secondly, no other study has identified Thr49 either, but Ser50 has been found in multiple large-scale MS experiments in addition to our study (Kettenbach et al. 2011; Santamaria et al. 2011; Sharma et al. 2014; Zhou et al. 2013). Along with our findings, these data may suggest either in the initial study the phospho-site may have been mis-assignment to Thr49 or that both sites can be phosphorylated by Aurora B however Ser50 is favoured in most experimental set-ups.

Since Ndc80-MT interactions are regulated by electrostatic forces, it is unlikely that this mis-association, if true, would invalidate studies which have used phospho-mimietic mutants of Thr49. Individual sites are not likely to have much individual impact, the important point is the overall change in charge (Alushin et al. 2012; DeLuca et al. 2011; DeLuca et al. 2006; Ciferri et al. 2008).

In our experiments Bub1 and BubR1 sites were seen to be well phosphorylated (13 of which are novel sites), which is consistent with previous data (Chan et al. 1999; Taylor et al. 2001; Asghar et al. 2015). Some of these sites are well known for instance BubR1 p670 and p676 whose phosphorylation correlates with tension-sensing and error correction respectively (Huang et al. 2008; Elowe et al. 2007), Several Bub1 sites are autophosphorylation sites, shown in italics in **Figure 3.14B** (Asghar et al. 2015). It was striking that the phosphorylation sites normally bracketed domains of know function rather than being within them. In particular the location of the novel site Ser223, which sits just upstream of the GLEBs motif fits with this idea. The GLEBS

motif creates an extended surface which interacts with Bub3's β-propeller (Larsen et al. 2007). It would be interesting to further investigate if the Ser223 phosphorylation does have any role in regulating this interaction.

Dsn1 phospho-sites were observed with a high degree of reproducibility over all our experiments. Dsn1 is known to be highly phosphorylated residue with 28 phospho-sites over its 40kDa (Hornbeck et al. 2015). Of these Ser100 and Ser109 are known Aurora B sites (Welburn et al. 2010; Yang et al. 2008). Their phosphorylation or the deletion of a short region containing Ser100 and Ser109 stabilises the Mis12 complex's interaction with kinetochores suggesting the unphosphorylated form has an inhibitory effect (Rago et al. 2015; Kim & Yu 2015) When a $Dsn1^{68-200}$ fragment containing Ser100 and Ser109 sequences is removed Dsn1 binds 60x more strongly to CENP-C (Petrovic et al. 2016). We notice that all but one of the phosphorylation sites we see are in the first 124 amino acids of Dsn1. Several of these conform to the (S/T)-P Cdk1 motif. It seems possible that this region with no clearly defined structure and the ability to be highly phosphorylated may allow Cdk1 to regulate aspects of Dsn1's activity.

Knl1 was the most phosphorylated protein identified in our study. We observed the phosphorylation of the SILK and RVSF motifs, however, only one MELT motif was seen to be phosphorylated, MELT12 (Thr875). We did also observe the SHT motif of MELT7 to be phosphorylated. Vleugel et al. (2015) have suggested a mechanism whereby Mps1 first phosphorylates the MELT motif creating its own substrate recognition site allowing it to then phosphorylate the downstream SHT motif. This mechanism suggest that the SHT motif is phosphorylated subsequently to the upstream MELT motif. MELT7 contains a lysine residue between the MELT and SHT motif, therefore Trypsin should be acting to separate the MELT from its SHT motif, however the tryptic peptide containing the MELT7 motif was not observed. V8 is

unable to create a peptide compatible with MS in this region. Therefore it is plausible that MELT7 is phosphorylated but not observed.

The majority of the phosphorylation sites found on Knl1 were not in these well-understood motifs. We found sites grouped either up- or down- stream of certain MELT motifs, as well as a considerable number of sites which were in the 1320-1850 region which has no defined structure or function (**Figure 3.14C**). Of those in the region 1320-1850, one appears to be a Cdk1 site and whilst a few look like Aurora targets the majority don't have a strong similarity to classic consensus motifs. None of these sites have been investigated, it would be interesting to look at this region in further detail. There is poor sequence conservation of these phospho-sites in different species. However, in general Knl1 shows a low level of sequence conservation between species with only the SILK, RVSF, MELT and coiled-coil regions being consistently observed in Knl1 homologs. This may mean that these sites are not functionally relevant acting as 'passenger' phosphorylation events (in the same way you have driver and passenger mutations). But considering those phospho-sites which have been investigated in mechanistic detail show exquisite levels of regulations, this hypothesis then jars with the idea that these kinases, capable of such fine levels of regulation also add many dozens of spurious phosphorylations.

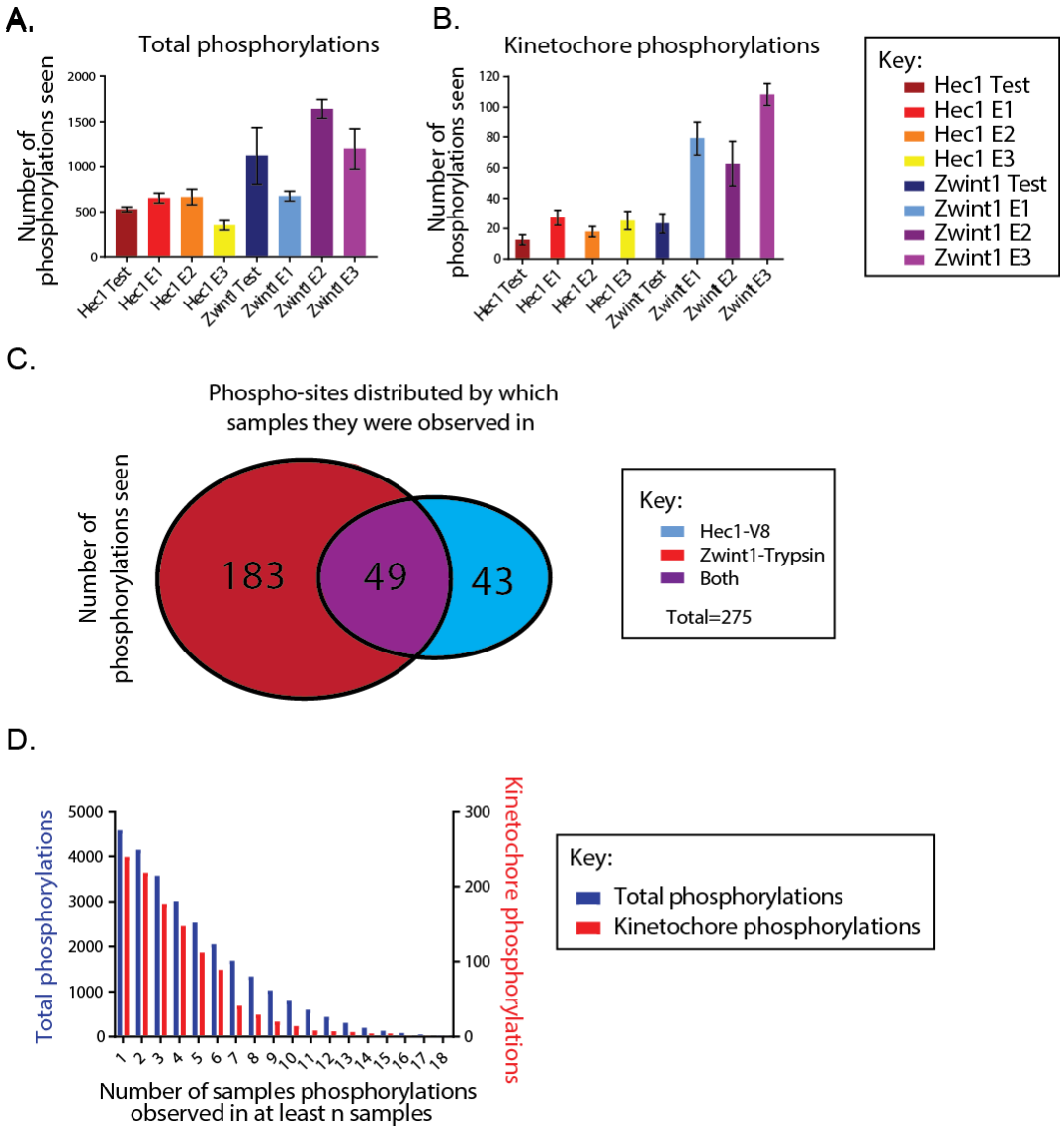


Figure 3.13 Analysis of the experiment outcomes from the pro-metaphase data set

HeLa Flp-in/TREx Ndc80-GFP and GFP-Zwint cells were processed for MS as previously stated (Figure 3.12). A) Graph shows the number of phosphorylation sites seen per sample. B) Shows the number of kinetochore related phosphorylation sitesseen per sample. C) Venn diagram show the level of overlap between the Ndc80 and Zwint cell lines with only a minority seen by both IP's. E) Graphically displays the relative level of reproducibility between samples, denoting in how many samples the same phospho-site was observed in. This shows the same trend for both the total number of phosphorylation events and the kinetochore specific phosphorylation events.

A.

Protein name	Phosphorylations identified	Novel sites identified
BUB1	23	7
BUBR1	12	6
KNL1	58	21
DSN1	15	1
INCENP	23	0
NDC80	8	0
NSL1	3	1
NUF2	1	0
PMF1	2	0
SKA3	2	0
SPC25	1	0
ZWINT	2	0

B.

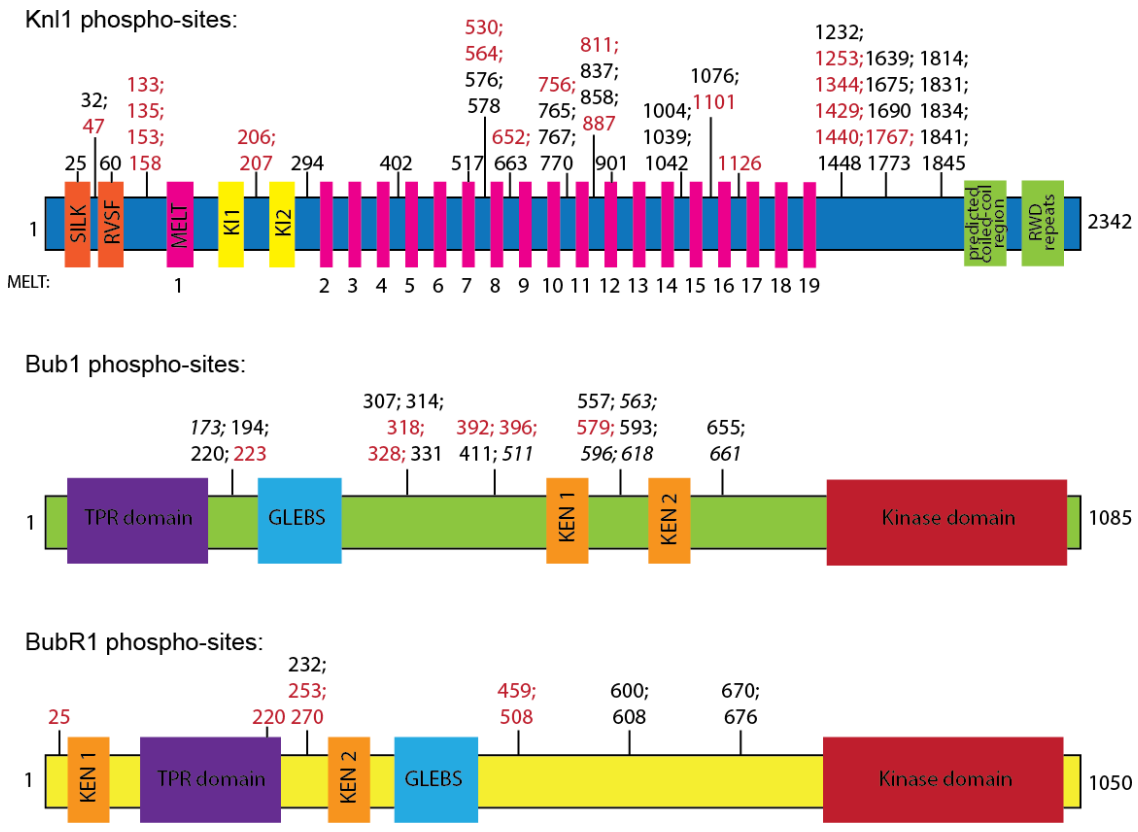


Figure 3.14 Identification of the novel sites found

A) Total output of MS experiments with Ndc80-GFP and GFP-Zwint cell lines, Table of the kinetochore related phospho-sites identified in the pro-metaphase samples shown. B)

Cartoon illustrating phospho-sites seen on Bub1, BubR1 and Knl1. Phospho-sites shown in red are novel. Novel sites are shown below in a table with red residues being the site of the phosphorylation. NB. Numbering for each protein is determined by the Uniprot Canonical sequence.

Gene names	Position	Localization prob	Score	Intensity	Amino acid	Sequence window
BUB1	223	0.791186	52.527	5049800	S	ERRVITISKSEYSVHSSLASKVDVEQVVMYC
BUB1	318	0.938089	103.42	489350000	S	VVETSHEDLPASQERSEVNPARMGPSVGSQQ
BUB1	328	0.999176	75.764	7924900	S	ASQERSEVNPARMGPSVGSQQELRAPCLPVT
BUB1	392	0.999894	59.585	140290000	T	ATSQSIAPPVPLKAQTVTDSMFAVASKDAGC
BUB1	396	0.90528	59.585	177250000	S	SIAPPVPLKAQTVTDSMFAVASKDAGCVNKS
BUB1	579	0.865717	108.86	568770000	S	KPKEEVPHAEEFLDDSTVWGIRCNKTLAPSP
BUB1B	25	0.999908	65.624	49251000	S	ALSEAMSLEGDEWELSKENVQPLRQGRIMST
BUB1B	220	0.791624	139.47	140800000	S	LLALEKEEEEEVFESSVPQRSTLAELKSKGK
BUB1B	253	1	56.569	8494600	S	ARAPIIRVGGALKAPSQNRGLQNPFPQQMQN
BUB1B	270	1	135.08	171700000	S	NRGLQNPFPQQMQNNSRITVFDENADEASTA
BUB1B	459	0.931935	83.243	16265000	T	KQIEEMEKKLKEIQTTQQERTGDQQEETMPT
BUB1B	508	0.882229	130.01	770090000	T	TLSSSVCQVNCCARETSLAENIWQEQPHSKG
CASC5	47	1	73.233	5074700	S	SPLQDLRGGNERVQESNALRNKKNSRRVSFA
CASC5	133	0.997722	94.295	182310000	T	LLIQNKKLEDNYCEITGMNTLLSAPIHTQMQ
CASC5	137	0.994227	94.295	182310000	T	NKKLEDNYCEITGMNTLLSAPIHTQMQQKEF
CASC5	153	1	86.014	166050000	S	LLSAPIHTQMQQKEFSIIEHTRERKHANDQT
CASC5	158	1	50.354	11589000	T	IHTQMQQKEFSIIEHTRERKHANDQTVIFSD
CASC5	206	0.93437	73.953	31790000	T	LLDNPISEKSTKIDTTSFLANLKLHTEDSRM
CASC5	207	0.93437	73.953	31790000	S	LDNPISEKSTKIDTTSFLANLKLHTEDSRMK
CASC5	530	0.907713	111.67	65073000	S	SHTVAIDNQIFKQDQSNVQIAAAPTPEKEMM
CASC5	564	0.999621	75.911	21856000	S	LMTTSEDGKMNVNCNSVPHVSKERIQQSLSN
CASC5	652	1	64.52	31365000	S	ECEEITKSRNEPFQRSDIIAKNSLTDTWNKD
CASC5	756	0.999993	108.75	189700000	S	TAISSHTVKSVLGQNSKLAEPLRKSLSNPTP
CASC5	811	1	64.191	22881000	T	VVIGFGPSELQELGKTNLEHTTGQLTTMNRQ
CASC5	887	0.99912	76.294	38079000	T	KIWGRKSVGGPKIDKTIVFSEDDKNDMDITK
CASC5	1101	0.999998	82.349	59542000	T	SKSQRRKSLKLKNDKTIVFSENHKNDMDITQ
CASC5	1126	1	125.53	212450000	S	DMDITQSCMVEIDNESALEDKEDFHLAGASK
CASC5	1253	1	61.161	3065700	T	AEKQALAVGNKIVLHTEQKQQLFAATNRTTN
CASC5	1344	1	52.527	69981000	S	SCLPNVISCTDNLEGSAMLLCDKDEEKANYC
CASC5	1429	0.994628	122.89	48458000	T	DQDLIKDPRNLLANQTLVYSQDLGEMTKLNS
CASC5	1440	0.997025	122.89	48458000	T	LANQTLVYSQDLGEMTKLNSKRVSFKLPKDQ
CASC5	1639	0.792597	88.986	86125000	S	HIVQATEIHNINIISSNAKDSRDEENKKSHN
CASC5	1767	1	171.47	156910000	T	SDSINIETEEKALIETYQKEISPYENKMGKT
CENPC1	276	0.80789	66.393	11884000	S	SFSTLFLETVKRKSESSPIVRHAATAPPHSC
DSN1	7	0.82109	71.933	9289800	S	_____MTSVTRSEIIDEKGPVMSKTHD
NSL1	22	0.89414	103.9	18533000	T	LVVLDPPWDKELAAGTESQALVSATPREDFR

3.3 Discussion

3.3.1 Summary

We have developed a MS based technique which allows analysis of the outer kinetochore's phosphorylation state during mitosis. Optimisation of the protocol has led to the development of a multi-step procedure including pre-treatment with a cell permeable phosphatase inhibitor, an immunoprecipitation which is eluted using a combination of Glycine and Urea elution's. In order to process the samples for MS FASP was used to digest proteins using both V8 and Trypsin in combination, and TiO_2 enrichments are used to increase identification of phospho-peptides. We were able to recapitulate others' results whilst also identifying novel phospho-sites.

3.3.2 Discussion

MS has been widely used to investigate the complex phospho-regulation which occurs during mitosis. In the last decade there have been many attempts to identify key targets of phospho-regulation. With the improvement in techniques and increase in the power of mass spectrometers themselves more and more phospho-sites have been obtained. Much of the data can be collected into two categories:

1) large-scale studies interested in identifying sites without deeply investigating their biological significance
2) focussed papers investigating a specific protein or group of interactors, using biochemical or biological techniques. In these MS is used to augment their data and to answer a specifically targeted questions

We wanted to create a protocol which bridged these two approaches with regards to the kinetochore. The development of an immunoprecipitation procedure capable of isolating the entire outer kinetochore allows a broader overview of phospho-regulation as well as providing a rich data set as a starting point for further biological investigations.

We developed a MS based approach capable of generating good coverage of the entire outer kinetochore. Our initial experiment using an in-gel digestion method previously used in our lab revealed how technically challenging this would be. Several KMN network components were missing, owing to the exclusion of the IgG bands. The sequence coverage, excluding the bait protein, varied between 7.35% and 31.7%. The gradient time allowed on the mass spectrometer allowed exhaustive sequencing of peptides present in the sample. Improvements needed to be made to increase the overall coverage as sequence coverage is critical to identifying phosphorylation events.

The FASP procedure offered a way to reduced cost and losses associated with in-gel digestion. FASP in place of in-gel proved capable of isolating the entire KMN network successfully. It also gave better sequence coverage than the in-gel experiments varying between 21.1% and 52.8%. This is likely to be an under-representation of the peptide coverage present because samples were only run on a single hour gradient.

Titanium dioxide was selected as the enrichment procedure as it is designed for small sample size and was simple and cost-effective to use. We found it gave a 5-10 fold increase in kinetochore sites identified. It also showed that Knl1 immunoprecipitations generated more phospho-data compared to Ndc80 immunoprecipitations. Knl1 itself is highly phosphorylated. Furthermore, it is in direct contact with other highly phosphorylated proteins such as the Bub proteins. Isolating the outer kinetochore using Knl1 rather than Ndc80, which is situate at the other end of the KMN network, allowed more phospho-sites to be seen. This data was later confirmed by the GFP-

Zwint immunoprecipitations which again showed more phosphorylation sites compared to Ndc80-GFP IPs.

Throughout this study we used the Ndc80 phosphorylation sites as an indicator of experimental success, or otherwise. To test the quality and robustness of our results, we looked for well-studied and well-established sites. *In silico* analysis identified the limitations using of trypsin alone. V8 in parallel with trypsin could augment our coverage and therefore our number of identifications. Interestingly in our final data set it was striking how only a minority of phospho-sites were identified by both digestion methods and pull-downs. Considering the pull-downs were equally able to isolate the proteins themselves, suggesting there was not a largescale deficiency in terms of protein, it leads us to conclude that the digestion method is largely responsible for the non-overlap of identifications.

Once we had developed a sound and effective method of identification we investigated if it might be possible to create a labelling technique. Dimethyl labelling led to a considerable loss of material and a poor outcome in terms of identifications. It was concluded the costs outweighed the benefits.

Following these rounds of optimisation, our new methodology was used to generate a comprehensive data set for analysis. Using Ndc80-GFP and GFP-Zwint cell lines, GFP immunoprecipitations were performed. Our data revealed numerous novel phospho-sites on a variety of core and SAC related components.

Overall the methodology had been improved significantly from its starting point, we are now able to isolate the outer kinetochore components with greater efficiency and retain associated phosphorylation sites with much greater success. There is still an issue with the reproducibility of individual phospho-sites within samples however this is not unusual within such experiments and can be largely be worked around if the sample size is large enough. The creation of this pipeline is a means to an end, allowing the

study of the phospho-state different attachment statuses which will be discussed in the next chapter.

Chapter 4: An unbiased analysis of the kinetochore in different k-MT attachment states

4.1 Introduction

The most profound change that occurs at the kinetochore is the attachment to the bipolar spindle. Microtubules bind kinetochores first laterally and then in a stable end-on fashion. This change from unattached to attached status causes a switch in behaviour. The loss of Aurora B and Mps1 activity from the outer kinetochore, and the kinetochore-bound phosphatases PP1 and PP2A-B56 reversing their kinase activity, leads to a widespread loss of phosphorylation (Funabiki & Wynne 2014). MS is an ideal way of investigating the specific changes of this large-scale change of state in an unbiased fashion.

Phosphorylation has been implicated in the binding and regulation of several of the key components at the kinetochore (Funabiki & Wynne 2014). The phosphorylation of the N-terminus of Ndc80 by Aurora B reduces its affinity for MT, and also enhances Mps1's ability to bind the Ndc80 complex (Ji et al. 2015). This has the effect of promoting SAC signalling, because Mps1 phosphorylation of MELT motifs on Knl1 is critical to the successful binding of the Bub components necessary to initiate the SAC signal (Primorac et al. 2013).

Of the MS studies done to date, some have used synchronisation techniques to look at the cell cycle, but none has aimed to separate the difference between attachment states. Many of the studies are too general, isolating mitosis as a single time point or fraction (Daub et al. 2008; Dephoure et al. 2008; Olsen et al. 2010).

Malik et al. (2009) were interested in the changes over the course of mitosis. However their synchronisation method relied upon a noscapine release. Noscapine decreases microtubule dynamics by altering the conformation of tubulin, so arrests cells with a bipolar spindle with a few outlying chromosomes (Ye et al. 1998). Their three time points were late prometaphase, a stage close to metaphase and post-metaphase. The difference between late prometaphase and metaphase (15mins post-release) is small thus the largescale switch in behaviour will be masked as the majority of chromosomes have not changed their status as aligned, attached kinetochores. Indeed Malik et al. only see 3% of all phospho-sites downregulated between prometaphase to metaphase. This experimental setup condenses the differences between these two mitotic stages.

The last chapter described how a methodology has been developed allowing isolation of the outer kinetochore to study phosphorylation status. Our objective is to couple this protocol with a preceding synchronisation step which creates two populations with distinct attachment status. Together they should allow an unbiased global comparison of the changes in phospho-regulation at the kinetochore upon K-MT attachment.

4.1.1 Aims

- Develop a synchronisation protocol capable of creating homogeneous unattached and attached kinetochore states
- Investigate how the phospho-status of the kinetochore changes upon attachment in an unbiased fashion

4.2 Results

4.2.1 Analysis of synchronous cell cycle timings

The objective is to study changes of state in as close to an unperturbed system as possible. In asynchronous HeLa cultures the mitotic index is about 5% of the cell population. In order to enrich for a mitotic population, researchers take one of two approaches; either drug-arrests halt progression at the time point of interest, or drug-arrests are used to block cell cycle progression at a specific stage before release into fresh medium so that cells proceed through the cell cycle in a synchronised manner. The latter method is used when there is no drug which precisely halts cell cycle progression at the point required. However, it results in a more mixed population, because individual cells can differ in progression timings post-block.

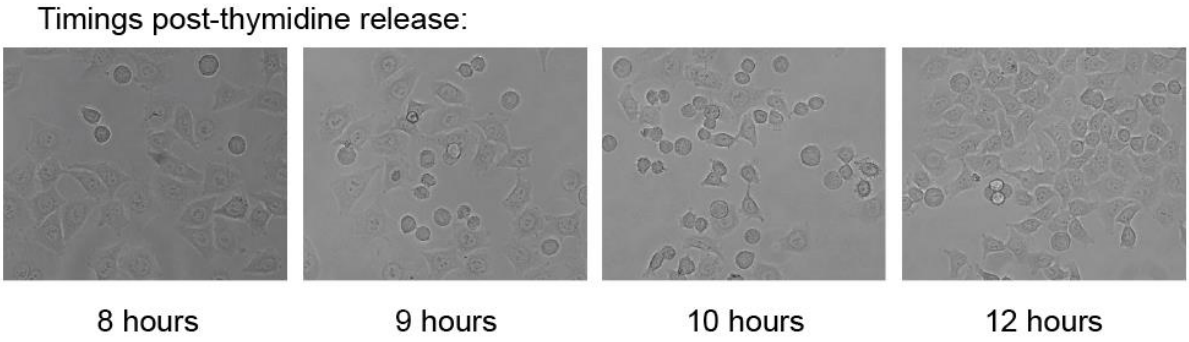
Thymidine is a drug which inhibits DNA replication by interrupting the deoxynucleotide metabolism pathway (Bjursell & Reichard 1973). Cells synchronised by thymidine accumulate in S-phase. It is commonly used as a synchronisation agent because it can be kept in the media for prolonged periods and is easy to wash out. HeLa cells were treated with Thymidine for 18 hours before being released into fresh media. Time points were taken every hour from 7 to 14 hours, to analyse mitotic progression of the population (**Figure 4.1A**). The mitotic peak was at 10 hours with ~ 60% cells in mitosis, but the population was relatively mixed. The thymidine release was insufficient to create a homogeneous population because of its relative temporal distance to mitosis. With over eight hours between release and collection, there was a considerable time for natural variation in cell cycle progression to dilute the synchronicity achieved. A thymidine release alone was evidently not sufficient. Therefore a different strategy needed to be considered.

Live cell imaging of GFP-Mad2 cells was used to assess mitotic timings in HeLa in more detail (**Figure 4.1B**). SiR-DNA was used to stain DNA, allowing mitotic state to be determined. Following nuclear envelope breakdown, cells rapidly congress their chromosomes to the metaphase plate with an average time of 19 minutes. Once all kinetochores are fully attached the SAC signal is lost. GFP-Mad2 is used as a marker as it is one of the first proteins to be lost upon SAC silencing. There is a lag of approximately 20 minutes, upon the loss of the last Mad2-positive kinetochore, before anaphase onset ensues. Most cells undergo mitosis within an hour. However, if chromosomes are incorrectly attached or become stranded at the poles, it can lead to a more prolonged mitosis because the SAC holds the cell in mitosis allowing the errors to be corrected. This was evident from the pronounced difference between the most rapid and slowest NEB-Anaphase onset time, 30 minutes and 106 minutes respectively. Overall the average time from NEB to Anaphase onset was 48 minutes (**Figure 4.1D**).

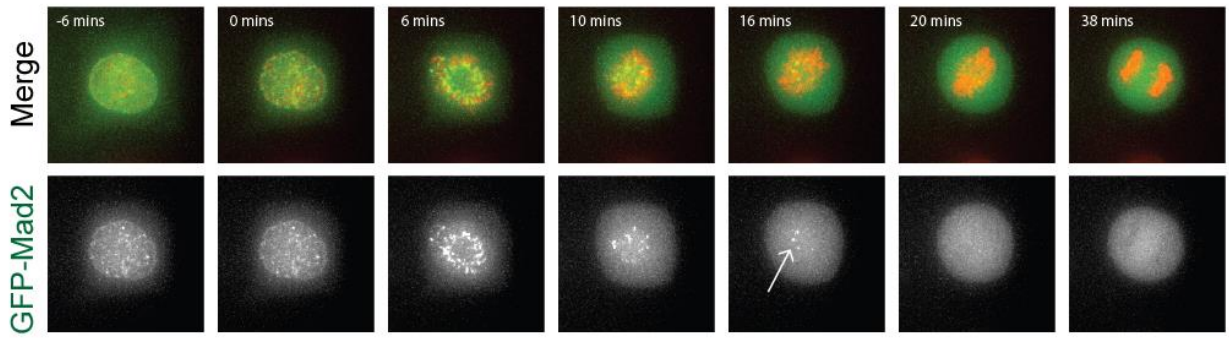
The timing from early prometaphase to metaphase was aproximately 15 minutes. This small time difference reflects a large switch in kinetochore status between unattached and attached K-MT states. When compared with an average division time of 24hrs, this accounts for 1% of the cell cycle.

One of my key aims was to accentuate the difference in phospho-state as much as possible by creating very homogeneous populations.

A.


Timings post-thymidine release:
8 hours
9 hours
10 hours
12 hours

B.


Merge
GFP-Mad2
-6 mins
0 mins
6 mins
10 mins
16 mins
20 mins
38 mins

C.

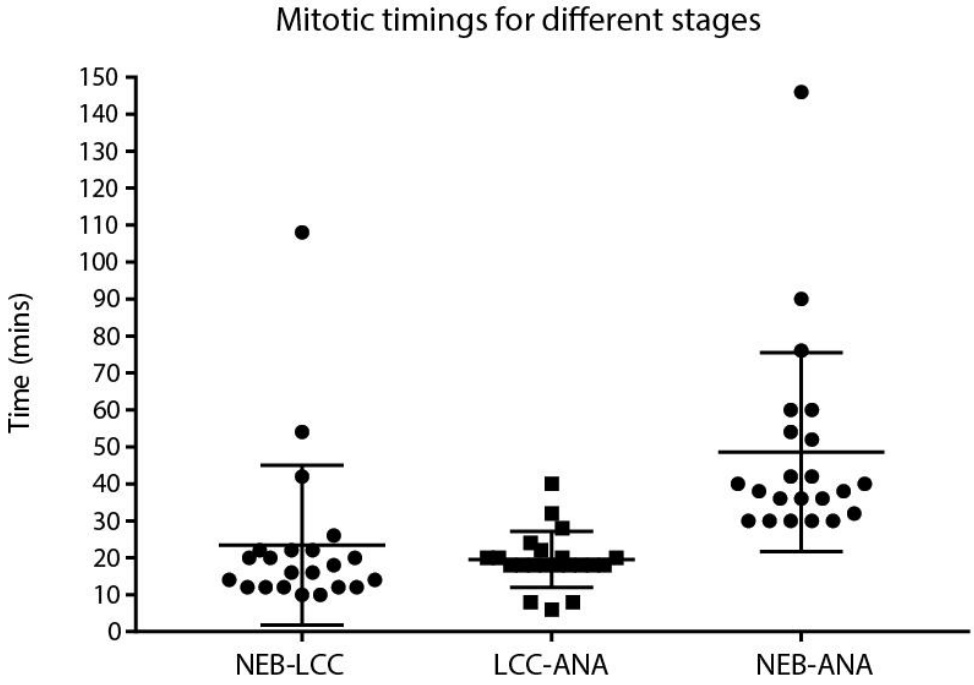

Mitotic timings for different stages
Time (mins)
150
140
130
120
110
100
90
80
70
60
50
40
30
20
10
0
NEB-LCC
LCC-ANA
NEB-ANA

Figure 4.1: Analysis of synchronous cell cycle timings.

A) HeLa cells were seeded 24hrs prior to Thymidine addition. Cells were treated with Thymidine for 18hrs before being released by washed four times in fresh media. Time points were taken every hour from 7hrs onwards. Pictures of a wide-field view using bright field in the following conditions; 8, 9, 10,12 hours post thymidine release. B) HeLa GFP-Mad2 cell lines were synchronised with Thymidine as above, samples were imaged live 8hours after Thymidine release. Samples were imaged at 2min intervals. Merge contains SiR-DNA. White arrow indicates last GFP-Mad2 foci. C) Graphically displaying mitotic timings of GFP-Mad2 cells over NEB to Anaphase. NEB = Nuclear envelope breakdown, LCC = Last chromosome congressed, ANA = Anaphase onset. (n=24 from two independent experiments).

4.2.2 Creating a release protocol

Following the limited success of a thymidine-release protocol it was necessary to consider other drugs which would be suitable. One potential concern about creating prolonged prometaphase populations is that it may cause an unnaturally hyper-phosphorylated state. For an initial study, however, it was decided that it represented the most promising way of obtaining two distinct states. Validation using cell biological techniques in an unperturbed system can then be used to confirm positive hits.

Nocodazole is the obvious candidate to create a prometaphase-like condition. It is a microtubule depolymerising drug which prevents the formation of the bipolar spindle, resulting in a completely unattached state. To create an attached metaphase population, the proteasome inhibitor MG132 can be used to prevent the destruction of

separase and cyclin B, which inhibits anaphase onset by preventing the separation of chromatid. Both these conditions mimic the prometaphase and metaphase populations well. Nocodazole kinetochores are SAC positive (shown by GFP-Mad2 foci), whereas MG132 cells display a fully aligned metaphase plate with an absence of SAC signalling (see **Figure 4.2A**). However, MG132 is toxic if left in for periods of more than three hours (Wu et al. 2002; Suraveera et al. 2012). Therefore, to get a homogenous population it is necessary to pre-synchronise the cells prior to a MG132 arrest.

To be a valid candidate the pre-synchronisation drug has to be stable and non-toxic to cells, easily washed out and relatively inexpensive so could be done on large scale. Drugs that affect bipolar spindle formation are good candidates as a bipolar spindle is a prerequisite to a successfully aligned metaphase population. **Figure 4.2B** shows a comparison of the arrest states. Nocodazole fully depolymerises microtubules and thus activates the SAC on all kinetochores. All kinetochores display GFP-Mad2 foci and lack Astrin staining, because the Astrin/Kinastrin complex only associates with attached kinetochores (Manning et al. 2010). STLC and Monastrol, both Eg5 inhibitors, prevent separation of the spindle pole bodies, creating a single nucleating point for microtubules which radiate out in a star shape (Skoufias et al. 2006; Mayer et al. 1999). GSK923925 is an inhibitor of CENP-E's motor function (Wood et al. 2010); it creates a phenotype closest to a metaphase plate with only a few outlying chromosomes left unable to congress to the metaphase plate.

To test which of these inhibitors is most suitable for the creation of a fully-attached kinetochore population, GFP-Mad2 cells were seeded in 6 well plates and arrested with Monastrol, STLC, Nocodazole and GSK923925 for 12hrs. Overnight treatment led to about 60-70% mitotic index. The cells were washed (2xPBS;3xDMEM) and released into MG132. At 2 hr and 3 hr time points coverslips were fixed and stained for tubulin and Astrin. These drug-releases were compared for the ability of cells to

form metaphase plates. GSK923925 proved difficult to wash out efficiently; 91% cells still showed peripheral SAC signalling chromosomes after extensive wash-out of the drug. Nocodazole could be washed out but with variable efficiency; 25% of cells were able to form a bipolar spindle after wash out. Although according to the literature STLC is more difficult to washout than Monastrol, no difference was observed in our hands. A possible explanation could be that STLC is indeed more difficult to wash out and does cause a slight delay in spindle reformation compared with Monastrol but due to the prolonged MG132 arrest imposed by our protocol after wash out this delay was not observed in our experiments. After careful consideration, the conditions chosen to proceed with were an STLC release into 3hr MG132 which was able to produce 86% of bipolar spindles.

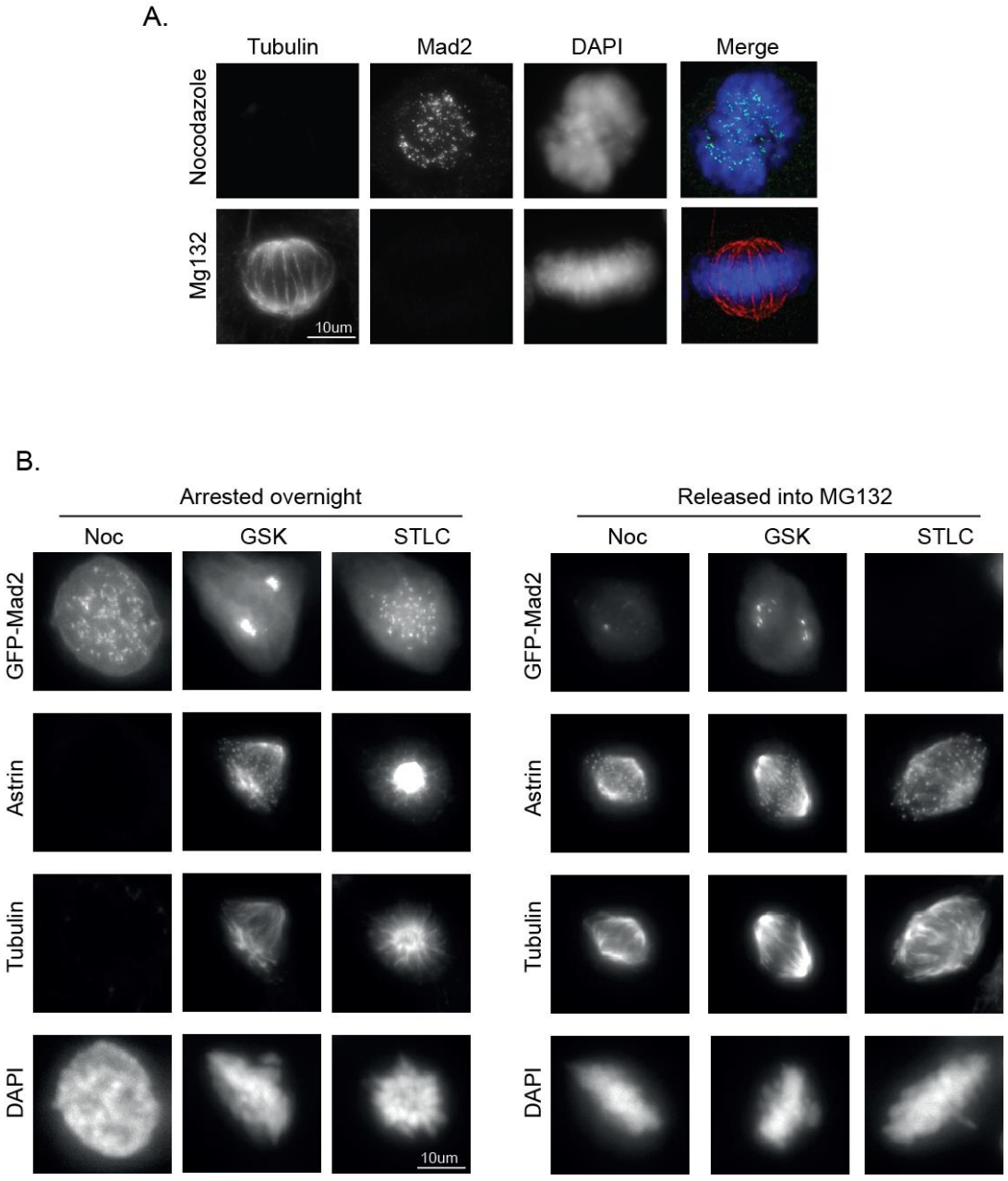


Figure 4.2: Synchronisation protocol established

A) HeLa cells were grown asynchronously before being treated with Nocodazole or MG132 for 3hours. Samples were stained for Tubulin to shows the spindle status and Mad2 to indicate its SAC status. B) HeLa cells were arrested for 14hrs in either GSK923925, Nocodazole and STLC a coverslip was fixed to give the arrested overnight fraction. Samples released into MG132 and left for 3hrs before fixing. GFP-Mad2 and Astrin are used as markers of unattached and attached kinetochores respectively.

4.2.3 Optimising for large-scale releases

For large scale experiments cells were synchronised in solution. Following rounds of optimisation the protocol illustrated in **Figure 4.3A** was established. To ensure the protocol worked with a high degree of reproducibility 4xPBS and 4xmedia washes were required (**Figure 4.3B**). Three 15cm dishes were combined in a single 50ml Falcon. Each wash used 50ml media and samples were mixed well to ensure the pellets were fully resuspended to aid release from an STLC arrest. Following each resuspension stage, cells were incubated for three minute at 37ºC followed by a two minute centrifugation step (at 600g). An increased number of washes were required to achieve a good wash out; this is possibly because the cells weren't agitated in the media but left in a falcon tube in the incubator such that they did naturally settle. The clumping of cells would be likely to impede the release of STLC from the cells as the local concentration difference is less pronounced between the media and cells if the cells clump.

After the final wash cells were plated into a single large 15cm dish with 50ml medium. 20 minutes later MG132 was added. An initial concern was that the release itself would be so time-intensive that it would result in the first cells progressing through into anaphase but this was never observed. After 3 hrs cells were counted using a haemocytometer and 30,000 cells were taken for cytospin. Cells were fixed with PTEMF and analysed by IF to confirm the success of release. We found it was possible to get 90% metaphase populations, with the remainder having largely reformed spindles with just a few checkpoint positive kinetochores (**Figure 4.3B**).

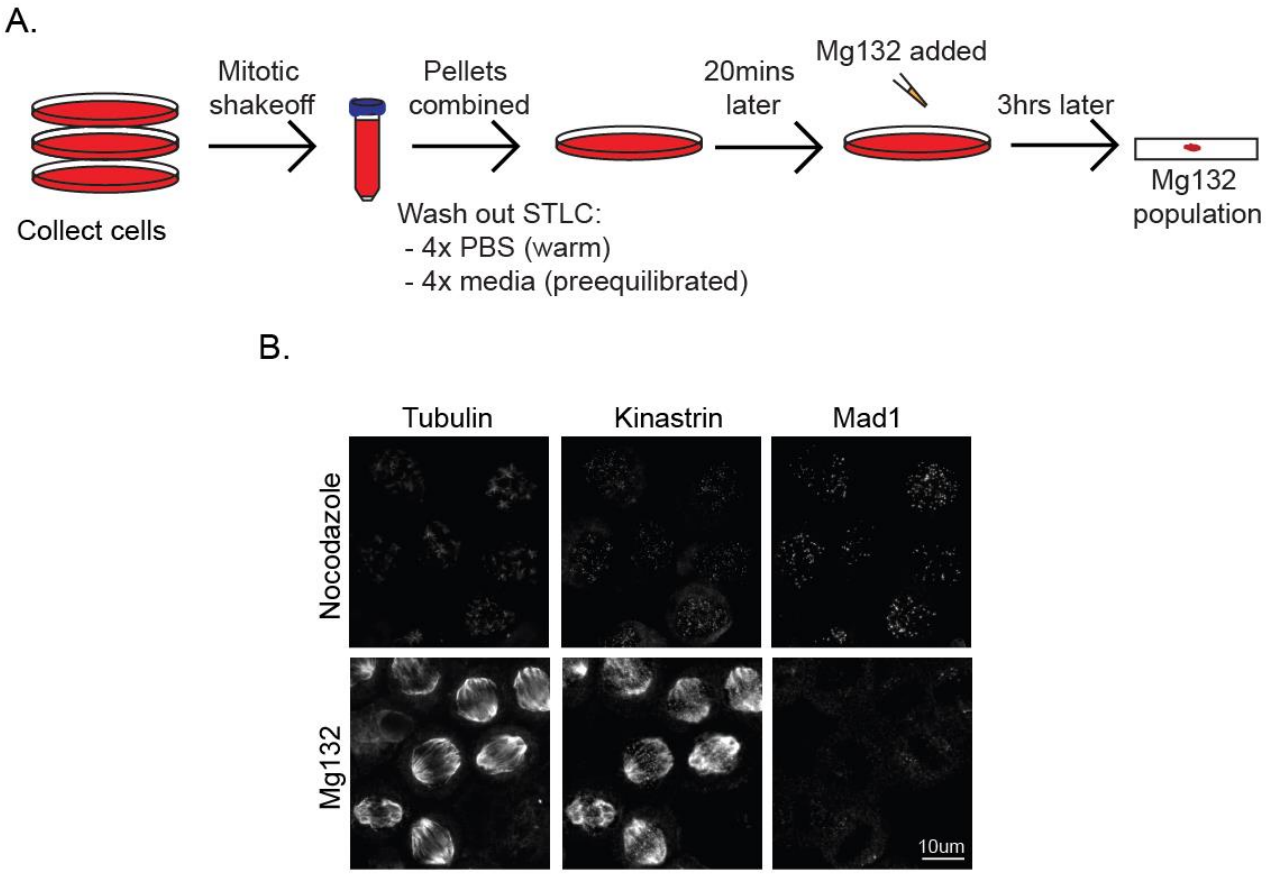


Figure 4.3: Synchronisation reoptimised for larger-scale

A) Schematic showing release protocol. HeLa cells were arrested in mitosis for 14hrs using STLC. Samples were collected via mitotic shake-off and three 15cm dishes combined into a single 50ml falcon. Cells were released from STLC via washes with PBS and media four washes each at prior to MG132 addition twenty minutes later. B) Cells were cytospun onto glass slides and the success of the release was determined by immunofluorescence. Tubulin was used to assess the reformation of the spindle whilst Kinastrin and Mad1 were used to assess the status of the SAC (off and on respectively). Experiments were discarded if <85% SAC silencing was achieved.

4.2.4 Confirming releases do recapitulate an attached state

A key consideration to the entire success of the project was that the attachment status would be maintained over the course of an immunoprecipitation procedure. Lysis causes total disruption to cellular structures with microtubules being dissociated during the lysis of cells in the cold. With the addition of micrococcal nuclease kinetochores are released into the supernatant (see **Figure 3.3**). It was unclear if the removal of the microtubule attachments by our lysis protocol would result in the re-association with the kinetochore of proteins, absent from the kinetochores in the attached state, during the course of the immunoprecipitation. It has been suggested that Mps1 might bind competitively with microtubules to the Ndc80 complex, exhibit competitive binding to the Ndc80 complex, with the presence of microtubule preventing binding (Ji et al. 2015; Hiruma et al. 2015). If Mps1 is able to re-associate and is not completely inactivated by the cold there was a risk it could lead to the re-association of other factors. Effectively the kinetochore might revert to a prometaphase-like state.

Whilst the core KMN network components and Knl1's direct interacting partner were isolated with similar efficiency in both the Nocodazole and MG132 fractions, the Bub proteins showed a marked reduction upon MT-binding consistent with the silencing of the SAC (**Figure 4.4 A and B**). This data confirms that the "attachment" status is maintained over the course of an immunoprecipitation.

The experiment was then repeated and processed for MS. This recapitulated the results above with no significant change in core components but a marked decrease in Bub1 and Bub3 in the MG132 fraction compared with Nocodazole (**Figure 4.4C**).

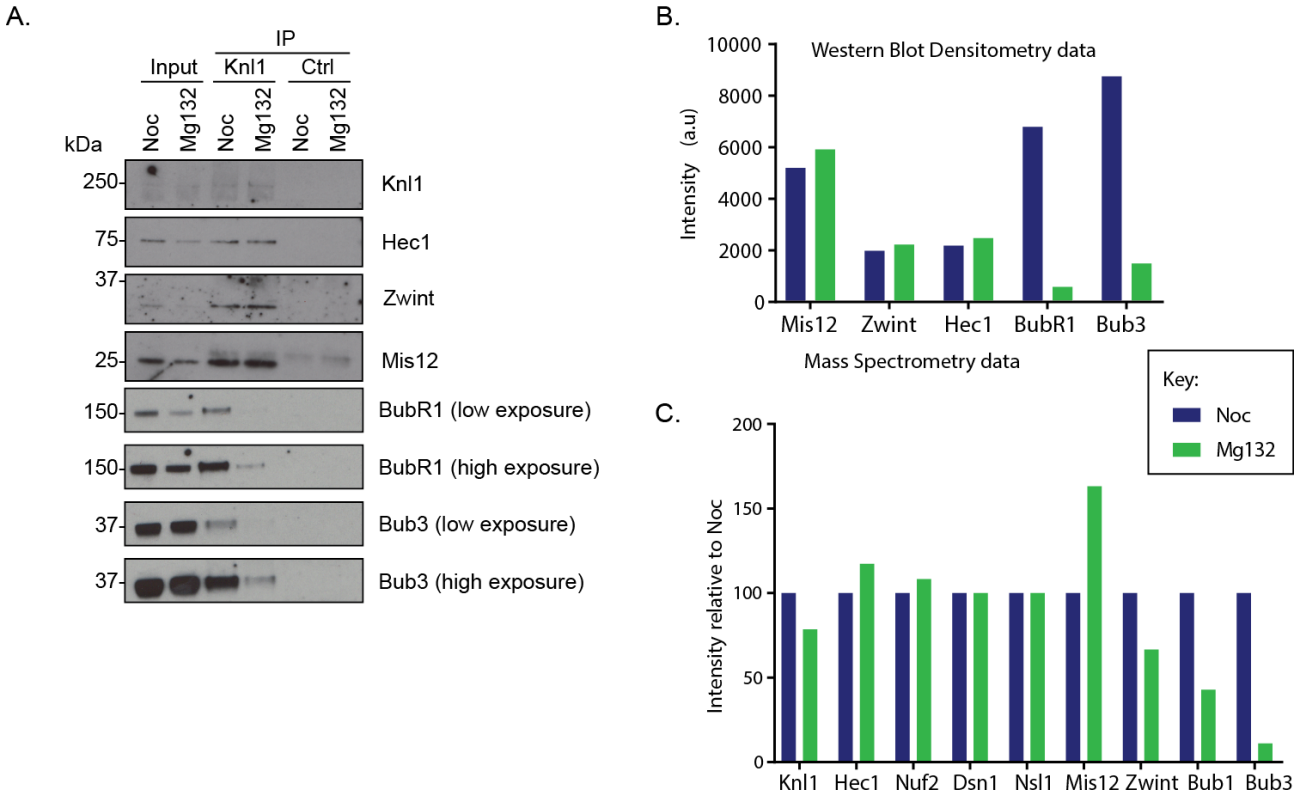


Figure 4.4: Immunoprecipitations are capable of identifying changes of attachment state

A) HeLa cells were arrested in mitosis using Nocodazole or STLC for 14hrs, the STLC samples were released into MG132 as previously described. 5mg Knl1 IP's were then performed and eluted in laemmli buffer. Identification of changes in kinetochore attachment state by immunoprecipitation. In both Nocodazole and MG132 fractions the core KMN network components and Knl1's direct interacting partner, Zwint, are isolated with the same efficiency. The Bub proteins are reduced in MG132. B) Densitometry of data shown in A). C) Experiment was repeated and following a glycine-urea elution processed for MS using trypsin. Their intensity relative to Nocodazole is shown.

4.2.5 Comparing kinetochore phospho-states depending on attachment status

Having created a protocol which is capable of isolating two distinct attachment states we wanted to analyse the difference in phosphorylation at the outer kinetochore. HeLa cells were synchronised as before (**Section 2.2.3**) and Knl1 immunoprecipitations were performed. Four samples were analysed per experiment; with the unattached vs attached states (labelled Noc and MG respectively) were separated into two and processed for MS using FASP, with one immunoprecipitation being digested with 1.5µg Trypsin, and the other with 1.5µg V8 (**Figure 4.5**). As prior experiments had confirmed that no kinetochore proteins were seen in negative immunoprecipitation samples, the negative immunoprecipitations were not run on the MS systems. Instead, as we were looking for the relative difference between Nocodazole and MG132 samples, they acted as each other's internal control. Samples were TiO_2 enriched in parallel and run on a QEX system on a 30 minute gradient. Analysis using MaxQuant allowed recombination of the samples to create a single 'sample' for each of the Nocodazole and MG132 fractions. Analysis using RawMeat revealed a good digestion efficiency (**Figure 4.5B**).

The experiment was performed in quadruple and analysed using Perceus software (Tyanova et al. 2016). Over the course of all four experiments 795 phospho-sites were identified, of which 131 were on proteins related to the kinetochore. These hits were filtered based on three factors; a measured intensity in at least one sample (which reduced the list to 112); a localisation score of >75% (91 hits), and with a score of over 50. This generated a final list of 82 kinetochore-related hits.

The exception to the filtering was when two adjacent phosphorylatable residues were each given a localisation score of 50%, meaning the software was sure one of them

was phosphorylated but was unable to ascertain which one based on the fragmentation patterns generated. This occurred twice: Ndc80 (pThr61 and pSer62) and Knl1 (pSer24 and pSer25). Both these sites have been well studied in the past, with Knl1 pSer24 and pSer25 making up part of a SILK motif, a motif associated with PP1 binding (Wakula et al. 2003; Hendrickx et al. 2009). However, it has been shown that in the case of Knl1 the RVSF motif, not the SILK motif, is responsible for PP1 (Liu et al. 2010), as mutations of the RVSF motif alone resulted in the loss of PP1 binding to Knl1 (Nijenhuis et al. 2014). pSer24 which was found to be an Aurora B regulated phospho-site (along with pSer60 of the RVSF motif) has been suggested to be dephosphorylated by PP2A-B56 allowing PP1 to associate with Knl1 (Welburn et al. 2010; Nijenhuis et al. 2014). Validation by low-throughput techniques in the case of pSer24 therefore suggests this is the correct residue.

In the case of Ndc80 both pThr61 and pSer62 have been seen separately using MS techniques in the past with Ciferri et al. (2008) assigning pSer62 as an Aurora B-regulated site *in vitro* (Ciferri et al. 2008; Nousiainen et al. 2006; Kettenbach et al. 2011). Our data shows a single phospho-site which cannot be conclusively localised to either residue. In **Chapter 3** we identified only Ser62 with a localisation probability of 82.5%. It may be that Aurora B is capable of phosphorylating either residue. In this case it is difficult to determine conclusively which residue is phosphorylated. In the downstream handling we therefore treated the pThr61/pSer62 site as a single entity.

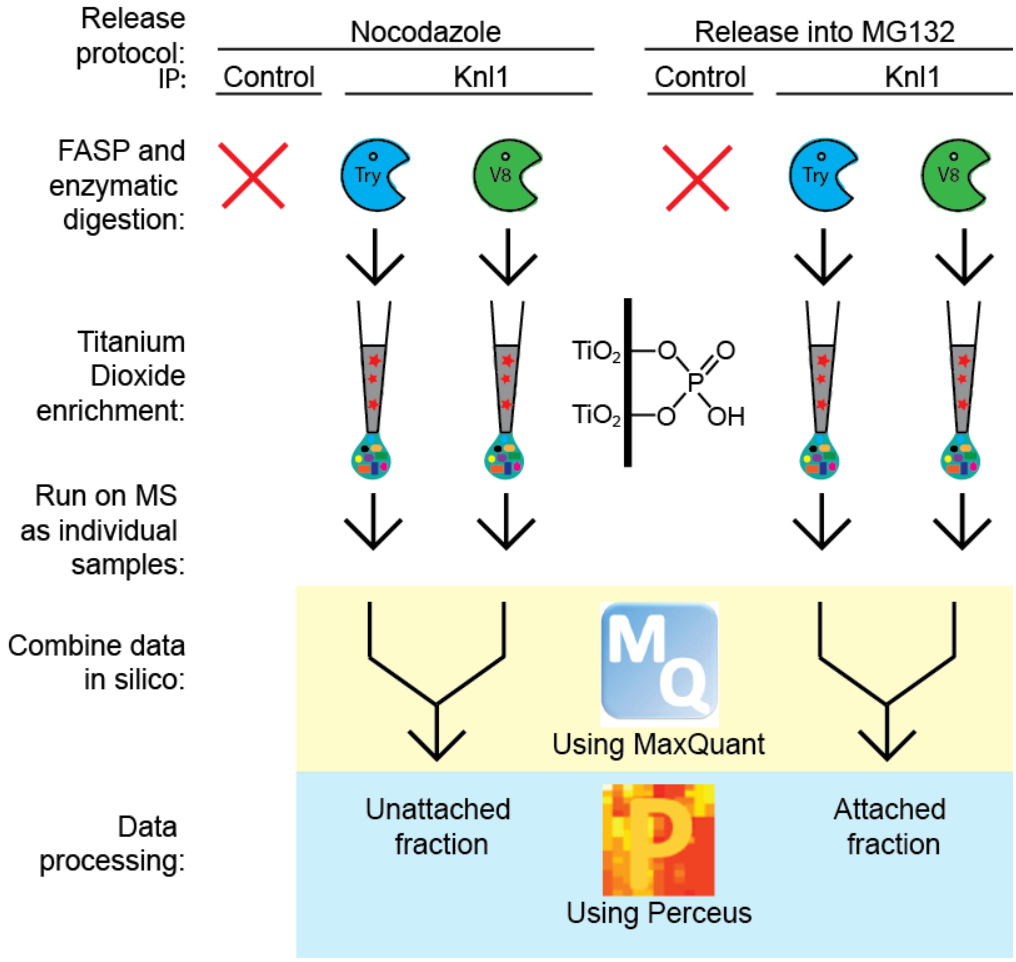
A comparison of the Pearson correlation coefficient indicated that the first experiment was much less comparable with the others (**Figure 4.6**). On average, comparing experiment 1 to experiments 2-4, the Pearson correlation coefficient (r) = 36.1% in Nocodazole and 42.6% in MG132. Whereas comparing experiments 2-4 to each other, r=76.83% in Nocodazole and 74.87% in MG132. We therefore excluded experiment 1 from statistical tests.

A two sample T-test was used to identify phospho-sites which differed significantly between the Nocodazole and MG132 samples. This data is shown on the volcano plot which separates phospho-sites based on the difference of their means between Nocodazole and MG132 fractions (x-axis) and $\log_{10}$ p-value (y-axis) (**Figure 4.7A**). The dotted line represents a p-value of 0.05 (equivalent to $-\log_{10}(0.05)=1.301$).

Out of the 82 sites found only 15 were significantly different between the two states. 18 phospho-sites were novel, seven of these were significantly different between the two states and are discussed later. The vast majority were on Knl1. The unchanging sites included 21 sites which corresponded to the motif (S/T)-P making them likely MAPK or Cdk1 sites. Some, such as Bub1 pSer661, are known Cdk1 sites (Dumitru et al. 2017). 15 others showed similarity to a Plk1 kinase consensus motif (D/E/N/Q)-X-(S/T)- Φ.

Finally, a few phospho-sites looked like Aurora sites with $(R/K)_{1-3}$-X-(S/T) like sequences. Of these, three out of the five are the SSILK and RVSF motifs on pSer24/Ser25 and pSer60 of Knl1 which are known Aurora B sites. Previous literature has suggested that these sites are dephosphorylated upon attachment to allow PP1 binding (Welburn et al. 2010; Nijenhuis et al. 2014). Our data shows no significant difference between the Nocodazole and MG132 condition This may be because of technical reasons (eg missing values with the pSer24/Ser25 phospho-peptide seen in only one out of the four experiments compared to three times in the MG132 experiments) but alternatively could indicate that these Aurora B sites remain phosphorylated for longer than previously assumed. However, it is a more general point that we saw fewer Aurora B type phosphorylation sites than in our previous data set.

A.


Release protocol:
IP:
Nocodazole
Release into MG132
Control
Knl1
Control
Knl1
FASP and enzymatic digestion:
Try
V8
Try
V8
Titanium Dioxide enrichment:
TiO2
TiO2
O
P
O
O
OH
Run on MS as individual samples:
Combine data in silico:
Using MaxQuant
Data processing:
Unattached fraction
Attached fraction
Using Perceus

B.

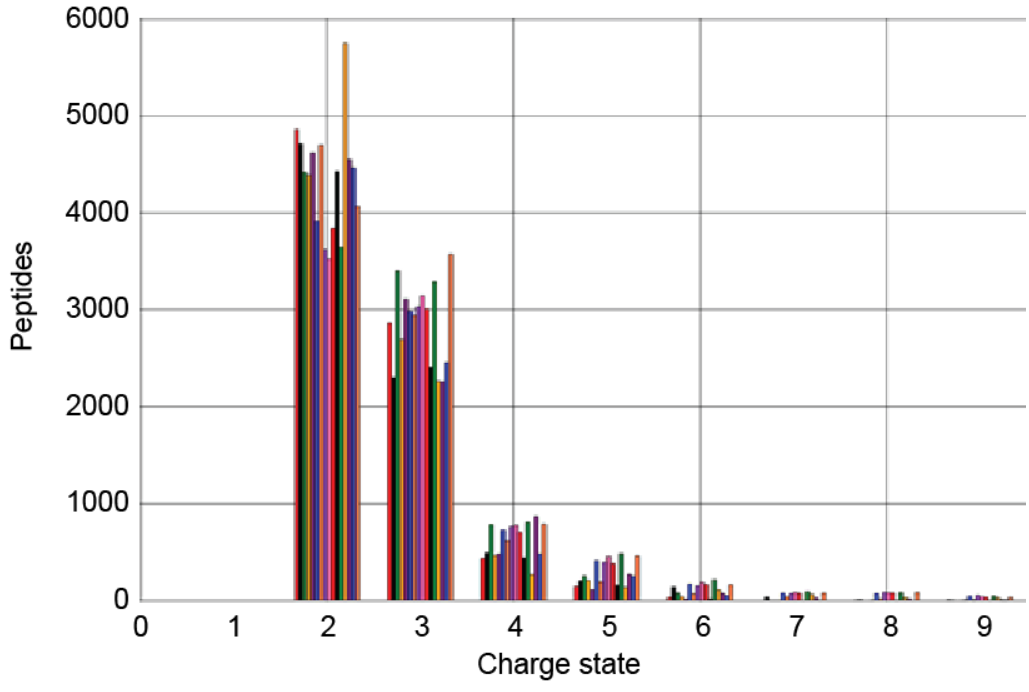

Peptides
6000
5000
4000
3000
2000
1000
0
0
1
2
3
4
5
6
7
8
9
Charge state

Figure 4.5 MS pipeline

A) Schematic showing the design of the experiment. 9 large HeLa dishes per condition were released into either Nocodazole or MG132 as previously described. Each sample was split into 3 at the immunoprecipitation stage (2 positive Knl1 and 1 negative control IP). The Knl1 samples were then processed separately being digested with different enzymes (V8 and Trypsin respectively). Data was recombined *in silico* to generate a single 'sample' per attached condition. B) Each FASP sample was run on a 30 minute gradient on a LC-QEX Mass spectrometry machine. Their peptide charge status was analysed via the RawMeat software package. Graph represents the distribution of peptide charge states, with peptide number on the y-axis and charge state on the x-axis. Each colour represents a sample. The high trend of 2+ and 3+ charge states denotes a good digestion by both V8 and Trypsin.

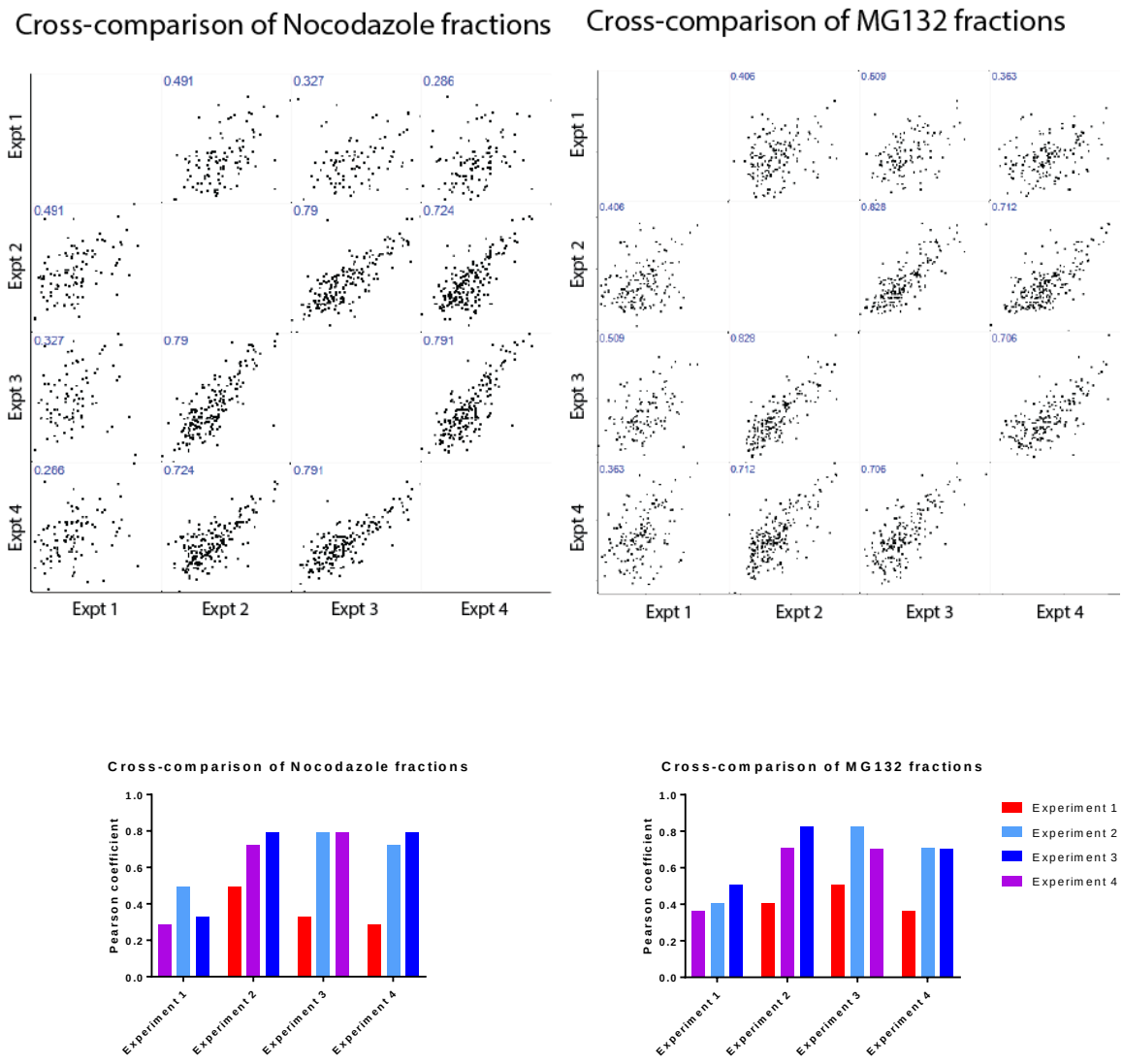


Figure 4.6 Analysis shows poor comparison of first experiment

A) The Knl1 dataset made up of four independent repeats was compared for its consistency. Data shows Pearson coefficient correlations for each experimental sample with respect to other samples digested with the same enzyme. B) The value of Pearson coefficient correlation for each comparison is shown graphically and denotes the similarity between the comparable samples. This shows the poor quality of the first test experiment



Figure 4.6 The majority of phospho-sites show reduced levels of phosphorylation upon MT attachment

Volcano plot of MS data shows the kinetochore-related proteins found. Most points are at the zenith of the plot showing most phosphorylation sites show no difference

in abundance between the attached and unattached state (on the x-axis) and therefore show very low p-values (on the y-axis). Points are colour coordinated with Bub proteins shown in blue, Knl1 in red, Ndc80 in green, Dsn1 in purple. Phospho-sites with a p-value of over 0.05 (shown by the dotted line) have the amino acid next to their data point.

4.2.6 Ndc80 pThr61/Ser62 and pSer69 show higher levels of phosphorylation upon MT attachment

We identified pThr61/pSer62 and pSer69 as phosphorylated sites in Ndc80. Previous *in vitro* data has identified these sites as Aurora B-regulated sites (Ciferri et al. 2008). The working hypothesis within the field is that Aurora B sites on the N-terminal of Ndc80 are largely lost upon amphitelic attachment due to the spatial separation of the outer kinetochore from centromeric Aurora B upon kinetochore attachment and the development of tension (DeLuca et al. 2011; Liu et al. 2009). Our data does not seem to support that for these two individual sites. They were significantly upregulated in the attached fraction. The phosphorylation site were seen consistently in all MG132 fractions with average intensity values of 1.94E9 and 1.37E9 for pThr61/pSer62 and pSer69 respectively. In the Nocodazole fractions they were less well identified; pThr61/pSer62 was seen in experiments 2 and 4 and pSer69 in experiments 2-4. However, in the Nocodazole fractions in which the phosphorylation sites were identified, there is a substantial drop in the intensity of the phosphorylation with intensity values on average sixty times and thirty times lower than in the MG132 fraction (**Figure 4.7**).

It is clearly not the case that pThr61/Ser62 and pSer69 are incompatible with MT attachment. Indeed, other MS studies which have used taxol-stabilised cells have

identified pThr61 and pSer62 and pSer69 (Kettenbach et al. 2011; Nousiainen et al. 2006). In agreement with our data, new work by DeLuca et al. (2018) suggests that pSer69 is regulated by Aurora A rather than Aurora B. Consistent with our data, they find that pSer69 is unusual compared to other tested phosphorylation sites (Ser44 and Ser55) in being maintained at a stable level from prometaphase to metaphase. Whilst our data agrees with the maintenance of the phospho-site we see a large increase in phosphorylation of our sites in the MG132 fractions. .

Earlier work by Zaytsev et al. (2014) suggested that low levels of Ndc80 phosphorylation need to be maintained in the attached state for correct K-MT dynamics in metaphase. Their findings showed retention of one Ndc80 phosphorylation is sufficient to maintain normal kinetochore oscillations, inter-kinetochore distance and relative k-fibre intensity, with a single phosphorylation fitted most closely with WT conditions. In the absence of any phosphorylation (i.e. Ndc80-9A mutant) there is a dampening effect on kinetochore oscillations, and an increase in the inter-kinetochore distance and relative k-fibre intensity.

The similarity in trend of pThr61/Ser62 and pSer69 may suggest it is regulated in the same way. Zaytsev et al. (2014) found that the requirement for maintenance of normal metaphase activity was not specific to Ser69 with other phospho-mimetic changes able to recapitulate this result. Deluca et al. (2018) also found that movement of the amino acid sequence containing Ser69 had no effect on Aurora A's ability to phosphorylate it.

This data confirms DeLuca et al. (2018) and Zaytsev et al. (2014) showing *in vivo* some Ndc80 phospho-sites are actually upregulated during metaphase. This suggests the view of Ndc80's N-terminal tail being phosphorylated by Aurora B in prometaphase, and being dephosphorylated after attachment, is overly simplistic. I suggest that it is not the case that Ndc80 phosphorylation sites are simply switched off at metaphase, but rather that there is an exchange of responsible kinase from Aurora

B to Aurora A. Rather than phosphorylation breaking K-MT connections, in metaphase they have a more subtle effect altering MT-dynamics.

	Seen in how many samples:		Average intensity:		Intensity nocodazole/ Intensity MG132
	Nocodazole	MG132	Nocodazole	MG132	
pThr61/pSer62	3	4	6.49E+07	1.94E+09	29.92
pSer69	2	4	2.26E+07	1.37E+09	60.58

Figure 4.7 Ndc80 phospho-sites increase in intensity post-attachment

A comparison of the phospho-data collected on Ndc80 phospho-sites showing the relative fold-change upon attachment

4.2.7 Knl1 sites are lost upon MT attachment

Of those phospho-sites which are significantly reduced following K-MT attachment the majority are on Knl1. Knl1 is known to be phosphorylated by Mps1 on MELT motifs which create a binding motif for the Bub complex to bind (Primorac et al. 2013) (See **0**). Upon microtubule binding Mps1 is lost from the kinetochore and phosphatases dephosphorylate Knl1 (Nijenhuis et al. 2014; Espert et al. 2014). This system has been validated by the use of phospho-specific antibodies against specific MELT motifs (Yamagishi et al. 2012; Espert et al. 2014). Other work has used Knl1-fragments with

varying MELT motifs to try and assess which MELTs are capable of generating a SAC response (Vleugel et al. 2013; Vleugel et al. 2015). Attempts to use immunoprecipitations have identified MELT7 *in vivo* and *in vitro* phosphorylation of MELT12 and MELT17 containing fragments has been found (Vleugel et al. 2015)

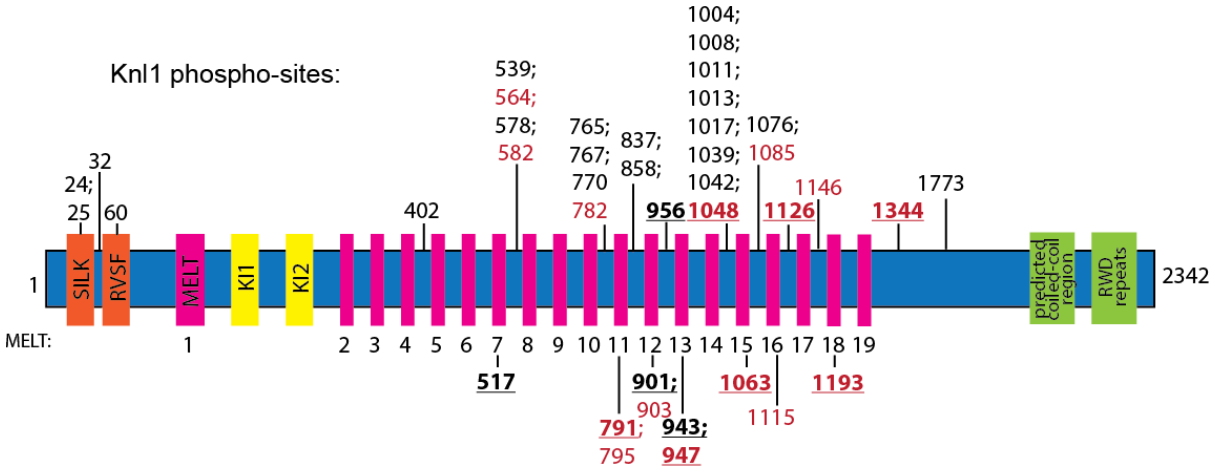
Our data has allowed us to identify which MELT motifs are active *in vivo*. We find multiple MELT motifs whose phosphorylation is significantly reduced upon MT-attachment. Of these MELT11, MELT15, and MELT18 have not been seen *in vivo* before (**Figure 4.9A**). We have indirect evidence that MELT7 may be active as the downstream SHT motif is phosphorylated. As discussed in **Chapter 3** the sequence of MELT7 is MELTKSHT leading to a separation of the MELT motif from its SHT motif into two separate peptides by the tryptic digest. Again consistent with **Chapter 3** we did not observe the MELT7 peptide. It is a possibility this peptide has qualities which make it difficult to observe by mass spectrometry. Comparing our *in vivo* data with Vleugel et al. (2015) suggests some overlap, with MELT7, MELT11, MELT12 able to recruit at least 50% normal Bub1 and BubR1 levels to the kinetochore. However they were unable to identify active MELT13, MELT15 and MELT18 which all give low relative levels of Bub proteins in their data set. Our data set is in line with the expected number of active MELTs, and represents a clear advance on previous methods and attempts to identify active MELT motifs (Zhang et al. 2014; Vleugel et al. 2015).

There were 11 significant Knl1 phosphorylation sites which were decreased in the MG132 fraction, of these 7 were associated with MELTs (**Figure 4.9B**). Of the remaining four, three are novel with only pSer956 being seen previously (Sharma et al. 2014; Mertins et al. 2013; Zhou et al. 2013; Santamaria et al. 2011; Hegemann et al. 2014; Olsen et al. 2010; Malik et al. 2009; Nousiainen et al. 2006). pSer956 seems likely to be a target of a proline-directed kinase as it has a Proline sequence at the +1 position. We considered whether any of the others may also be Mps1 sites. However

Mps1 has a strong preference for Thr residues with only 10% of the phospho-sites found *in vitro* being Ser (Hennrich et al. 2013). Overall they look very similar to Plk1 sites which are characterised by E/D/N/Q at the -2 and a hydrophobic residue at +1 (Dou et al. 2011). However it is impossible to assign them to Plk1 confidently due to the relative similarity between Mps1 and Plk1's consensus sequences (Dou et al. 2011).

Two sites on the Bub proteins were seen as significant. Indeed the most highly significantly reduced site was Bub1 pSer307 which has been found in a variety of other MS studies previously (Sharma et al. 2014; Zhou et al. 2013; Hegemann et al. 2014; Dephoure et al. 2008; Mertins et al. 2013). BubR1 pSer384 was also seen with a p-value <0.05. This has also been reported before by Grosstessner-Hain et al. (2011) and Santamaria et al. (2011). However the loss of this phospho-site can be largely attributed to the loss of the Bub proteins from the kinetochore upon SAC silencing. Once the relative loss of Bub1 and BubR1 from the kinetochore is factored in most of the phosphorylation events appear unchanged over the course of attachment.

A.



B.

Gene name	Phospho-site	Localisation Probability	MaxQuant Score	p-value (-log10)	Difference Noc vs MG132	Novel Site?	Motif if relevant
BUB1	307	0.999	163.9	3.65	-3.4	No	
BUBR1	384	0.998	50.897	1.42	-1.3	No	
KNL1	517	0.999	112.82	2.22	-1.47	No	SHT7
KNL1	791	1	142.97	1.35	-2.89	Yes	MELT11
KNL1	901	1	107.92	2.52	-1.99	No	MELT12
KNL1	943	0.968	66.13	1.45	-2.65	No	MELT13
KNL1	947	0.784	66.13	1.45	-2.65	Yes	SHT13
KNL1	956	0.999	112.82	2.22	-1.47	No	
KNL1	1048	1	112.55	1.95	-5.16	Yes	
KNL1	1063	1	157.11	3.23	-1.12	Yes	MELT15
KNL1	1126	1	171.15	1.46	-1.81	Yes	
KNL1	1193	0.943	86.18	1.72	-3.25	Yes	MELT18
KNL1	1344	1	89.47	1.77	-1.35	Yes	
NDC80	61	0.499	199.8	1.39	3.17	No	
NDC80	62	0.499	199.8	1.39	3.17	No	
NDC80	69	1	199.8	1.5	2.15	No	

Figure 4.8 Knl1 is phosphorylated on multiple MELT motifs

A) Schematic showing phospho-sites seen on Knl1. Those underlined are significantly downregulated upon attachment. Those in red are novel to our study. B) Table of those kinetochore phospho-sites which are significantly altered upon attachment (p-value greater than 0.05). The last column shows any relevant data know about the sites

4.3 Discussion

4.3.1 Summary

In order to create a metaphase-like state a release protocol was developed. Several drugs were assessed for their ability to arrest cells in a pro-metaphase like state which can be released into MG132. They were compared for their ability to reform a bipolar spindle with attached kinetochores. Using the protocol developed in **Chapter 3** immunoprecipitations of Knl1 in attached and unattached states were processed by mass spectrometry. Our data shows Ndc80 and Knl1 phospho-sites exhibit a switch in behaviour upon attachment.

4.3.2 Discussion

Here we have created a methodology which allows the comparison of phospho-sites in different attachment states by combining a large-scale release protocol (**Figure 4.3**) with the MS pipeline developed in **Chapter 3**. Our data shows out of the 82 kinetochore sites identified, only 15 underwent significant levels of variation upon attachment. Of these only two Ndc80 sites were upregulated (**Figure 4.8**). The remainder were downregulated and localised to Knl1 (**Figure 4.9**). Our data does show the importance of collecting proteome data alongside phospho-data. With the Bub complexes being lost from the kinetochore as the SAC is silenced, the loss of phosphorylation could be due to the activity of phosphatase, or the absence of Bubs associating with Knl1, or a combination of both.

Compared to our data set in **Chapter 3** we were able to see fewer sites. There are various factors that may account for this; fewer samples were run (8 compared to 31); only one protein was used to isolate the kinetochore; a calyculin A treatment was not utilised (the experiments were performed prior to this final stage of optimisation). This may explain why other Ndc80 phosphorylation sites were not observed. It is interesting to posit that a comparison of the two data sets may allow us to uncover which phospho-sites are more labile, with Calyculin A being necessary to maintain those sites with the shortest half-life.

Our data, largely fits the overarching themes within the field; we do not find large numbers of significantly altered sites. Those we do identify are well studied and understood in some detail. To our knowledge, however, this is the first time multiple MELT motifs have been seen to be regulated *in vivo*. Furthermore our work supports new research on the importance of maintaining some level of phosphorylation on the N-terminal of Ndc80 (DeLuca et al. 2018; Zaytsev et al. 2014).

Although our primary focus was on the phospho-sites which exhibit differential regulation depending on attachment status there is a considerable number of unchanged sites which may be equally interesting. For example, Ser24/25 on Knl1 which in our experiments appears unchanged upon attachment but have previously been suggested to be dephosphorylated following microtubule binding to the kinetochore (Nijenhuis et al. 2014).

The release protocol was a bottle neck to the experimental setup. It was found to have variable levels of success, such that several experiments had to be aborted due to incomplete reformation of a bipolar spindle, and a largely non-attached kinetochore population. One possible change which might help this process is to follow the mitotic shake off transferring cells to a suspension flask. With gently mixing over the 3 minute wash to prevent cells clumping together by gravity we may be able to materially improve the drug release and reproducibility of the process. On the other hand we

could try to ensure greater reproducibility by increasing the length of the MG132 treatment. MG132 as with other proteasome inhibitors are toxic due to the formation of reactive oxygen species which induce apoptosis (Wu et al. 2002) and due to exhaustion of the available amino acid pool (Suraweera et al. 2012). It has been shown that these toxic effects can be alleviated adding cysteine to the growth medium to overcome amino acid starvation (Suraweera et al. 2012). This is something we will try in the future.

This protocol represents a bridge between studies of the past which have either been very large-scale or in-depth. It has been shown to be capable of generating distinct mitotic states and identifying novel phospho-sites on a range of proteins. Having established the feasibility of the protocol it would be interesting to assess how proteins whose localisation alters over the prometaphase to metaphase are phospho-regulated. Potential targets of this strategy might be the Astrin or Ska complexes and members of the MCC. The first two are recruited upon attachment to kinetochores, and the last set are recruited to unattached kinetochores and lost post-attachment.

Chapter 5: The phosphorylation of Astrin by Plk1 is critical to timely mitotic progression

5.1 Introduction

The ability to create load-bearing attachments between kinetochores and microtubules is critical to successful chromosome segregation. Central to this is the KMN network which acts synergistically to enhance microtubule binding through Ndc80 and Knl1 (Cheeseman et al. 2006). However fully-formed attachments involve multiple other proteins which help maintain the KMN network's binding to the dynamic microtubule polymers including MT binding factors such as EB1 and CLIP-170 and motor proteins such as Dynein and CENP-E (Cheeseman & Desai 2008; Kumar & Wittmann 2012). In budding yeast the Dam1 complex, made up of 10 monomers which form a ring structure, encloses the microtubule helping the kinetochore remain coupled to the depolymerising microtubule via interactions with Ndc80 (Lampert et al. 2010; Lampert et al. 2013). In metazoans the Ska1 complex, formed of three subunits (Ska1, Ska2 and Ska3) which form a W-shape upon trimerisation, is believed to be a functional homologue of Dam1, facilitating MT-k interactions and allowing kinetochores to move progressively along depolymerising microtubules (Welburn et al. 2009; Schmidt et al. 2012). Other work has also implicated the Astrin-Kinastrin complex as having a contributing role in formation of a stable MT-k interface (Kern et al. 2017).

Astrin is a mitotic spindle-associated protein which was first described in 2002 (Gruber et al. 2002) and further characterised in 2007 (Thein et al. 2007). Astrin RNA interference experiments have shown the formation of multipolar, disorganised spindles and the loss of sister chromatid cohesion (Thein et al. 2007; Gruber et al.

2002; Dunsch et al. 2011). Cells exhibit delayed chromosome congression and mitotic arrests (Dunsch et al. 2011). Furthermore depletion of Astrin eliminates CENP-E and CENP-F recruitment to the kinetochore (Thein et al. 2007). It impairs k-MT attachments causing metaphase delays, and defects in spindle bipolarity and sister chromatid cohesion (Thein et al. 2007). *In vivo* Astrin forms a complex with Kinastrin (also known as SKAP) Dynein light chain (DYNLL1), Shugoshin-like2, Plk1 and MYCBP (Schmidt et al. 2010; Dunsch et al. 2011; Kern et al. 2017). Of these Kinastrin is the only major interacting partner with Astrin binding 2 copies of Kinastrin per complex, the other interactions all appear sub-stochiometric (Dunsch et al. 2011). Astrin and Kinastrin show the same pattern of localisation; during prophase and prometaphase they localise to spindle poles and are found along spindle microtubules. As attachments form Astrin-Kinastrin is recruited to the outer kinetochore and remains associated through anaphase (Dunsch et al. 2011).

Astrin-Kinastrin's shared localisation, depletion phenotypes and the fact that depletion of one is enough to prevent localisation of the other speaks to them acting as a complex. The Astrin-Kinastrin complex localises in the opposite way to SAC components and is only recruited to attached, aligned microtubules. It is thus used as a marker for SAC-silenced kinetochores. The timing of their association with the kinetochore therefore makes a compelling argument that Astrin-Kinastrin may play a role in stabilising MT-k attachments and act as a "ready" signal demonstrating a readiness for the onset of chromosome segregation.

Recent work has elucidated how Astrin-Kinastrin may facilitate correct attachments by acting as a cross-linker between MT and kinetochores. The complex is known to interact with microtubules through Kinastrin. Kinastrin has two distinct ways of interacting with MT; first directly through 135-225aa region which interacts with the interface between α- and β-tubulin (Friese et al. 2016; Kern et al. 2016), secondly Kinastrin can bind EB1 and EB3 proteins via a SXIP motif granting plus end tracking

activity (Tamura et al. 2015; Wang et al. 2012). Together these interactions allow the Astrin-Kinastrin complex to stream along microtubules towards kinetochores (Dunsch et al. 2011). Indeed, Kinastrin has been shown to aid MT polymerisation *in vitro* suggesting a role in the stabilisation of MT plus ends (Dunsch et al. 2011).

Astrin-Kinastrin's binding partner at the kinetochore has long been unknown, with conventional MS only revealing members of the complex. Recently Kern et al. (2017) managed (with the help of formaldehyde crosslinking and MS) to identify peptides of Ndc80 complex components in an Astrin immunoprecipitation. Their work suggests that the Astrin interacts with kinetochores via at least two domains; its N-terminal region (aa1-464) interacts with Ndc80 through Ndc80's CH domain (aa 80-201), and Astrin's C-terminal region (aa694-1193) forms another kinetochore interaction site with an as yet unidentified kinetochore component. Kern postulates it may be CENP-L/N which appears in reciprocal immunoprecipitations however this has not yet been fully validated. These results suggest Astrin could act as a final MT-k stabiliser with Kinastrin working alongside Ndc80 in making links to microtubules.

Although conserved throughout vertebrates, in rodents viability is not compromised in Astrin and Kinastrin knockouts but it does affect fertility, so may be required for meiosis (Grey et al. 2016; Xue et al. 2002). However it is clearly important in humans with Astrin and Kinastrin being implicated in disease. Kinastrin and Astrin have both been deemed oncogenes (C. S. Lee et al. 2014; Zhang et al. 2016). Studies in lung and cervical cancer have shown that overexpression of Astrin can lead to a poor prognosis (Välk et al. 2010; Yuan et al. 2014). In a study of prostate cancer it was shown downregulation of Astrin reduced tumour volume and ability to metastasise *in vivo* (Zhang et al. 2016). Lee et al. (2014) found point mutations of Kinastrin in 19% of cutaneous squamous cell carcinomas. Further analysis found the most common mutation (p.Ser24Phe), never identified in non-cancerous skin, arose early in tumorigenesis with the authors postulating these cells may be more prone to

aneuploidy. However, more recent analysis of Kinastrin revealed that the most commonly expressed isoform of Kinastrin does not contain the Ser24 amino acid in the expressed protein, raising doubts over the role of the residue in carcinogenesis (Kern et al. 2016). Nevertheless, taken together these studies suggest that the correct expression and functioning of the Astrin-Kinastrin complex is critical for accurate error-free mitosis.

Whilst considerable work has been performed to elucidate the activity of Astrin and Kinastrin, little is known about how their sub-stochiometric binding partners act as part of the complex. Of particular interest is Plk1, which has a known role in regulating kinetochore-microtubule attachments, during prometaphase its activities help stabilise initial attachments (Liu et al. 2012). It exhibits a very dynamic localisation pattern over the course of mitosis in line with its varied roles over the course of mitosis (Barr et al. 2004).

5.1.1 Aims

- Investigate biochemically how Plk1 interacts with the Astrin-Kinastrin complex
- Understand the effect of Plk1's binding to Astrin

5.2 Results

5.2.1 Plk1 and Astrin interact during mitosis

Plk1 is well established as a key driver of cell cycle progression, acting on hundreds of different phospho-sites on a multitude of targets (Kettenbach et al. 2011). This in itself has created difficulties in picking apart individual biological functions, particularly later in mitosis, as inhibition or depletion of Plk1 leads to the formation of monopolar spindles. Plk1 is known to have multiple targets at the kinetochore including INCENP, Mps1, Bub1 and Cdc20 (Liu et al. 2012; Ikeda & Tanaka 2017; von Schubert et al. 2015; O'Connor et al. 2016; Jia et al. 2016). Lera et al.'s (2016) work shows that although direct binding to the kinetochore is required for correct alignment and separation of chromosomes, direct binding to target proteins is probably not required. Plk1 may, once bound, act on a small number of interactors within range.

The location of Plk1 was assessed over the course of mitosis and analysed by immunofluorescence to see if it co-localised with Astrin. HeLa cells were grown asynchronously and stained for both Plk1 and Astrin (**Figure 5.1A**). Consistent with previous data Plk1 is initially recruited to centrosomes during prophase (Golsteyn et al. 1995). During prometaphase it also binds the inner centromere and can be seen as a single foci. As chromosomes become attached to the mitotic spindle, Plk1's localisation shifts subtly. Rather than a single point it creates a dumbbell structure the 'bell' of which co-localises with Astrin (see **Figure 5.1B**). As anaphase progresses Plk1 can still be observed on the kinetochores, yet the bulk of Plk1 is relocated to the midzone.

The co-localisation of Astrin and Plk1 fits with previous published work from our lab which documented an interaction between the Astrin-Kinastrin complex and Plk1.

Dunsch et al. (2011) found Plk1 as a sub-stochiometric component of the complex through both Astrin and Kinastrin pull-downs. In order to confirm this interaction we performed reciprocal immunoprecipitations for both Astrin and Plk1 (**Figure 5.1C**). Western blots showed that both were capable of isolating each other, confirming Plk1 as a bone fide interaction partner of the Astrin-Kinastrin complex.

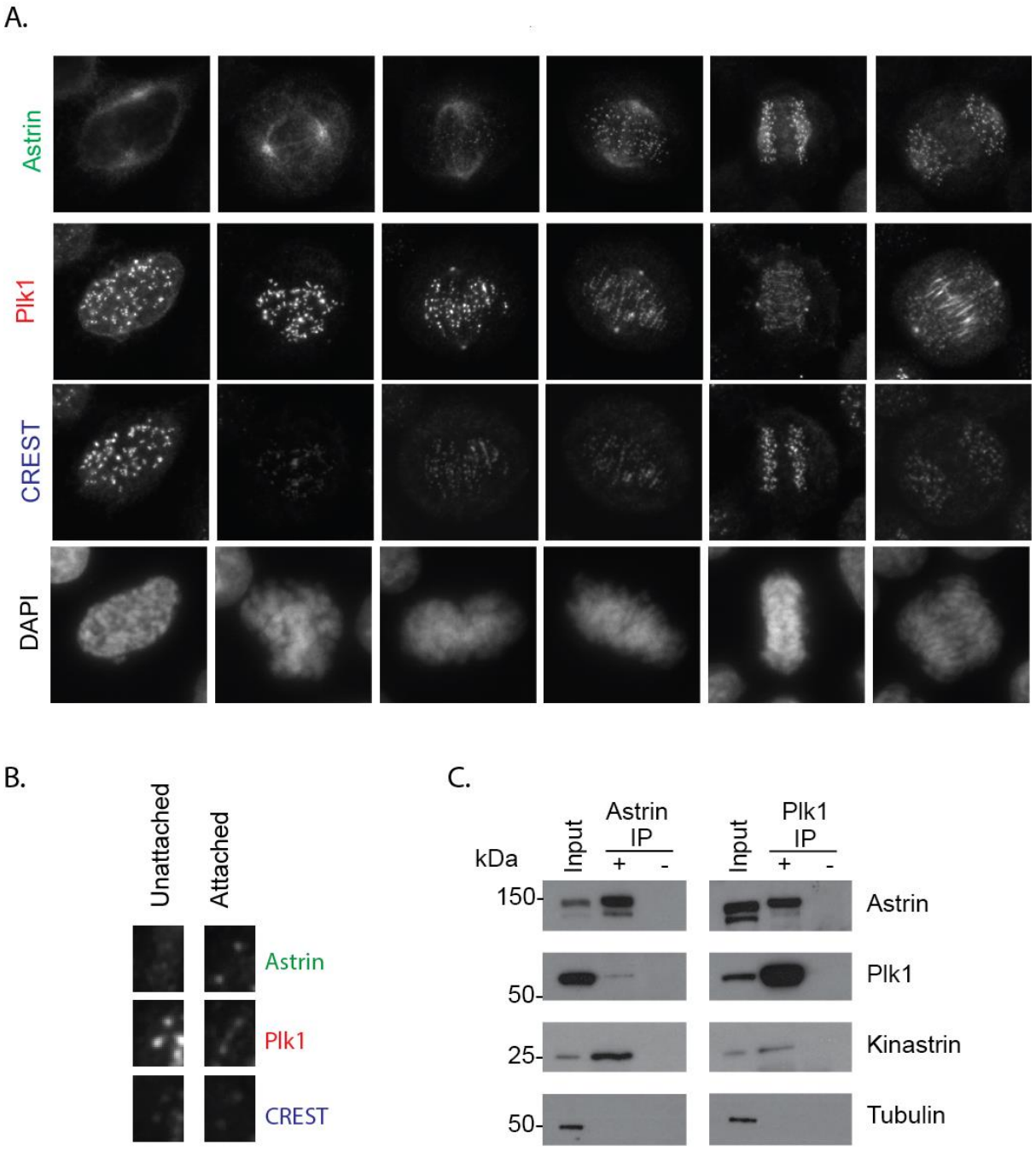


Figure 5.1: Plk1 and Astrin do interact during mitosis

A) Asynchronous HeLa cells were stained with Plk1 and Astrin. Upon Astrin recruitment to the kinetochore at metaphase, Plk1 co-localises with Astrin. B) Blow up of unattached and attached kinetochores shows upon attachment Astrin and Plk1 are localised at the kinetochore. C) HeLa cells were arrested with STLC for

14hours, cells were lysed and Astrin and Plk1 immunoprecipitations were performed. Western blots were run for members of the Astrin complex and both interactors were able to isolate each other. Tubulin was run as a negative control.

5.2.2 Plk1 binds via its PBD through a PBD-binding motif on Astrin

Next, we wanted to investigate whether Plk1 was a direct interactor of Astrin or whether it was binding through another member of the complex. Astrin's amino acid sequence contains three potential PBD binding motifs; SS65/66, ST110/111 and ST936/937. In order to determine whether any of these are required for Plk1 binding we used Flag-Astrin constructs where the candidate PBD binding sites had been mutated to a double alanine. These were transfected for 24hrs into HEK293T cells before an overnight Nocodazole arrest. Cells were collected via a mitotic shake-off and a Flag-immunoprecipitation was performed. Corroborating previous data in the lab, western blots showed that Plk1 binds Astrin through a single PBD-binding motif, ST110/111 (**Figure 5.2**). Western blots also confirmed that the mutant PBD-binding region did not affect complex formation, with both Kinastrin and DYNLL1 still associating with Astrin. Overall this data confirms that Astrin and Plk1 are direct interactors.

To investigate Plk1's method of binding we performed a far western blot. Purified Flag=Astrin^{WT} and Astrin$^{ST110/111AA}$ were incubated with active Cdk1-cyclin B to allow the PBD binding site to be primed. Samples were run on a gel and renatured before being incubated with purified GST-Plk1 with either a wild-type or mutant polo box domain (PBD^{WT} and PBD^{HKAA} respectively). Samples were then western blotted for GST and Astrin (**Figure 5.**3B). A coomassie stain was also performed to show the presence of the negative control - GFP protein (**Figure 5.3A**). The Astrin western blot

confirmed equal loading and the GST blot showed that both the PBD and its binding site ST110/111 are required for the Astrin-Plk1 interaction to occur.

A.

3 Possible PBD-binding sites:

SS65/66:	SNNSSPVDF
ST110/111:	QISSTPKTS
ST936/937:	EPESTPVPL

B.

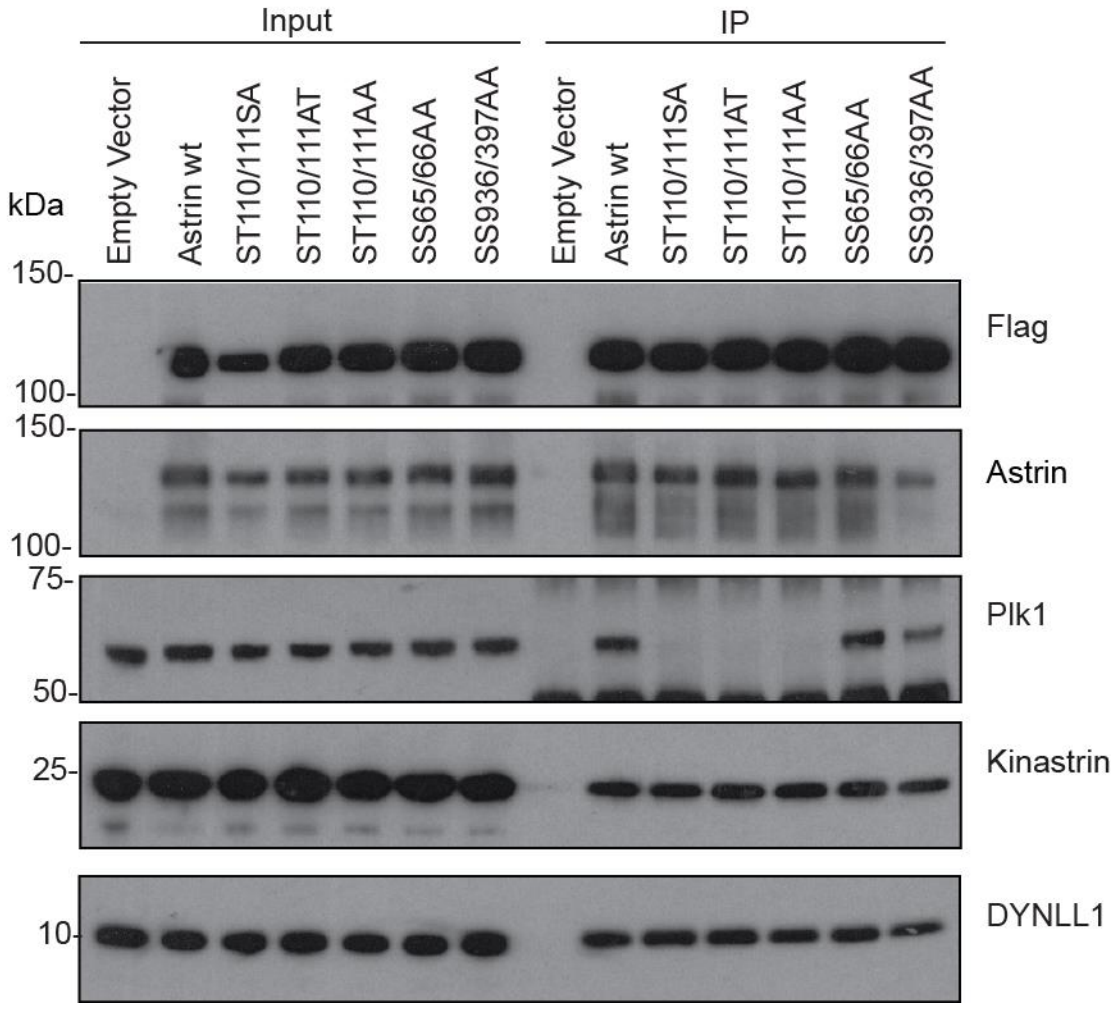


Figure 5.2 Plk1 binds Astrin through ST110/11

A) Shows the three potential PBD-binding sites within Astrin. B) Flag-tagged Astrin proteins containing mutated PBD-binding regions were transfected for 24hrs into HEK293T

cells. HEK293T cells mitotic were arrested for 14hrs with STLC before a mitotic shake-off was performed. Flag IP's were performed and eluted in laemmli buffer. Western blots were performed to analyse the binding of Plk1. Data shows point mutants of either of the 110/111 residues was sufficient to prevent Plk1 associating with Astrin.

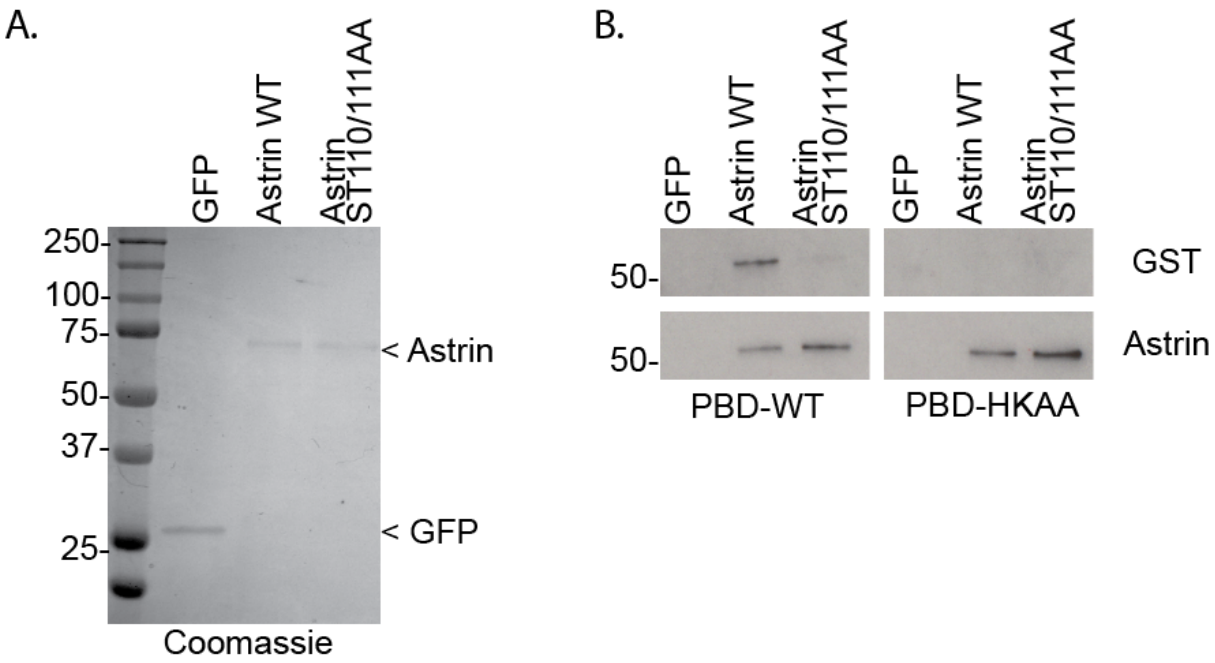


Figure 5.3 Plk1 binds Astrin through its PBD site

A) His-tagged Astrin constructs (either WT or ST110/111AA) or GFP protein (as a negative control) was loaded onto a coomassie gel and stain to confirm samples equal loading of the Astrin constructs. B) 1µg of His-tagged Astrin constructs (either WT or ST110/111AA) or GFP protein was incubated with 100ng Cdk1/CycB1 (Abcam) then denatured in laemmli buffer. Samples were transferred onto a nitrocellulose membrane, reanatured and incubated with 1 µg of His-GST-tagged Plk1-PBD constructs (either WT or HKAA mutants) for 8hrs. The far western confirms Plk1 binds via its polo box domain interacting with Astrin ST110/111AA.

5.2.3 Plk1 phosphorylates Astrin in vivo

Having confirmed that Plk1 directly interacts with the Astrin-Kinastrin complex through a binding site on Astrin we wanted to investigate whether Plk1 phosphorylates Astrin. HeLa samples were treated with a variety of drugs and inhibitors to mimic different mitotic states (described below). Western blots were run on the lysate to see if Astrin ran differently which might be suggestive of post translational modifications being present (**Figure 5.4A**).

This data clearly shows Astrin undergoes substantial changes during mitosis. When cells are arrested in S-phase using thymidine, Astrin presents as a duplet band which shifts up to a single band as cells enter mitosis (in Nocodazole). During an STLC arrest, which creates a monopolar spindle, we expect some of the kinetochores to be attached. Here Astrin seems to be slightly more highly phosphorylated than in the Nocodazole condition. In the presence of BI-2536, a Plk1 inhibitor, the phosphorylation level drops slightly, back to the level found in the Nocodazole condition. This suggests that in the presence of microtubules Astrin becomes phosphorylated by Plk1. Finally, of particular interest is the MG132 sample which clearly shows that Astrin, in a situation where all kinetochores are attached and stabilised, is even more highly shifted. These changes are most likely caused by phosphorylation.

In order to investigate Plk1's activity on Astrin further we undertook a MS-based approach where we compared samples with and without Plk1 inhibitor, BI-2536. Two populations of GFP-Astrin cells were arrested overnight in STLC. One of the populations was treated for 30mins with BI-2536 prior to mitotic shake-off; the other was left untreated. Large-scale GFP pull-downs were performed and samples were eluted with glycine followed by urea. Western blots were used to confirm the success of the immunoprecipitations (**Figure 5.4B**). Samples were then prepared by FASP;

10% was taken for a proteomic analysis whilst the remainder was TiO_2 enriched. Proteomic analysis confirmed western blot results showing the amounts of Astrin immunoprecipitated were fairly similar between the two conditions, allowing us to assign any differences in phosphorylation level to activity of kinases as opposed to differences in efficiency of pull-down (**Figure 5.4C**). All members of the Astrin-Kinastrin complex were identified in the proteomic analysis with the exception of Sgo2 (**Figure 5.4D**). This is in agreement with previous in odata which showed Sgo2 interacts at very low levels and was only observed by mass spectrometry in Kinastrin immunoprecipitations (Dunsch et al. 2011).

Our data revealed that although Astrin is highly phosphorylated, with 53 sites identified, only a few sites are dependent on Plk1 (**Figure 5.5A**). Of those that remain constant, one is the Cdk1 site ST110/111, confirming Plk1 is not able to self-prime. Analysis indicated there were four probable Plk1 sites (**Figure 5.5B**). Our data shows these sites were all strictly restricted to the STLC samples, and completely absent from the BI-treated samples. However as discussed in previous chapters, the experimental design can lead to phospho-peptide loss. Although all sites are clearly very reproducible, pSer157 and pSer353 were only observed in three experiments each, which accounts for the lower p-value for these sites (**Figure 5.6**). All these sites were seen with high localisation scores apart from pSer411, which has two phosphorylatable residues directly beside it hindering the assignment (**Figure 5.7**).

Ser353 fits with the Plk1 consensus motif of (E/N/D(Q))X(S/T)$\oplus$ (Nakajima et al. 2003; Santamaria et al. 2011; Dou et al. 2011). Santamaria et al. noted in their analysis that although their work had broadened the Plk1 consensus motif, from the original (D/E)-X-(S/T)-Φ sequence, it still did not account for all Plk1 substrates. Our phospho-sites, of Ser157 and Ser159, both have S/T in the -2 sites (**Figure 5.5C)**). Also if Ser411 is a misassignment and the phosphorylation is actually present on Ser413, this too would

have a phosphorylatable residue two amino acids upstream. Interestingly in Santamaria et al.'s data there were numerous phospho-sites with the motif (S/T)-X-(S/T)-Φ which were validated as Plk1 sites using *in vitro* phosphorylation assays. The phosphorylation of the (S/T) at the -2 position would create an acidic site mirroring a Plk1 consensus motif. It is intriguing to suggest that phosphorylation of Ser155 would create a sequence similar to the Plk1 consensus motif, leading to Plk1's activity at Ser157 which would then stimulate the phosphorylation of Ser159. In this system it is not clear if the primary upstream residue is phosphorylated by another kinase or Plk1 itself. Upon binding Astrin, Plk1 may have a low level of activity allowing phosphorylation of these upstream sites, which then stimulates its activity creating a positive feedback loop.

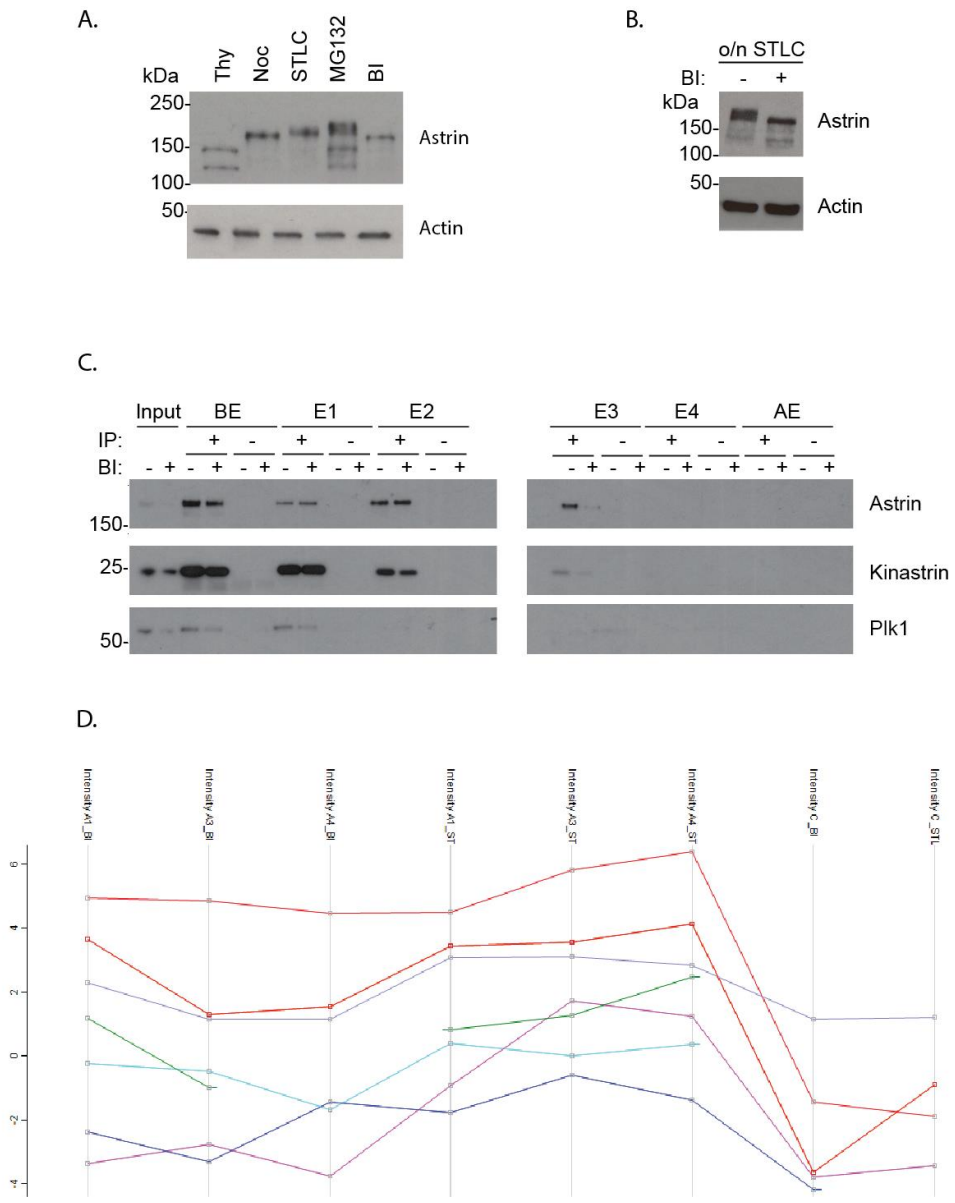
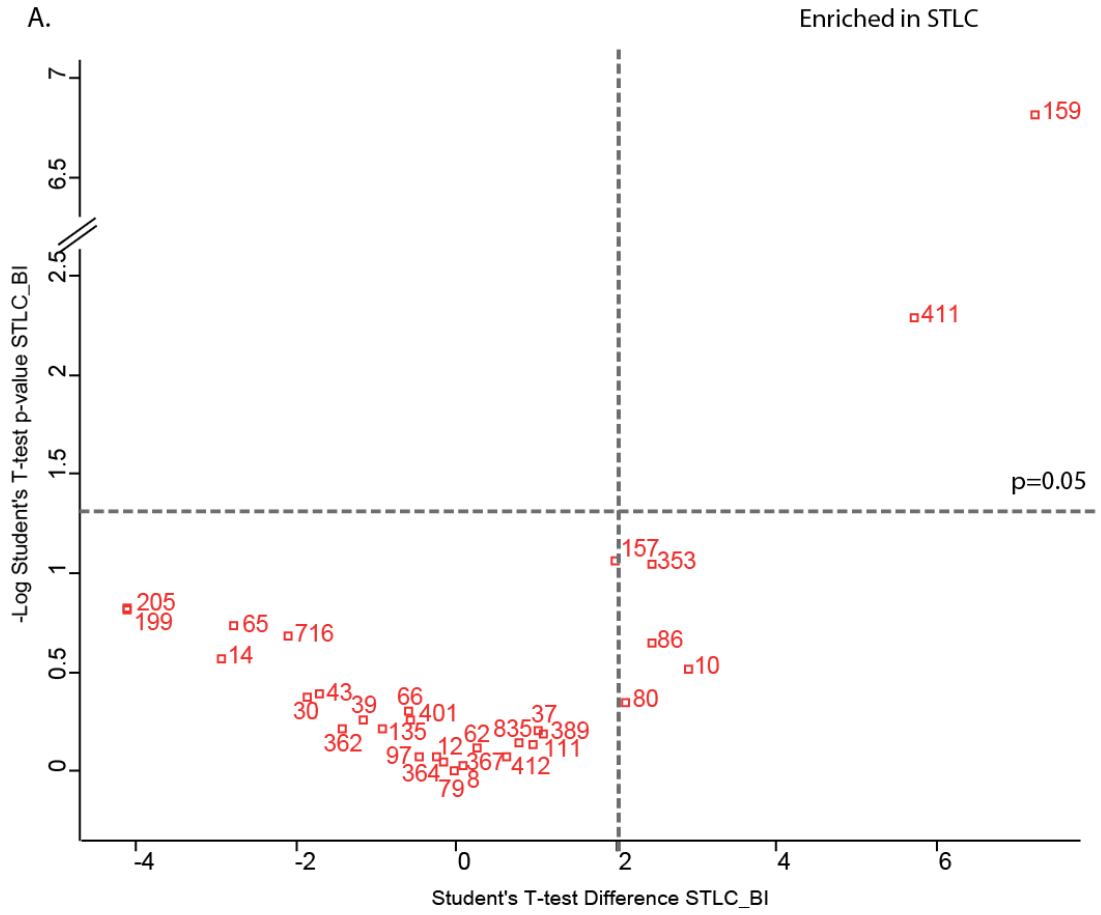


Figure 5.4 Astrin is phosphorylated by Plk1

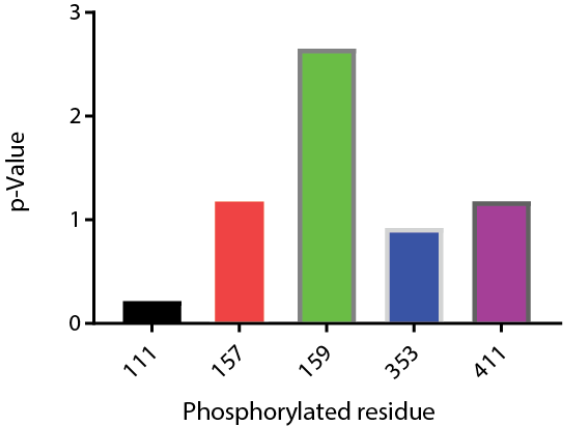
A) HeLa samples were treated for 14hrs with one of: thymidine, Nocodazole, STLC, MG132 or BI-2536. Samples were collected via mitotic shake-off. Following lysis Astrin samples were western blotted and Astrin's running pattern was analysed. B) HeLa samples were treated overnight in STLC, one sample was inhibited with BI-2536 for 30minutes. Following lysis Astrin samples were western blotted. C) HeLa cells were arrested for 14hrs in STLC, Half the samples are treated for 30mins with +BI-2536 prior to collection via mitotic shake-off. Astrin immunoprecipitations of

STLC and STLC+BI-2536 are performed, samples were eluted with Urea and western blotted to confirm elution and immunoprecipitation. BE= before elution, AE= After elution, E1-4= elutions 1-4. D) Proteomic analysis of the Astrin immunoprecipitations showed Astrin levels were largely equivalent between conditions. Astrin is shown in orange, Kinastrin in red, GFP in Green, Plk1 in grey and Dynein light chain in blue

A.



B.



C.

Residue	Amino acid sequence
S157	DtMAETNSISLNGP
S159	MAETNSISLNGPLRT
S353	LEKGVNTSVMLENLR
S411	VGTkHSTSETEQLLC

Figure 5.5 Plk1 phosphorylates Astrin at 4 residues

A) Volcano plot showing Astrin phospho-sites. Numbers represent the amino acid which is phosphorylated. On the y-axis is the p-value - anything over 1.3 is significant (p-value of 0.05). On the x-axis is the fold change between experiments. Phospho-sites only present in STLC fall on the right hand side of the volcano plot. B) A graph of the p-value for Plk1-dependent sites in comparison with the confirm Cdk1 site (p111) shows Cdk1 site is not significantly altered in our experiment whilst those suspected Plk1-dependent sites have values greater than 1. C) Table showing the amino acid sequence of Plk1-dependent phospho-sites. The phosphorylated residue is shown in red font.

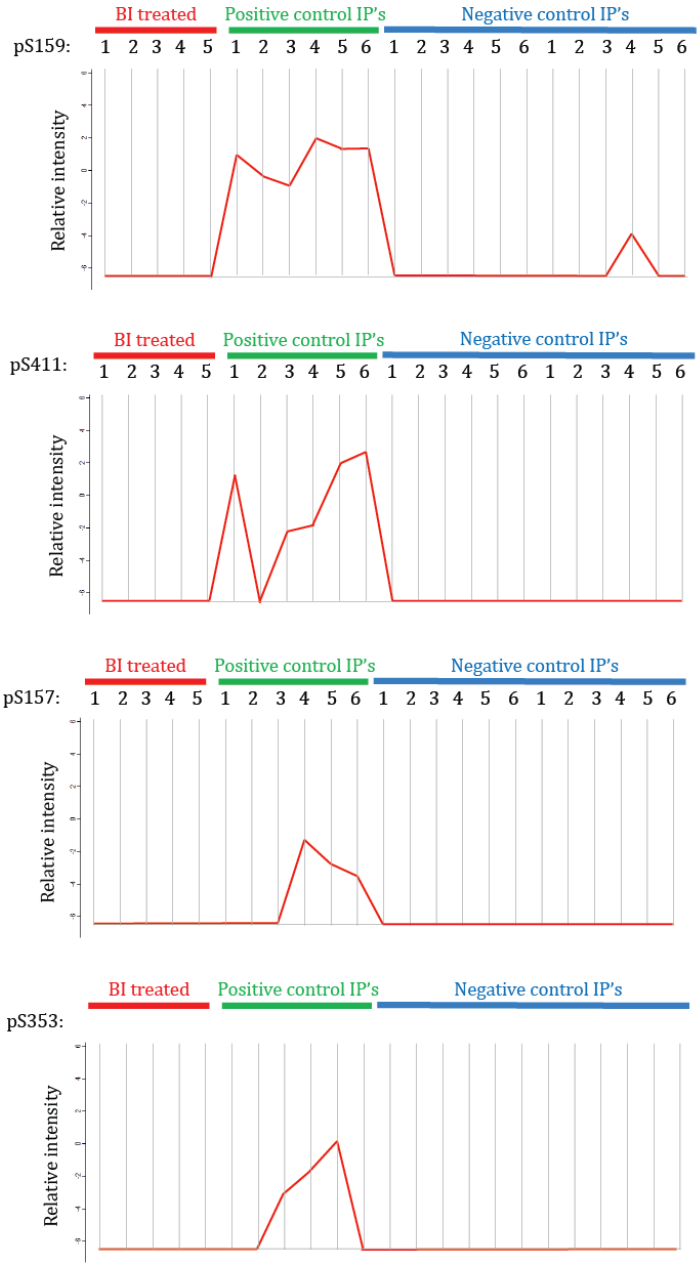
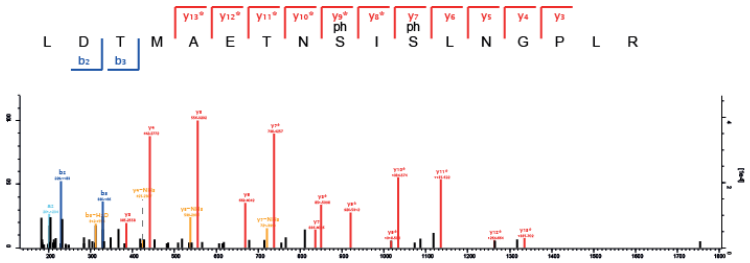


Figure 5.6 Reproducibility of Plk1-dependent phosphorylation sites

Phospho-site is indicated on graphs as a red line. Where the red line intersects with the grey lines indicates the relative intensity of signal in that single experiment. Experiments are grouped by type: BI-2536 treated (red) or STLC treated (green) or negative controls (blue). If the phospho-site was not observed the signal runs at -6.5 (the bottom of the graph). This data shows pSer157 was seen in all six STLC immunoprecipitations whilst pSer353 and pSer159 were seen in three.

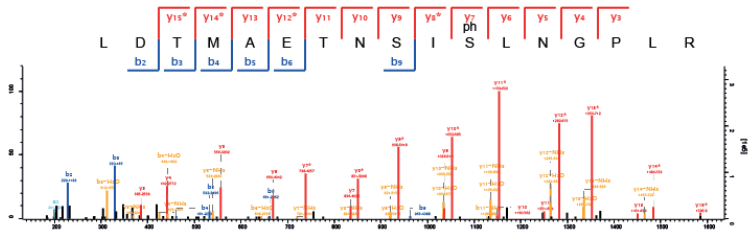
Plk1 site: pS157

Score: 78.0
Localisation probablility: 99.10%



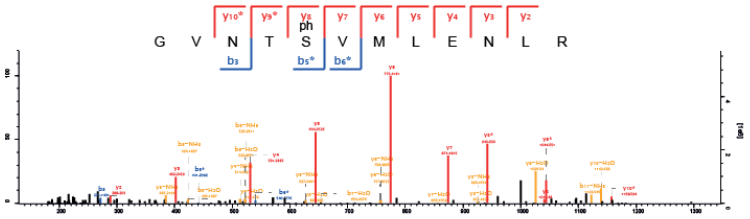
Plk1 site: pS159

Score: 235.2
Localisation probablility: 99.98%



Plk1 site: pS353

Score: 127.3
Localisation probablility: 96.11%



Plk1 site: pS411

Score: 180.3
Localisation probablility: 71.53%

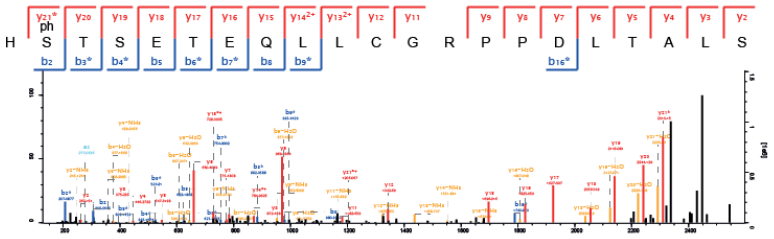


Figure 5.7 Fragmentation patterns for Plk1 dependent phosphorylation sites

Fragmentation patterns for Plk1-dependent phosphorylation sites are shown. The graphical representation shows individual ions found in the fragmentation patterns. These ions are then indicated by red and blue lines on the peptide sequence to show the sequencing of the phospho-peptide. The peptide with the fragmentation pattern which best shows the localisation of the phosphorylation is shown. These fragmentation patterns are used by MaxQuant to generate a Score and Localisation probability shown on the left.

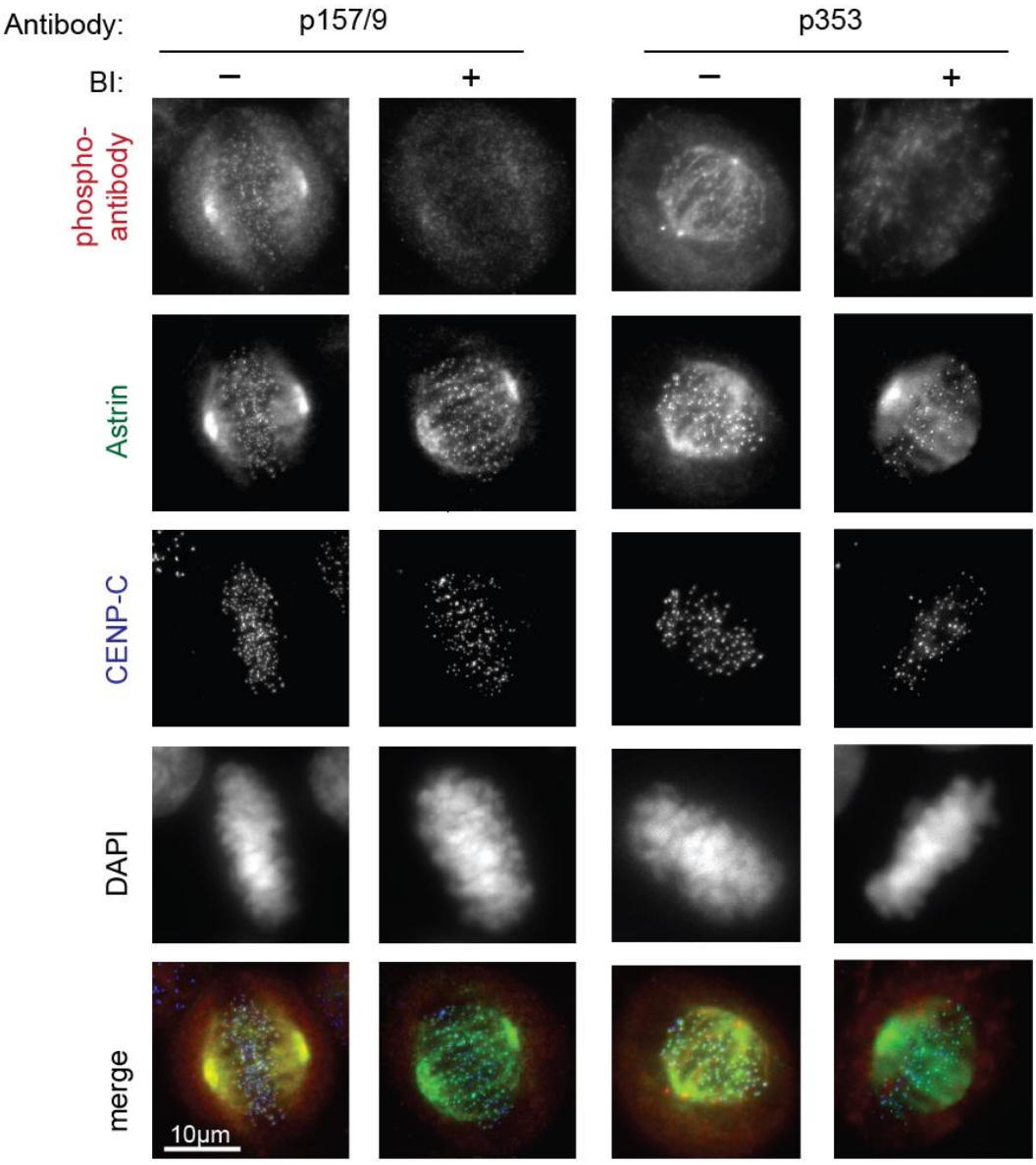
5.2.4 Confirming phospho-sites found

In order to investigate the function of Plk1's phosphorylation of Astrin we generated a phospho-specific antibody against pSer157/159 and pSer353 phosphorylation. The phospho-antibodies were tested by immunofluorescence. Phospho-staining with pSer157/159 revealed it co-localised with Astrin at the kinetochore and spindle pole but was not strongly present on the spindle, whilst pSer353 localisation was seen on the spindle and looked very similar to Astrin. Following a 30min treatment with BI-2536, phospho-staining was lost confirming Astrin pSer157/159 and pSer353 are dependent on Plk1 activity (**Figure 5.8**).

This *in vivo* data confirms our mass spectrometry data, showing three out of the four phospho-sites found are indeed dependent on Plk1 activity. Furthermore the data generated by mass spectrometry on pSer353 and pSer159 phospho-sites was very close to the significance cut-off of a p-value of 0.05. This data confirms our method is sound and that missing values, whilst affecting the p-value, do not signify an absence of biological significance.

In order to confirm the staining is specific to Astrin, an RNA interference protocol was implemented. HeLa cells were lysed and western blotted to confirm the success of the Astrin RNAi. Samples were also stained for Kinastrin which also showed a reduction in Astrin depleted samples (in line with previous data) (**Figure 5.9A**). The staining of both Astrin and phospho-antibodies was absent in cells depleted of Astrin, indicating that the pSer157/9 and pSer353 phospho-signal is specific to Astrin (**Figure 5.9B**).

A.


Antibody:
p157/9
p353
BI:
–
+
–
+
phospho-antibody
Astrin
CENP-C
DAPI
merge
10μm

B.

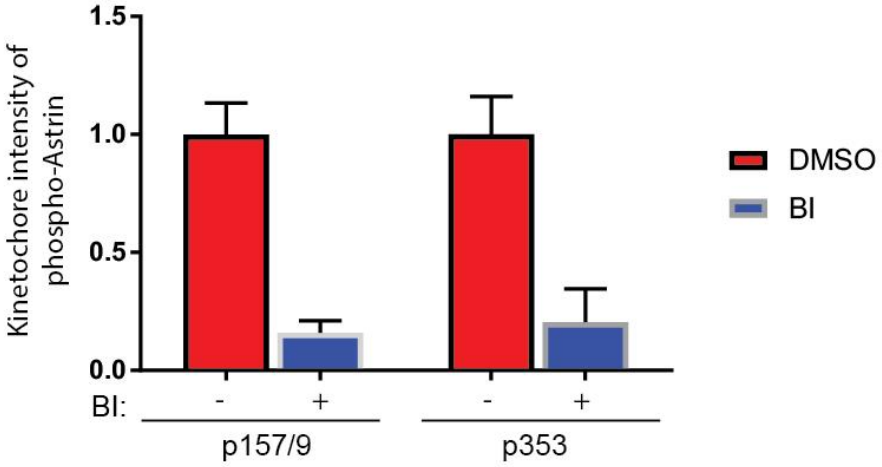
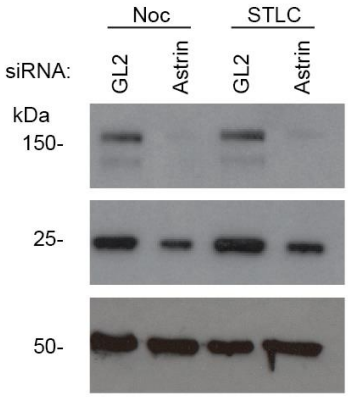

Kinetochore intensity of phospho-Astrin
1.5
1.0
0.5
0.0
BI:
-
+
-
+
p157/9
p353
DMSO
BI

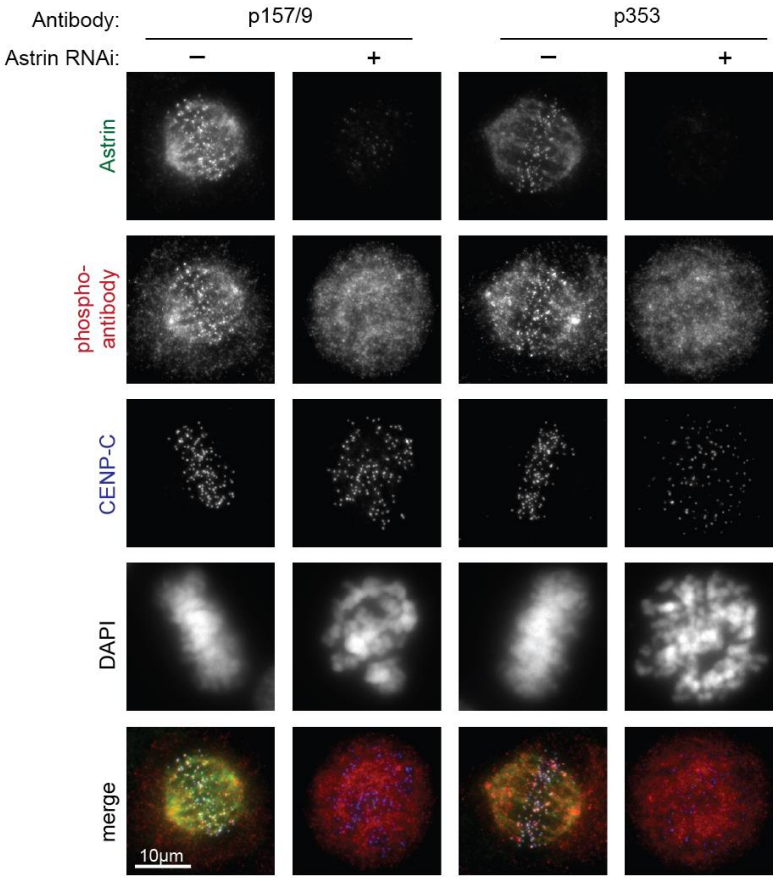
Figure 5.8 Validation of phospho-antibodies

A) HeLa cells were grown asynchronously and treated with BI-2536 for 15 minutes prior to fixation. Cells were stained with Astrin and pSer157/9 and pSer353 antibodies. Data shows the loss of phospho-staining upon BI-2536 treatment. B) Quantification of phospho-staining normalized to the mean of the DMSO treated control; error bars indicate the SD (10 kinetochore are measured per cell with 10 cells counted in three independent experiments)

A.


Noc
STLC
siRNA:
GL2
Astrin
GL2
Astrin
kDa
150-
25-
50-

B.


Antibody:
p157/9
p353
Astrin RNAi:
–
+
–
+
Astrin
phospho-antibody
CENP-C
DAPI
merge
10μm

C.

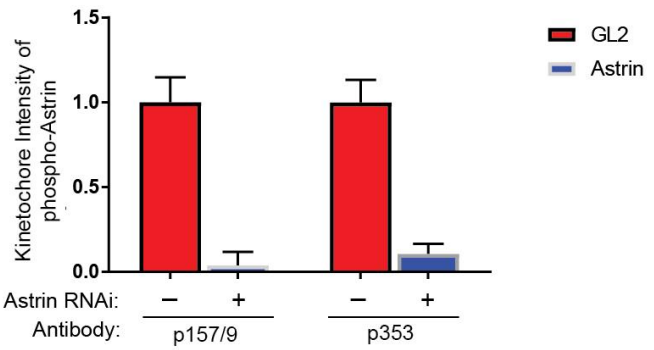

Kinetochore Intensity of phospho-Astrin
1.5
1.0
0.5
0.0
GL2
Astrin
Astrin RNAi:
–
+
–
+
Antibody:
p157/9
p353

Figure 5.9 Phospho-antibodies are specific to Astrin

A) HeLa cells were treated with Astrin RNAi for 60 hours prior to lysis. 14hrs before collection by mitotic shake-off Nocodazole and STLC were added. Western blot confirms Astrin was successfully depleted, which also caused a reduction in Kinastrin, which is in line with previous literature. Tubulin was used as a loading control. B) HeLa cells were depleted of Astrin and stained for Astrin and pSer157/9 and pSer353 antibodies. Data shows the loss of phospho-staining upon Astrin depletion. C) Quantification of phospho-staining normalized to the mean of the GL2 treated control; error bars indicate the SD (10 cells and 10 kinetochore are measured per cell for three independent experiments)

5.2.5 The PBD mutant is unable to be phosphorylated by Plk1 but able to reform bipolar spindle

We wanted to assess the role of Astrin-bound Plk1. It has been shown in previous studies that direct binding of Plk1 to the kinetochore is necessary for its ability to phosphorylate targets (Lera et al. 2016), so we would expect preventing the Astrin-Plk1 binding would be enough to prevent Plk1's activity at this site. Having already confirmed that the PBD-binding site ST110/11AA is required for Plk1's binding to Astrin, we chose to create a PBD-binding mutant of Astrin as a means of removing Plk1. To study it we used an siRNA approach, knocking down endogenous Astrin and replacing it with transiently expressed GFP-Astrin. Two constructs were created using the Flp-In TREx system, GFP-Astrin WT and GFP-Astrin ST110/111AA. The Flp-In

TREx system allows different GFP-tagged constructs to be inducibly expressed under the same promoter leading to comparable expression levels. GFP-Astrin cell lines showed the same localisation pattern to endogenous Astrin (**Figure 5.10**).

The key to successful rescue assays is being able to knock down the endogenous proteins effectively. Using an siRNA targeting the 3' UTR of Astrin, (Dunsch et al. 2011) we were able to knock down the endogenous Astrin whilst not affecting the Astrin transgene. Cell lines were induced six hours prior to siRNA and samples were depleted of Astrin for 60hrs before fixation (**Figure 5.11A**). Cell lines which had been depleted without induction of the transgene led to a classic Astrin phenotype displaying difficulties in producing a bipolar spindle **(**Error! Reference source not found.**B**). As expected following induction of GFP-Astrin WT bipolarity was restored and Astrin was able to accumulate on the kinetochores, suggesting attachment was also restored. Induction of GFP-Astrin ST110/111AA seemed to cause no obvious phenotype, with bipolarity and attachment looking remarkably similar to GFP-Astrin WT (**Figure 5.11 B-C**).

The only clear difference between the GFP-Astrin WT and GFP-Astrin ST110/111AA cells was the lack of phospho-staining in the Astrin PBD-binding mutant. This shows that direct binding of Astrin and Plk1 is necessary for the phosphorylation of Astrin (**Figure 5.11B-C**).

This was a very interesting result, here we show that the presence of the Astrin-Kinastrin complex which is unable to recruit Plk1, is sufficient to generate bipolar spindles. Cold-stable assays performed by Zoe Geraghty showed that the formation of K-MT attachments were stable. This confirms that phosphorylation is not required for the formation of a stable spindle or microtubule attachments. This is slightly surprising as we may have expected the phosphorylation and aspects of Astrin's function to be linked. However, it is not inconsistent with other published work; Kern et al. (2017) found an Astrin construct with an N-terminal deletion was able to rescue bipolarity.

In order to identify if there are any physiological consequences of Astrin-bound Plk1 we performed live cell microscopy.

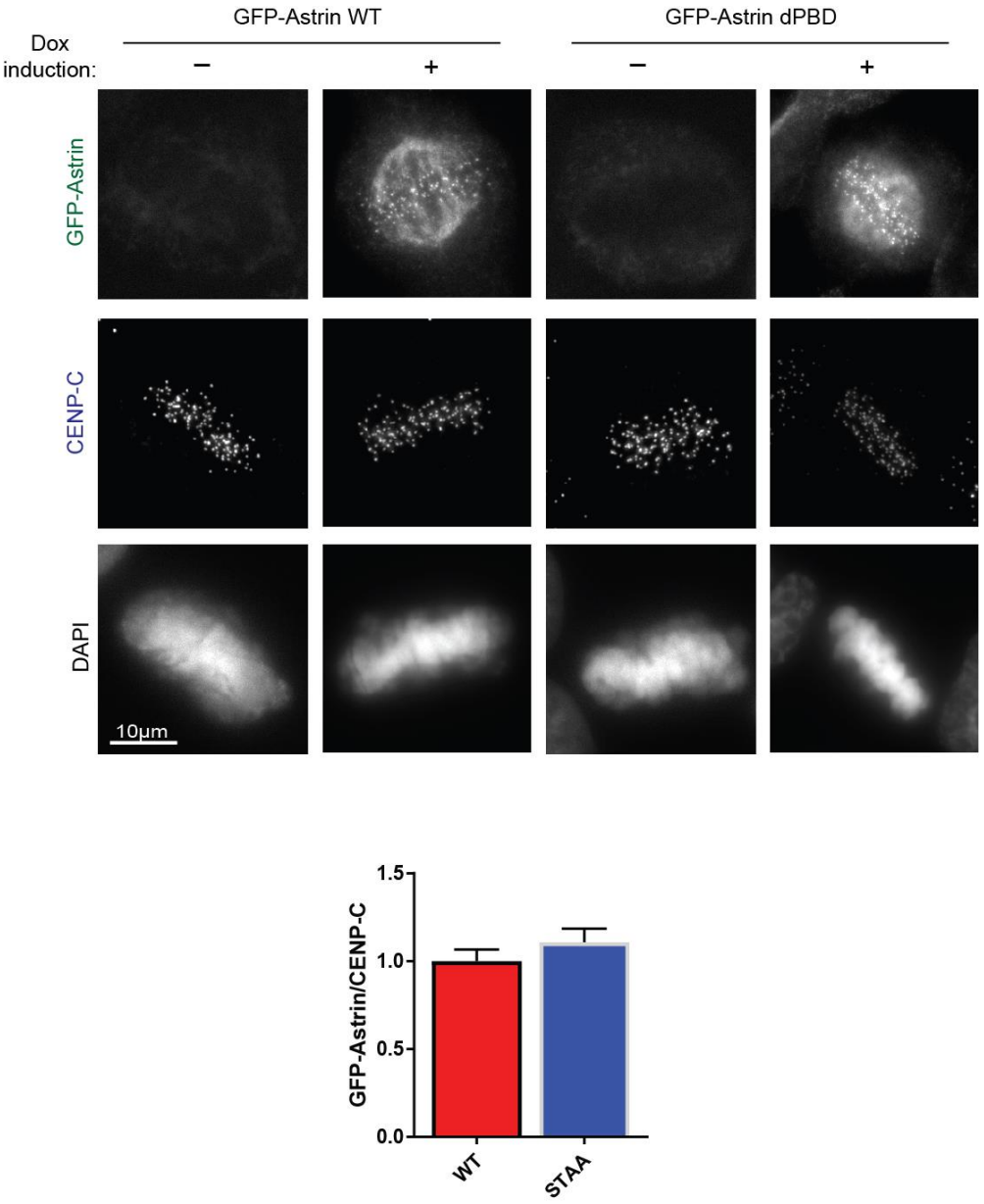
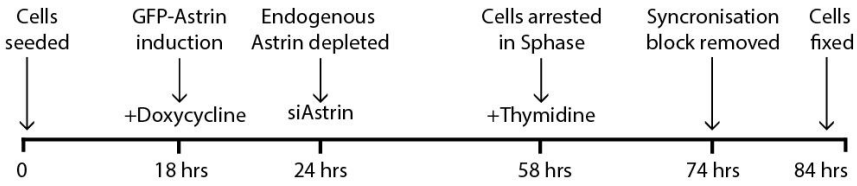


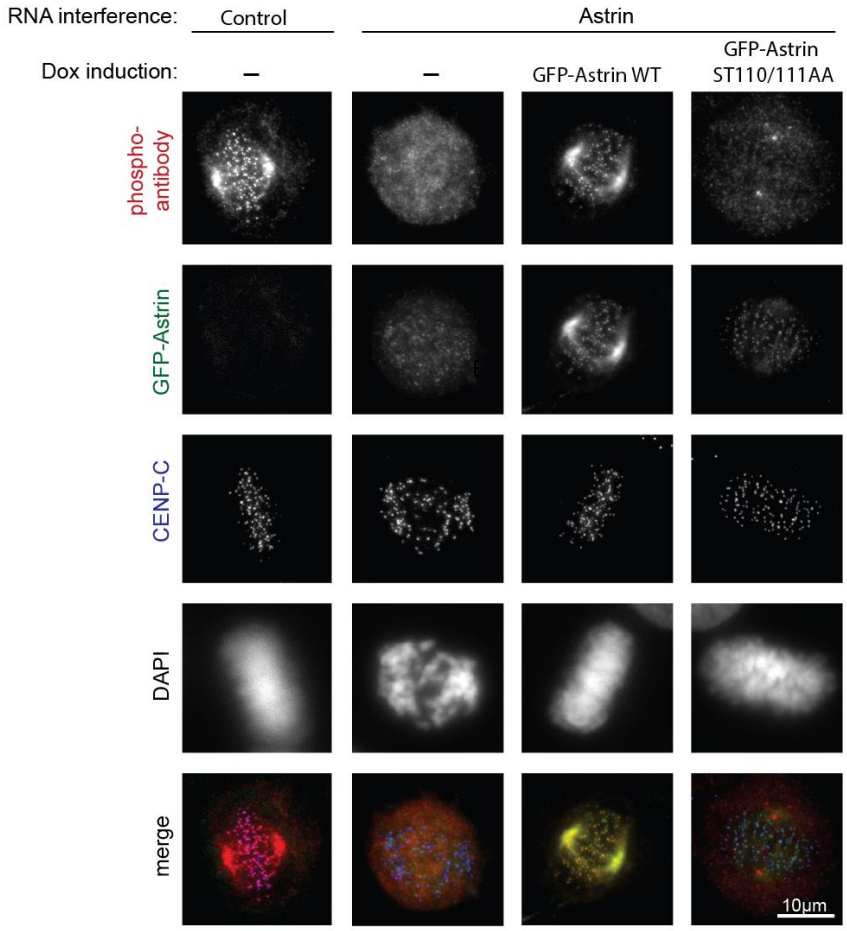
Figure 5.10 Generating GFP-Astrin cell lines

A) HeLa Flp-in/TREx GFP-Astrin cell lines were created and induced for 24hrs prior to immunofluorescence analysis of mitotic cells. This confirmed correct localisation without leaky expression. B) GFP-Astrin's kinetochore intensity was quantified against CENP-C. Quantification of kinetochore Astrin normalized to the mean of the GFP-Astrin cell lines; error bars indicate the SD (10 cells and 10 kinetochore are measured per cell for two independent experiments)

A.


Cells seeded
GFP-Astrin induction
+Doxycycline
Endogenous Astrin depleted
siAstrin
Cells arrested in Sphase
+Thymidine
Syncronisation block removed
Cells fixed
0
18 hrs
24 hrs
58 hrs
74 hrs
84 hrs

B.


RNA interference:
Control
Astrin
Dox induction:
–
–
GFP-Astrin WT
GFP-Astrin ST110/111AA
phospho-antibody
GFP-Astrin
CENP-C
DAPI
merge
10µm

C.

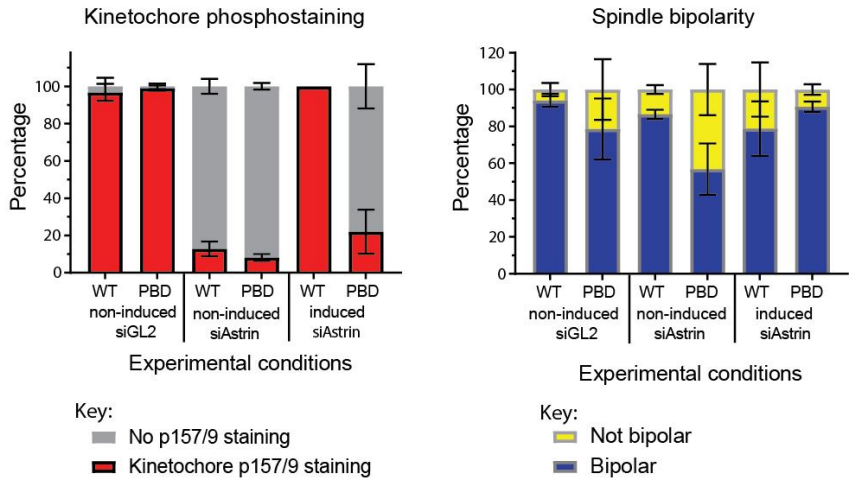

Kinetochore phosphostaining
Percentage
WT non-induced siGL2
PBD non-induced siGL2
WT non-induced siAstrin
PBD non-induced siAstrin
WT induced siAstrin
PBD induced siAstrin
Experimental conditions
Key:
No p157/9 staining
Kinetochore p157/9 staining
Spindle bipolarity
Percentage
Experimental conditions
Key:
Not bipolar
Bipolar

Figure 5.11 siRNA 3' UTR capable of efficiently depleting endogenous Astrin

A) Schematic of RNAi procedure used for the HeLa Flp-in/TREx GFP-Astrin cell lines showing timing of drug additions and RNAi depletion. B) Flp-in cells were depleted of either Astrin or GL2 (as a control). Non-control samples had doxycycline added as shown in part A). Cells were fixed in PTEMF and stained for p157/9, CENP-C and DAPI. C) Counts were performed of the percentage showing bipolar spindles and kinetochore phospho-staining. Quantification performed from two independent repeats n=100.

5.2.6 ST110/111AA Astrin exhibits a delayed congression and anaphase onset phenotype

So far we have established that Plk1-bound Astrin phosphorylates Astrin but no phenotype has yet been observed in fixed cells. To get a more detailed analysis of these mutants, live cell microscopy was performed. Endogenous Astrin was depleted by siRNA, and the GFP-Astrin cells were induced as before (**Figure 5.12**). Cells were arrested using Thymidine for 16hrs before the thymidine was washed out, allowing the cell cycle to proceed in a more synchronous manner. Following the thymidine washout doxycycline was added back into the media, along with SiR-Hoechst to visualise the DNA. 9-10 hrs after washout cells were imaged at two minute intervals.

In GFP-Astrin WT cell lines, Astrin was recruited to the bipolar spindle and could be seen at the kinetochores in more highly expressing cells. Chromosomes rapidly congressed to the metaphase plate and, following a short arrest whilst the last of the SAC was silenced, cells proceeded into anaphase in a timely manner (**Figure 5.12A**). The average timing between nuclear envelope breakdown (NEB) and formation of the

metaphase plate, (measured as the time until last chromosome congression (LCC) was 16 minutes. The SAC silencing delay between last chromosome congressed (LCC)-Anaphase onset was 23 minutes (**Figure 5.12B)**. These timings are directly comparable to the non-siRNA uninduced controls with values for NEB-LCC and LCC-Anaphase of 15 and 21 minutes respectively. In contrast, GFP-Astrin ST110/111AA cells showed an elongated mitosis. There was a clear delay in LCC timing with cells showing difficulties in congressing a few last chromosomes to the metaphase plate. 22% of cells failed to congress their chromosomes to a metaphase plate and apoptosed prior to the end of the movie. The remaining 78% managed to congress their chromosomes but with an average time of 52 minutes - over double that of GFP-Astrin WT cells.

Interestingly, a further delay was noticed with the average LCC-Anaphase onset timing taking 57 minutes in GFP-Astrin ST110/111AA rather than 23 minutes in the GFP-Astrin WT. This was even taking into account the 5% minority which, following longer NEB-LCC timings, showed virtually no delay with anaphase onset occurring almost immediately after LCC. No differences in the speed of anaphase were observed.

This data confirms the fixed cell work we have done. The live experiments confirm that cells are able to create a bipolar spindle. Even when cells were delayed in mitosis for several hours we observed no breakdown into multipolar spindles. Previous work showed an Astrin depletion phenotype which caused issues with the creation and maintenance of the bipolar spindle, maintenance of sister chromatid cohesion as well as problems with chromosome attachment and alignment (Dunsch et al. 2011). Here we have managed to separate these observations into Plk1 dependent and independent roles. The core complex of Astrin and Kinastrin is sufficient to maintain a bipolar spindle and chromosome are able to align. However, Astrin ST110/111AA cells do have a subtle phenotype, elucidated by live microscopy. Plk1-bound Astrin

seems to have a role in the formation of K-MT attachments and progress into anaphase.

In conclusion, suggest that whilst the phosphorylation sites seem important for aiding initial attachment and timing of anaphase onset, the mere presence of the core Astrin-Kinastrin complex is enough to achieve attachment and in most case alignment.

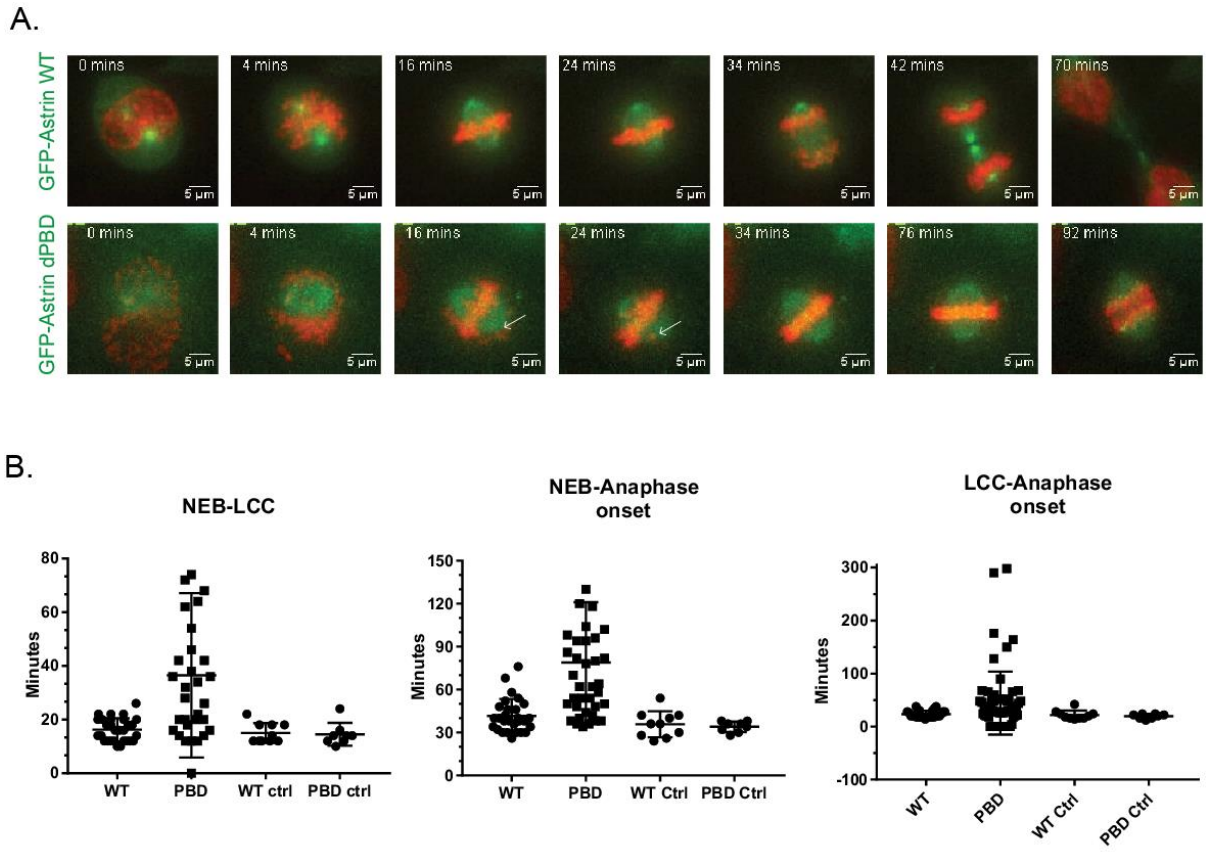


Figure 5.12 Live cell imaging of GFP-Astrin variants

A) Rescue experiments were performed as in Figure 5.13. SiR-DNA was added to stain DNA during the release step. Cells were imaged every two minutes over 10 hour period. Stills show representative images, in the dPBD cell there are a minority of chromosomes which take longer to congress. Following congression there is a further delay before anaphase onset occurs. B) Quantification of mitotic timings from nuclear envelope breakdown (NEB) to anaphase onset. Data represents the result of five independent repeats WT n=28, PBD=46

5.3 Discussion

5.3.1 Summary

Here we have confirmed that Plk1 is an important component of the Astrin-Kinastrin complex. We have identified the Plk1 binding site on Astrin as ST110/111 and have confirmed that Plk1 does bind through its polo box domain. Short term inhibition of Plk1 combined with MS showed Astrin to be directly phosphorylated by Plk1 on several residues towards its N-terminus. Two of these sites were confirmed using phospho-antibodies. Using rescue assays with Astrin PBD-binding mutant it has been shown that phosphorylation by Plk1 is important for timely mitotic congression and anaphase onset.

5.3.2 Discussion

The Astrin-Kinastrin complex is important for successful chromosome alignment and spindle bipolarity. It is therefore unsurprising it is highly expressed in mitosis (Kern et al. 2016). Previous work by Dunsch et al. (2011) identified Plk1 as an interactor of the Astrin-Kinastrin complex. Our work confirms this interaction and shows they interact through a single key interacting site on Astrin in a classical way; Plk1's PBD binding a PBD-binding domain.

Plk1 therefore binds within the same region as the region that has been suggested for the Ndc80 interaction (which binds somewhere in the region 1-464), towards the N-terminus of Astrin in what is presumed to be an unstructured region. It has been suggested that the Astrin N-terminus faces outward from the outer kinetochore (Kern

et al. 2017), and would therefore recruit Plk1 exactly to the interface between the outer kinetochore and the microtubule. It is an interesting idea that recruiting Plk1 to aligned, attached outer kinetochores might phosphorylate sites, creating a "ready" signal denoting a kinetochore's readiness for anaphase onset, and completing the process of forming stable attachments.

In order to determine whether Plk1 phosphorylates members of the Astrin-Kinastrin complex, Astrin immunoprecipitations were performed in the presence and absence of Plk1 inhibitor. Although all members of the Astrin-Kinastrin complex except Sgo2 were identified by proteomic MS (consistent with Dunsch et al.'s work which only saw Sgo2 with Kinastrin pull-downs). Only Astrin was significantly phosphorylated following phospho-enrichment. Our data confirms what others have found, showing Astrin is a highly phosphorylated protein (Sharma et al. 2014; Olsen et al. 2010; Kettenbach et al. 2011; Santamaria et al. 2011). The majority of sites seen fall within the first 400 or so amino acids which contain a relatively unstructured region and the head domain of Astrin (Kern et al. 2017). It is also the region of Plk1 and Ndc80 binding, and leaves open the question of whether Astrin phosphorylation (by Plk1 or other kinases) is required for binding to the kinetochore.

Our data suggested only four of the phospho-sites seen were downregulated upon Plk1 inhibition; pSer157, pSer159, pSer353, pSer411. Of these sites only pSer353 looks like a classic Plk1 motif, pSer157 and pSer159 both show S/T at site -2 which has been seen in multiple large scale MS analyses of Plk1 substrates (Santamaria et al. 2011). It would be interesting to assess pSer411 *in vitro* to confirm it as a direct Plk1 site. The remaining sites were confirmed *in vivo* using phospho-antibodies of pSer157/9 and pSer353. It was observed that 15 minute inhibition of Plk1 was sufficient to prevent Astrin phosphorylation.

Currently we are working on creating phospho-mimetic and phospho-null cell lines for these four mutations in order to identify their specific effect. However there are

significant benefits to beginning this study by using the PBD-binding mutant of Astrin as it prevents the interaction of Plk1 with Astrin. We showed here direct binding of Plk1 was necessary for phosphorylation of Astrin. Should there be other proteins which Plk1-bound Astrin acts on in the same way, the PBD-binding mutant will also negate this effect. Our Astrin immunoprecipitations are only capable of isolating the Astrin complex itself but we know in binding to the kinetochore Astrin is in contact with, and in close proximity to many other proteins (Kern et al. 2017). These proteins may be key Plk1 targets which are not identified in our pull-down MS experiments. Furthermore there is always a risk using MS of missing identification of phospho-sites, so there may be other Plk1 phospho-sites on Astrin missed in this analysis. In order to maximise our chances of identifying a phenotype we created GFP-Astrin WT and PBD-binding mutant (ST110/111AA) cell lines using the Flp-in system.

This allowed us to use an siRNA approach to deplete Astrin whilst expressing GFP-Astrin transgenes. We found that Astrin ST1110/111AA was capable of localising correctly and maintaining a bipolar spindle. Indeed in fixed analysis it appeared identical to WT Astrin. A more detailed analysis was undertaken using immunofluorescence live cell microscopy. This revealed that Astrin was unable to recruit Plk1 and showed a marked delay in congression timing. This is in agreement with Thein et al. (2007) which showed a similar phenotype when Astrin was depleted, with the majority of chromosomes congressed whilst others struggled to enter the metaphase plate. In contrast to Thein et al. however, no breakdown of the spindle was observed even when cells were arrested for several hours. Thus for the first time, we are able to separate the two effects observed in an Astrin depletion: congression issues and loss of bipolarity following arrest. It appears that presence of Astrin is sufficient to maintain bipolarity however Plk1's binding is necessary to aid chromosome congression. One possible explanation we investigated was whether

Plk1's binding and phosphorylation of Astrin affect its ability to bind stably to kinetochores.

The live cell experiments also revealed a delay in anaphase onset compared to controls. This has not been observed before as siRNA mediated depletion of Astrin normally leads to prolonged arrests in prometaphase because the cell has problems with both congression and multipolarity of spindles, with the result that it has not previously been possible to analyse timings to anaphase (Thein et al. 2007; Dunsch et al. 2011). Within the field Astrin is often used as a marker of kinetochore attachment.

One intriguing possibility is that Astrin's phosphorylation mirrors the formation of the SAC, with Mps1 phosphorylating MELT motifs to generate the SAC signal preventing anaphase onset. Following attachment Mps1 is lost and PP1 and PP2A-B56 reverse these phosphorylation events. Astrin is recruited and at the kinetochore Plk1 phosphorylates Astrin generating an anaphase-ready signal.

We suggest two roles for Plk1-bound Astrin: firstly Plk1 binding Astrin is necessary to congress a minority of chromosomes to the metaphase plate, and secondly Plk1's phosphorylation of Astrin might allow timely anaphase onset to occur. Clearly this research is a work in progress and more experiments need to be done to prove this hypothesis.

Chapter 6: Concluding remarks

The mitotic kinetochore represents one of the most dynamic and intriguing proteinaceous interaction platforms known. Since the discovery of many of the major proteins in the SAC in the early 1990s, our understanding of how they are recruited to and interact at the kinetochore has improved significantly (Hoyt et al. 1991; Li & Murray 1991; Weiss & Winey 1996; Musacchio 2015). The network of protein inter-dependencies has made teasing out roles difficult. Inhibition experiments have been hampered because many important kinetochore kinases have roles earlier in mitosis as well (Combes et al. 2017). Much work has been done to elucidate the functions of the kinetochore, but several questions remain about how the recruitment and activity of proteins are regulated.

It is clear that phosphorylation events have an important role in the regulation of successful mitosis. In both the error correction pathway and the SAC, the key players are kinases - Aurora B and Mps1 respectively. Mass spectrometry has emerged as the most attractive way of studying such processes, as it allows an unbiased analysis of phosphorylation sites present *in vivo* under a variety of conditions.

Our study builds on the work of others, employing an immunoprecipitation-based method in conjunction with a synchronisation protocol. Using an immunoprecipitation step to enrich relevant kinetochore factors has provided us with considerable insight to the kinetochore phospho-proteome. The methodology also naturally excludes non-kinetochore bound pools of protein because they may undergo differential patterns of phosphorylation irrelevant to their activity at the kinetochore. This allows us to distil phosphorylation sites important to kinetochore regulation.

By adding a further synchronisation technique, we were able to identify proteins which underwent differential phosphorylation upon attachment. We found only a few phospho-sites which showed a significant alteration in phospho-status, which suggests that the kinetochore does not undergo a widespread phosphorylation switch-off upon MT attachment. Instead individual phosphorylations appear to be regulated according to site-specific needs. This has been alluded to in other studies which are beginning to show just how finely-tuned activity can be using phospho-regulation (Zaytsev et al. 2014).

6.1.1 Observations from our study

Taking the whole data set of MS results that we gathered, we found over 50 novel sites. The majority of these were on key KMN network components. Because they were direct interaction partners with the isolated bait protein, they were well observed in all samples. This increased the sequence coverage and likelihood of phospho-site identification. We found that the more MS runs we performed, the more sites we identified, which suggests that there may well be additional phospho-sites to be found if further experiments can be run more extensively in future.

We observed that the inclusion of a pre-lysis Calyculin A inhibitor treatment allowed stabilisation of labile phosphorylation sites. This enabled the identification of eight phospho-sites on the N-terminal of Ndc80, confirming previous published work, an improvement over the two seen in our earlier experiments. In future, comparisons of experimental data with and without Calyculin A treatments may allow us to infer the dynamics of phospho-sites. Those with a longer half-life would be in both samples whilst those with a shorter half-life would only be observed in the Calyculin A treated samples.

Work on post-translational modifications can be split into three broad questions which lead on from each other:

- Which sites are modified?
- What is the site's function?
- How is it regulated?

Currently, phospho-sites are being discovered far more rapidly than we can investigate their mechanisms of action.

In **Chapters 3 and 4**, we focused on the first of these goals, and also looked at two distinct mitotic states. Our method represents a bridge between large lysate-based studies and single kinetochore-protein studies. Our comparative analysis of prometaphase and metaphase cells allowed the identification of six active MELT motifs which undergo significant dephosphorylation upon attachment. However the most interesting result appears to be the upregulation of Ndc80 pThr61/Ser62 and pSer69. This represents a shift in perspective, the current simplistic model of kinetochore phosphorylation is that it is high at unattached kinetochores and reduced or lost upon attachment. Whilst DeLuca et al. (2018) reported the maintenance of p69 at metaphase, here we find evidence of significant increase in phosphorylation upon attachment.

In **Chapter 5**, I analyse one of the key protein complexes implicated in stabilising microtubule-kinetochore interactions, the Astrin/Kinastrin complex previously analysed in our lab (Thein et al. 2007; Dunsch et al. 2011). We identified Plk1 phosphorylation sites, pSer157, pSer159, pSer353 and pSer411 on Astrin. To elucidate the biological impact of these phosphorylations we analysed an Astrin mutant defective for Plk1-binding. We demonstrate that Astrin does not require Plk1 binding or phosphorylation to allow bi-polar spindle formation, and that Plk1 binding is exclusively required for timely chromosome congression and anaphase onset. Our work thus provides evidence for a role for Plk1 in regulating Astrin's ability to form mature attachments.

In our analysis of the prometaphase state we found multiple phosphorylations on Knl1 sites which contain an acidic residue or phosphorylatable residue at the -2 position. These therefore have characteristics of Plk1 sites. It may therefore be worthwhile to investigate Plk1 further as it has very interesting activity at the kinetochore with known roles in both activating and silencing the checkpoint. Here we have evidence for the activity of Plk1 at prometaphase (on Knl1) and at metaphase (on Astrin). We postulated that Astrin-bound Plk1 may be recruited to the attached kinetochore and through phosphorylation create a 'ready' signal demonstrating a kinetochore's readiness for anaphase onset.

Together this data allows us to speculate that, rather than the kinetochore going from a phospho-on to a phospho-off status, its phospho-sites may be regulated on a more individual basis dependent on specific need. Therefore kinases may transfer responsibility with Aurora B, Mps1 and Plk1 active at the unattached kinetochore handing over to Aurora A and Plk1. This places Plk1 in the role of mercenary, playing a role in both systems, with its activity possibly dependent on its binding interactor (or pay-lord).

6.1.2 Future directions for our MS methodology

Having validated our methodology, there are several avenues that would be fascinating to explore. These would involve: using crosslinking mechanisms to improve coverage of the more transiently bound proteins; understanding how proteins are differentially regulated depending on their localisation; and increasing the temporal resolution of our system.

Crosslinking would allow the identification of transient interactors of the kinetochore. As a starting point, it would be interesting to study known transiently kinetochore-

associated proteins including Mps1, Ska, Astrin, Mad proteins, and the RZZ complex. In immunoprecipitation and MS analysis performed by our group, Astrin, Mad and RZZ components can be isolated as sub-complexes but were not seen to associate with any kinetochore components. Previously Kern et al. (2017) have used a short 10 minute formaldehyde crosslinking to isolate Ndc80 with Astrin. It would be interesting to incorporate this step into my protocol. It might it allow us to isolate more transient interactors of the kinetochore, and increase our coverage of those interactors we see, like the Bub proteins. Overall this should allow analysis of these proteins' phosphorylation when complexed with the outer kinetochore. This would represent a way of expanding our data set to include proteins where regulation and binding are not yet well understood.

Up to now we have looked at kinetochore-bound proteins, but this may only be half the picture. It would be fascinating to compare and contrast the phosphorylations on kinetochore-bound and free-solution protein pools. Our protocol is already set up to do this. In future experiments we could load the immunoprecipitation flow-through on FASP filters and run it as an unbound sample. These samples would contain proteins such as Mps1, the free pool of Mad and Bub proteins, which as stated above maybe differently phospho-regulated. The flow-through would be considerably more complex than the immunoprecipitated fraction. However, it would not represent the entire lysate, because clarification would remove chromatin-bound and membrane-bound proteins along with cytoskeletal elements. It would still be highly complex such that longer mass spectrometry gradients and possibly even fractionation techniques were required. This may be quite a costly approach but would allow comparison of the different phospho-states of any protein which has a free-pool and kinetochore-localised pool.

An alternative avenue of investigation would be to do a more targeted small scale comparison. We could follow our kinetochore immunoprecipitation with, for example,

an MCC immunoprecipitation using the flow-through before proceeding to MS. That would allow a direct comparison of two different pools and give greater understanding of how SAC proteins are differentially regulated depending on their localisation and complex-associations.

Finally, our analysis represents two time points during mitosis; our results show that the kinetochore is highly phosphorylated both at prometaphase and metaphase, and also that there are relatively few sites that experience significant change upon attachment. It would be interesting to understand the temporal regulation of how the phospho-sites are laid down early in mitosis and the timing of their loss later in mitosis. Clarifying the timing may help our understanding of the sequence of events required for successful kinetochore regulation. This represents an ambitious goal but these types of studies are becoming possible. Recently Cundell et al. (2016) used an *ex-vivo* model to investigate PP2A-B55 phosphatase's dephosphorylation rates and how the dephosphorylation of substrates is temporally controlled.

Obviously investigating the laying-down of phosphorylations is different from analysing their removal, and such an analysis would require the creation of a large population of highly synchronised HeLa cells, a challenging task with current methods. There are potentially ideas and workarounds which could make such a study possible.

It has been observed that decreasing temperature from 37ºC to 19ºC during early-prophase prevents cells entering mitosis. Instead they enter antephase where mitotic chromosomes decondense and enter a terminal G2-like state (Pines & Rieder 2001). Upon warming they rapidly re-enter mitosis. A development of our protocol to combine a thymidine release with a cold-stop could allow a highly synchronous terminal G2 population to be prepared on a large scale.

Following entry into mitosis, cells become committed to mitosis during mid-prophase regardless of temperature changes. A shift to low temperatures at this stage has

effects on mitotic timing. For instance, when CFPAC1 cells are cooled to 19ºC in prophase, it takes approximately 5½ hours to reach metaphase, 8½ hours to anaphase I, and 9 hours to anaphase II (Rieder & Cole 2002; Rieder & Maiato 2004). Using this kind of method might allow mitosis to be stretched temporally, creating populations which would differ in their phospho-status. This would be an exciting experiment, challenging to implement, but potentially very rewarding because it would allow us to track phosphorylations and protein: kinetochore associations over mitosis.

6.1.3 Conclusion

Overall our mass spectrometry protocol represents a step forward, allowing temporal analysis of kinetochore-bound proteins without the need for weeks of mass spectrometry running time. Here we have identified numerous novel sites which merit further investigation. Our comparative analysis of pro-metaphase and metaphase-like cells identified six MELT motifs which undergo significant dephosphorylation upon attachment. Of particular interest is the observation of up-regulated phospho-sites on the N-terminal tail of Ndc80.

The Astrin-Kinastrin complex is now commonly used as a marker of attached kinetochores. However its function and regulation are not yet thoroughly understood. The data we present here showed that Astrin binds to Plk1 via a PBD-binding motif allowing Plk1 to directly phosphorylate Astrin. These phosphorylations appear important in chromosomal congression and timely anaphase onset. This is currently an ongoing project and we hope to understand the mechanisms further that control this, via phospho-mimetic and phospho-null mutants, as well as investigating the SAC status of the outlying and delayed chromosomes.

Chapter 7: Bibliography

Abad, M.A. et al., 2014. Structural basis for microtubule recognition by the human kinetochore Ska complex. *Nature communications*, 5, p.2964.

Akiyoshi, B. et al., 2010. Tension directly stabilizes reconstituted kinetochore-microtubule attachments. *Nature*, 468(7323), pp.576–579.

Alexander, J. et al., 2011. Spatial exclusivity combined with positive and negative selection of phosphorylation motifs is the basis for context-dependent mitotic signaling. *Science Signaling*, 4(179).

Alfieri, C. et al., 2016. Molecular basis of APC/C regulation by the spindle assembly checkpoint. *Nature*, 536(7617), pp.431–436.

Alushin, G.M. et al., 2012. Multimodal microtubule binding by the Ndc80 kinetochore complex. *Nature Structural & Molecular Biology*, 19(11), pp.1161–1167.

Alushin, G.M. et al., 2012. Multimodal microtubule binding by the Ndc80 kinetochore complex. *Nature Structural and Molecular Biology*, 19(11), pp.1161–1167.

Alushin, G.M. et al., 2010. The Ndc80 kinetochore complex forms oligomeric arrays along microtubules. *Nature*, 467(7317), pp.805–810.

Andersson, L. & Porath, J., 1986. Isolation of phosphoproteins by immobilized metal (Fe3+) affinity chromatography. *Analytical Biochemistry*, 154(1), pp.250–254.

De Antoni, A. et al., 2012. A small-molecule inhibitor of Haspin alters the kinetochore functions of Aurora B. *Journal of Cell Biology*, 199(2), pp.269–284.

De Antoni, A. et al., 2005. The Mad1/Mad2 Complex as a Template for Mad2 Activation in the Spindle Assembly Checkpoint. *Current Biology*, 15, pp.214–225.

Aravamudhan, P., Goldfarb, A.A. & Joglekar, A.P., 2015. The kinetochore encodes a mechanical switch to disrupt spindle assembly checkpoint signalling. *Nature Cell*

Biology, 17(7), pp.868–879.

Asghar, A. et al., 2015. Bub1 autophosphorylation feeds back to regulate kinetochore docking and promote localized substrate phosphorylation. *Nature Communications*, 6, pp.1–14.

Axton, J.M. et al., 1990. One of the protein phosphatase 1 isoenzymes in Drosophila is essential for mitosis. *Cell*, 63(1), pp.33–46.

Bader, J.R. & Vaughan, K.T., 2010. Dynein at the Kinetochore: Timing, Interactions and Functions. *Semin Cell Dev Biol*, 21(3), pp.269–275.

Bakhoum, S.F. et al., 2009. Genome stability is ensured by temporal control of kinetochore-microtubule dynamics. *Nature Cell Biology*, 11(1), pp.27–35.

Barisic, M. et al., 2014. Kinetochore motors drive congression of peripheral polar chromosomes by overcoming random arm-ejection forces. , 16(12).

Barisic, M. et al., 2010. Spindly/CCDC99 Is Required for Efficient Chromosome Congression and Mitotic Checkpoint Regulation. *Molecular biology of the cell*, 21(22), pp.1968–1981.

Barisic, M. & Geley, S., 2011. Spindly switch controls anaphase: Spindly and RZZ functions in chromosome attachment and mitotic checkpoint control. *Cell Cycle*, 10(3), pp.449–456.

Barr, F.A., Elliott, P.R. & Gruneberg, U., 2011. Protein phosphatases and the regulation of mitosis. *Journal of Cell Science*, 124(14), pp.2323–2334.

Barr, F.A., Silljé, H.H.W. & Nigg, E.A., 2004. Polo-like kinases and the orchestration of cell division. *Nature Reviews Molecular Cell Biology*, 5(6), pp.429–440.

Bjursell, G. & Reichard, P., 1973. ARTICLE : Effects of Thymidine on Deoxyribonucleoside Triphosphate Pools Chinese Hamster Ovary Cells Effects of Thymidine on Deoxyribonucleoside Pools and Deoxyribonucleic Acid Synthesis Chinese Hamster

Ovary Cells * Triphosphate in. *The Journal of Biological Chemistry*, 248(11), pp.3904–3909.

Boersema, P.J. et al., 2009. Multiplex peptide stable isotope dimethyl labeling for quantitative proteomics. *Nature Protocols*, 4(4), pp.484–494.

Bolanos-Garcia, V.M. & Blundell, T.L., 2011. BUB1 and BUBR1: Multifaceted kinases of the cell cycle. *Trends in Biochemical Sciences*, 36(3), pp.141–150.

Burkhart, J.M. et al., 2012. Systematic and quantitative comparison of digest efficiency and specificity reveals the impact of trypsin quality on MS-based proteomics. *Journal of Proteomics*, 75(4), pp.1454–1462.

Caldas, G. V., DeLuca, K.F. & DeLuca, J.G., 2013. KNL1 facilitates phosphorylation of outer kinetochore proteins by promoting Aurora B kinase activity. *The Journal of cell biology*, 203(6), pp.957–969.

Caldas, G. V et al., 2014. The RZZ complex localizes to the N-terminus of KNL1 to mediate robust Mad1 kinetochore localization in human cells. *Manuscript in Preparation*.

Carroll, C.W. et al., 2009. Centromere assembly requires the direct recognition of CENP-A nucleosomes by CENP-N. *Nature Cell Biology*, 11(7), pp.896–902.

Carroll, C.W., Milks, K.J. & Straight, A.F., 2010. Dual recognition of CENP-A nucleosomes is required for centromere assembly. *Journal of Cell Biology*, 189(7), pp.1143–1155.

Chan, G.K.T. et al., 1999. Human BUBR1 is a mitotic checkpoint kinase that monitors CENP-E functions at kinetochores and binds the cyclosome/APC. *Journal of Cell Biology*, 146(5), pp.941–954.

Chan, Y.W. et al., 2012. Aurora B controls kinetochore-microtubule attachments by inhibiting Ska complex-KMN network interaction. *Journal of Cell Biology*, 196(5), pp.563–571.

Chao, W.C.H. et al., 2012. Structure of the mitotic checkpoint complex. *Nature*, 484(7393),

pp.208–213.

Cheeseman, I.M. et al., 2006. The Conserved KMN Network Constitutes the Core Microtubule-Binding Site of the Kinetochore. *Cell*, 127, pp.983–997.

Cheeseman, I.M. & Desai, A., 2008. Molecular architecture of the kinetochore-microtubule interface. *Nature reviews. Molecular cell biology*, 9(january), pp.33–46.

Chen, Y. et al., 1997. HEC, a novel nuclear protein rich in leucine heptad repeats specifically involved in mitosis. *Molecular and cellular biology*, 17(10), pp.6049–6056.

Ciferri, C., Pasqualato, S., Screpanti, E., Varetti, G., Santaguida, S., Dos Reis, G., Maiolica, A., Polka, J., De Luca, J.G., De Wulf, P., Salek, M., Rappsilber, J., Moores, C. a., et al., 2008. Implications for Kinetochore-Microtubule Attachment from the Structure of an Engineered Ndc80 Complex. *Cell*, 133, pp.427–439.

Ciferri, C., Pasqualato, S., Screpanti, E., Varetti, G., Santaguida, S., Dos Reis, G., Maiolica, A., Polka, J., De Luca, J.G., De Wulf, P., Salek, M., Rappsilber, J., Moores, C.A., et al., 2008. Implications for Kinetochore-Microtubule Attachment from the Structure of an Engineered Ndc80 Complex. *Cell*, 133(3), pp.427–439.

Clarke, P.R. & Zhang, C., 2008. Spatial and temporal coordination of mitosis by Ran GTPase. *Nature reviews. Molecular cell biology*, 9(june), pp.464–477.

Cuijpers, S.A.G. & Vertegaal, A.C.O., 2018. Guiding Mitotic Progression by Crosstalk between Post-translational Modifications. *Trends in Biochemical Sciences*, 43(4), pp.251–268.

Cundell, M.J. et al., 2016. A PP2A-B55 recognition signal controls substrate dephosphorylation kinetics during mitotic exit. *Journal of Cell Biology*, 214(5), pp.539–554.

Daub, H. et al., 2008. Kinase-Selective Enrichment Enables Quantitative Phosphoproteomics of the Kinome across the Cell Cycle. *Molecular Cell*, 31(3),

pp.438–448.

DeLuca, J.G. et al., 2002. hNuf2 inhibition blocks stable kinetochore-microtubule attachment and induces mitotic cell death in HeLa cells. *Journal of Cell Biology*, 159(4), pp.549–555.

DeLuca, J.G. et al., 2006. Kinetochore Microtubule Dynamics and Attachment Stability Are Regulated by Hec1. *Cell*, 127(5), pp.969–982.

DeLuca, J.G. & Musacchio, A., 2012. Structural organization of the kinetochore-microtubule interface. *Current Opinion in Cell Biology*, 24(1), pp.48–56.

DeLuca, K.F. et al., 2018. Aurora A kinase phosphorylates Hec1 to regulate metaphase kinetochore – microtubule dynamics. *Journal of Cell Biology*, 217(1).

DeLuca, K.F., Lens, S.M.A. & DeLuca, J.G., 2011. Temporal changes in Hec1 phosphorylation control kinetochore-microtubule attachment stability during mitosis. *Journal of Cell Science*, 124(4), pp.622–634.

Dephoure, N. et al., 2008. A quantitative atlas of mitotic phosphorylation. *Proceedings of the National Academy of Sciences*, 105(31), pp.10762–10767.

Dimitrova, Y.N. et al., 2016. Structure of the MIND Complex Defines a Regulatory Focus for Yeast Kinetochore Assembly. *Cell*, 167(4), p.1014–1027.e12.

Dou, Z. et al., 2011. Quantitative mass spectrometry analysis reveals similar substrate consensus motif for human Mps1 kinase and Plk1. *PLoS ONE*, 6(4).

Dumitru, A.M.G. et al., 2017. Cyclin A/Cdk1 modulates Plk1 activity in prometaphase to regulate kinetochore-microtubule attachment stability. *eLife*, 6, pp.1–23.

Dunsch, A.K. et al., 2011. The astrin-kinastrin/SKAP complex localizes to microtubule plus ends and facilitates chromosome alignment. *Journal of Cell Biology*, 192(6), pp.959–968.

Elia, A.E.H. et al., 2003. The molecular basis for phosphodependent substrate targeting and regulation of Plks by the Polo-box domain. *Cell*, 115(1), pp.83–95.

Elia, A.E.H., Cantley, L.C. & Yaffe, M.B., 2003. Proteomic screen finds pSer/pThr-binding domain localizing Plk1 to mitotic substrates. *Science*, 299(5610), pp.1228–1231.

Elowe, S. et al., 2007. Tension-sensitive Plk1 phosphorylation on BubR1 regulates the stability of kinetochore-microtubule interactions. *Genes and Development*, 21, pp.2205–2219.

Elowe, S. et al., 2010. Uncoupling of the spindle-checkpoint and chromosome-congression functions of BubR1. *Journal of Cell Science*, 123(1), pp.84–94.

Ems-Mcclung, S.C. et al., 2013. Aurora B inhibits MCAK activity through a phosphoconformational switch that reduces microtubule association. *Current Biology*, 23(24), pp.2491–2499.

Espert, a. et al., 2014. PP2A-B56 opposes Mps1 phosphorylation of Knl1 and thereby promotes spindle assembly checkpoint silencing. *The Journal of Cell Biology*, 206(7), pp.833–842..

Espeut, J. et al., 2012. Microtubule binding by KNL-1 contributes to spindle checkpoint silencing at the kinetochore. *Journal of Cell Biology*, 196(4), pp.469–482.

Fachinetti, D. et al., 2013. A two-step mechanism for epigenetic specification of centromere identity and function. *Nature Cell Biology*, 15(9), pp.1056–1066.

Feist, P. & Hummon, A.B., 2015. Proteomic challenges: Sample preparation techniques for Microgram-Quantity protein analysis from biological samples. *International Journal of Molecular Sciences*, 16(2), pp.3537–3563.

Foley, E. a., Maldonado, M. & Kapoor, T.M., 2011. Formation of stable attachments between kinetochores and microtubules depends on the B56-PP2A phosphatase. *Nature Cell Biology*, 13(10), pp.1265–1271.

Foley, E. a & Kapoor, T.M., 2013. Microtubule attachment and spindle assembly checkpoint signalling at the kinetochore. *Nature reviews. Molecular cell biology*, 14(1), pp.25–37.

Foltz, D.R. et al., 2006. The human CENP-A centromeric nucleosome-associated complex. *Nature Cell Biology*, 8(5), pp.458–469.

Friese, A. et al., 2016. Molecular requirements for the inter-subunit interaction and kinetochore recruitment of SKAP and Astrin. *Nature Communications*, 7.

Fu, J. et al., 2009. A single amino acid change converts Aurora-A into Aurora-B-like kinase in terms of partner specificity and cellular function. *Proceedings of the National Academy of Sciences*, 106(17), pp.6939–6944.

Funabiki, H. & Wynne, D.J., 2014. Making an effective switch at the kinetochore by phosphorylation and dephosphorylation. *Chromosoma*, 122(3), pp.135–158.

Gaitanos, T.N. et al., 2009. Stable kinetochore-microtubule interactions depend on the Ska complex and its new component Ska3/C13Orf3. *EMBO Journal*, 28(10), pp.1442–1452.

Gascoigne, K.E. & Cheeseman, I.M., 2011. Kinetochore assembly: If you build it, they will come. *Current Opinion in Cell Biology*, 23(1), pp.102–108.

Gassmann, R. et al., 2010. controls spindle checkpoint silencing in human cells Removal of Spindly from microtubule- attached kinetochores controls spindle checkpoint silencing in human cells. *Genes & development*, 24, pp.957–971.

Glover, D.M., Hagan, I.M. & Tavares, Á.A.M., 1998. Polo-like kinases: A team that plays throughout mitosis. *Genes and Development*, 12(24), pp.3777–3787.

Golsteyn, R.M. et al., 1995. Cell-Cycle Regulation of the Activity and Subcellular-Localization of Plk1, A Human Protein-Kinase Implicated in Mitotic Spindle Function. *Journal of Cell Biology*, 129(6), pp.1617–1628.

Granvogl, B., Plöscher, M. & Eichacker, L.A., 2007. Sample preparation by in-gel digestion

for mass spectrometry-based proteomics. *Analytical and Bioanalytical Chemistry*, 389(4), pp.991–1002.

Gregan, J. et al., 2011. Merotelic kinetochore attachment: Causes and effects. *Trends in Cell Biology*, 21(6), pp.374–381.

Grey, C. et al., 2016. SKAP, an outer kinetochore protein, is required for mouse germ cell development. *Reproduction*, 151(3), pp.239–251.

Griffis, E.R., Stuurman, N. & Vale, R.D., 2007. Spindly, a novel protein essential for silencing the spindle assembly checkpoint, recruits dynein to the kinetochore. *Journal of Cell Biology*, 177(6), pp.1005–1015.

Grosstessner-Hain, K. et al., 2011. Quantitative Phospho-proteomics to Investigate the Polo-like Kinase 1-Dependent Phospho-proteome. *Molecular & Cellular Proteomics*, 10(11), p.M111.008540.

Gruber, J. et al., 2002. The mitotic-spindle-associated protein astrin is essential for progression through mitosis. *Journal of cell science*, 115(Pt 21), pp.4053–4059.

Guimaraes, G.J. et al., 2008. Kinetochore-microtubule attachment relies on the disordered N-terminal tail domain of Hec1. *Current Biology*, 18(22), pp.1778–1784.

Gupta, N. et al., 2010. Analyzing protease specificity and detecting in vivo proteolytic events using tandem mass spectrometry. *Proteomics*, 10(15), pp.2833–2844.

Guse, A. et al., 2011. In vitro centromere and kinetochore assembly on defined chromatin templates. *Nature*, 477(7364), pp.354–358.

Hanisch, A., Silljé, H.H.W. & Nigg, E.A., 2006. Timely anaphase onset requires a novel spindle and kinetochore complex comprising Ska1 and Ska2. *EMBO Journal*, 25(23), pp.5504–5515.

Hans, F. et al., 2009. Molecular Distinctions between Aurora A and B: A Single Residue

Change Transforms Aurora A into Correctly Localized and Functional Aurora B. *Molecular biology of the cell*, 20, pp.3491–35.

Harashima, H., Dissmeyer, N. & Schnittger, A., 2013. Cell cycle control across the eukaryotic kingdom. *Trends in Cell Biology*, 23(7), pp.345–356.

Hegemann, B. et al., 2014. Systematic Phosphrylation Analysis of Human Mitotic Protein Complexes. *Science Signaling*, 198(4), pp.2658–2666.

Hendrickx, A. et al., 2009. Docking Motif-Guided Mapping of the Interactome of Protein Phosphatase-1. *Chemistry and Biology*, 16(4), pp.365–371.

Hengge, A.C., 2013. Chemistry and mechanism of phosphatases, diesterases and triesterases. *Biochim Biophys Acta.*, 1834(1), pp.415–416.

Hennrich, M.L. et al., 2013. Universal quantitative kinase assay based on diagonal SCX chromatography and stable isotope dimethyl labeling provides high-definition kinase consensus motifs for pka and human mps1. *Journal of Proteome Research*, 12(5), pp.2214–2224.

Hertz, E.P.T. et al., 2016. A Conserved Motif Provides Binding Specificity to the PP2A-B56 Phosphatase. *Molecular Cell*, 63(4), pp.686–695.

Hiruma, Y. et al., 2015. Competition between MPS1 and microtubules at kinetochores regulates spindle checkpoint signaling. *Science*, 348(6240), pp.1264–1267.

Hochegger, H., Takeda, S. & Hunt, T., 2008. Cyclin-dependent kinases and cell-cycle transitions: Does one fit all? *Nature Reviews Molecular Cell Biology*, 9(11), pp.910–916.

Hofmann, C. et al., 1998. Saccharomyces cerevisiae Duo1p and Dam1p, Novel Proteins Involved in Mitotic Spindle Function. *Journal of Cell Biology*, 143(6), pp.1029–1040.

Hori, T. et al., 2008. CCAN Makes Multiple Contacts with Centromeric DNA to Provide Distinct Pathways to the Outer Kinetochore. *Cell*, 135(6), pp.1039–1052. Hori, T. et al.,

2013. The CCAN recruits CENP-A to the centromere and forms the structural core for kinetochore assembly. *Journal of Cell Biology*, 200(1), pp.45–60.

Hori, T. & Fukagawa, T., 2012. Establishment of the vertebrate kinetochores. *Chromosome Research*, 20(5), pp.547–561.

Hornbeck, P. V. et al., 2015. PhosphoSitePlus, 2014: Mutations, PTMs and recalibrations. *Nucleic Acids Research*, 43(D1), pp.D512–D520.

Howell, B.J. et al., 2001. Cytoplasmic dynein/dynactin drives kinetochore protein transport to the spindle poles and has a role in mitotic spindle checkpoint inactivation. *Journal of Cell Biology*, 155(7), pp.1159–1172.

Howell, B.J. et al., 2004. Spindle Checkpoint Protein Dynamics at Kinetochores in living cells. *Current Biology*, 14, pp.953–964.

Howman, E. V. et al., 2000. Early disruption of centromeric chromatin organization in centromere protein A (Cenpa) null mice. *Proceedings of the National Academy of Sciences*, 97(3), pp.1148–1153.

Hoyt, M.A., Totis, L. & Roberts, B.T., 1991. S. cerevisiae genes required for cell cycle arrest in response to loss of microtubule function. *Cell*, 66(3), pp.507–517.

Huang, H. et al., 2008. Phosphorylation sites in BubR1 that regulate kinetochore attachment, tension, and mitotic exit. *Journal of Cell Biology*, 183(4), pp.667–680.

Huang, Y. et al., 2005. Statistical Characterization of the Charge State and Residue Dependence of Low Energy CID Peptide Dissociation Patterns. , 77(18), pp.5800–5813.

Huisin'T Veld, P.J. et al., 2016. Molecular basis of outer kinetochore assembly on CENP-T. *eLife*, 5(DECEMBER2016), pp.1–24.

Hunter, T., 2012. Why nature chose phosphate to modify proteins. *Philosophical*

Transactions of the Royal Society B: Biological Sciences, 367(1602), pp.2513–2516.

Ikeda, M. & Tanaka, K., 2017. Plk1 bound to Bub1 contributes to spindle assembly checkpoint activity during mitosis. *Scientific Reports*, 7(1), pp.1–15.

Izawa, D. & Pines, J., 2015. The mitotic checkpoint complex binds a second CDC20 to inhibit active APC/C. *Nature*, 517(7536), pp.631–634.

Janczyk, P. et al., 2017. Mechanism of Ska Recruitment by Ndc80 Complexes to Kinetochores. *Developmental Cell*, 41(4), p.438–449.e4.

Jelluma, N. et al., 2010. Release of Mps1 from kinetochores is crucial for timely anaphase onset. *Journal of Cell Biology*, 191(2), pp.281–290.

Jeyaprakash, A.A. et al., 2012. Structural and Functional Organization of the Ska Complex, a Key Component of the Kinetochore-Microtubule Interface. *Molecular Cell*, 46(3), pp.274–286.

Jeyaprakash, A.A. et al., 2007. Structure of a Survivin-Borealin-INCENP Core Complex Reveals How Chromosomal Passengers Travel Together. *Cell*, 131(2), pp.271–285.

Ji, Z. et al., 2017. A sequential multi-target Mps1 phosphorylation cascade promotes spindle checkpoint signaling. *eLife*, 6, pp.1–23.

Ji, Z., Gao, H. & Yu, H., 2015. Kinetochore attachment sensed by competitive Mps1 and microtubule binding to Ndc80C. *Science*, 348(6240), pp.1260–1264.

Jia, L., Li, B. & Yu, H., 2016. The Bub1-Plk1 kinase complex promotes spindle checkpoint signalling through Cdc20 phosphorylation. *Nature Communications*, 7, pp.1–14.

Johnston, K. et al., 2010. Vertebrate kinetochore protein architecture: Protein copy number. *Journal of Cell Biology*, 189(6), pp.937–943.

Kalantzaki, M. et al., 2015. Kinetochore-microtubule error correction is driven by differentially regulated interaction modes. *Nature Cell Biology*, 17(4), pp.421–433.

Kang, J. et al., 2007. Autophosphorylation-dependent activation of human Mps1 is required for the spindle checkpoint. *Proceedings of the National Academy of Sciences*, 104(51), pp.20232–20237.

Kapoor, T.M. et al., 2006. Chromosomes Can Congress to the Metaphase Plate Before Biorientation. *Science*, 311(January), pp.388–392.

Kasuboski, J.M. et al., 2011. Zwint-1 is a novel Aurora B substrate required for the assembly of a dynein-binding platform on kinetochores. *Molecular Biology of the Cell*, 22(18), pp.3318–3330.

Kato, H. et al., 2013. A conserve mechanism for centromere nucleosome recognition by centromeric protein CENP-C. *Science*, 725(May), pp.1110–1114.

Kawashima, S.A. et al., 2010. Phosphorylation of H2A by Bub1 prevents chromosomal instability through localizing shugoshin. *Science*, 327(5962), pp.172–177.

Kelly, A. et al., 2010. Survivin reads phosphorylated Histone H3 Threonine 3 to Activate the mitotic kinase Aurora B. *Science*, 330(August), pp.235–239.

Kern, D.M. et al., 2016. A mitotic SKAP isoform regulates spindle positioning at astral microtubule plus ends. *Journal of Cell Biology*, 213(3), pp.315–328.

Kern, D.M. et al., 2017. Astrin-SKAP complex reconstitution reveals its kinetochore interaction with microtubule-bound Ndc80. *eLife*, 6, pp.1–20.

Kettenbach, A.N. et al., 2011. Quantitative phosphoproteomics identifies substrates and functional modules of Aurora and Polo-like kinase activities in mitotic cells. *Science Signaling*, 4(179), pp.1–16.

Kim, H.J. et al., 2010. Specific primary sequence requirements for Aurora B kinase-mediated phosphorylation and subcellular localization of TMAP during mitosis. *Cell Cycle*, 9(10), pp.2027–2036.

Kim, S. & Yu, H., 2015. Multiple assembly mechanisms anchor the KMN spindle checkpoint platform at human mitotic kinetochores. *Journal of Cell Biology*, 208(2), pp.181–196.

Kirschner, M. & Mitchison, T., 1986. Beyond self-assembly: from microtubules to morphogenesis. *Cell*, 45, pp.329–342.

Klare, K. et al., 2015. CENP-C is a blueprint for constitutive centromere-associated network assembly within human kinetochores. *Journal of Cell Biology*, 210(1), pp.11–22.

Klein, U., Nigg, E. & Gruneberg, U., 2006. Centromere targeting of the chromosomal passenger complex requires a ternary subcomplex of Borealin, Survivin, and the N-terminal domain of INCENP. *Molecular and Cellular Biology*, 17(2), pp.2547–2558.

Kline, S.L. et al., 2006. The human Mis12 complex is required for kinetochore assembly and proper chromosome segregation. *Journal of Cell Biology*, 173(1), pp.9–17.

Kops, G.J.P.L. et al., 2005. ZW10 links mitotic checkpoint signaling to the structural kinetochore. *Journal of Cell Biology*, 169(1), pp.49–60.

Kops, G.J.P.L., Saurin, A.T. & Meraldi, P., 2010. Finding the middle ground: How kinetochores power chromosome congression. *Cellular and Molecular Life Sciences*, 67, pp.2145–2161.

Kops, G.J.P.L. & Shah, J. V., 2012. Connecting up and clearing out: How kinetochore attachment silences the spindle assembly checkpoint. *Chromosoma*, 121, pp.509–525.

Krenn, V. et al., 2012. Structural analysis reveals features of the spindle checkpoint kinase Bub1-kinetochore subunit Knl1 interaction. *Journal of Cell Biology*, 196(4), pp.451–467.

Kruse, T. et al., 2013. Direct binding between BubR1 and B56-PP2A phosphatase complexes regulate mitotic progression. *Journal of Cell Science*, 126(5), pp.1086–1092.

Kumar, P. & Wittmann, T., 2012. +TIPs: SxIPping along microtubule ends. *Trends in Cell Biology*, 22(8), pp.418–428.

Lampert, F. et al., 2013. Molecular requirements for the formation of a kinetochore-microtubule interface by Dam1 and Ndc80 complexes. *Journal of Cell Biology*, 200(1), pp.21–30.

Lampert, F., Hornung, P. & Westermann, S., 2010. The Dam1 complex confers microtubule plus end-tracking activity to the Ndc80 kinetochore complex. *Journal of Cell Biology*, 189(4), pp.641–649.

Lampson, M. a. & Cheeseman, I.M., 2011. Sensing centromere tension: Aurora B and the regulation of kinetochore function. *Trends in Cell Biology*, 21(3), pp.133–140.

Lampson, M.A. et al., 2004. Correcting improper chromosome–spindle attachments during cell division. *Nature Cell Biology*, 6(3), pp.6–237.

Lan, W. et al., 2004. Aurora B phosphorylates centromeric MCAK and regulates its localization and microtubule depolymerization activity. *Current Biology*, 14(4), pp.273–286.

Larsen, N. a et al., 2007. Structural analysis of Bub3 interactions in the mitotic spindle checkpoint. *Proceedings of the National Academy of Sciences of the United States of America*, 104(4), pp.1201–1206.

Lassila, J.K., Zalatan, J.G. & Herschlag, D., 2012. *Biological phosphoryl-Tranfer reactions: understanding mechanism and catlysis*,

Lawrimore, J., Bloom, K.S. & Salmon, E.D., 2011. Point centromeres contain more than a single centromere-specific Cse4 (CENP-A) nucleosome. *Journal of Cell Biology*, 195(4), pp.573–582.

Lee, C.S. et al., 2014. Recurrent point mutations in the kinetochore gene KNSTRN in cutaneous squamous cell carcinoma. *Nat Genet.*, 46(10), pp.1060–1062.

Lee, K.S. et al., 2008. Mechanisms of mammalian polo-like kinase 1 (Plk1) localization: Self- versus non-self-priming. *Cell Cycle*, 7(2), pp.141–145.

Lee, K.S. et al., 2014. Mechanisms underlying Plk1 polo-box domain-mediated biological processes and their physiological significance. *Mol Cells*, 37(4), pp.286–294.

Lera, R.F. et al., 2016. Decoding Polo-like kinase 1 signaling along the kinetochore-centromere axis. *Nat Chem Biol.*, 12(6), pp.411–418.

Li, R. & Murray, a W., 1991. Feedback control of mitosis in budding yeast [published erratum appears in Cell 1994 Oct 21;79(2):following 388]. *Cell*, 66(Figure 1), pp.519–531.

Li, X. & Nicklas, R.B., 1995. Mitotic forces control a cell-cycle checkpoint. *Nature*, 373(6515), pp.630–632.

Li, Y. et al., 2007. Kinetochore dynein generates a poleward pulling force to facilitate congression and full chromosome alignment. *Cell research*, 17, pp.701–712.

Liebler, D.C. & Ham, A.J.L., 2009. Spin filter-based sample preparation for shotgun proteomics. *Nature Methods*, 6(11), p.785.

Lin, Y.T. et al., 2006. Hec1 sequentially recruits Zwint-1 and ZW10 to kinetochores for faithful chromosome segregation and spindle checkpoint control. *Oncogene*, 25(52), pp.6901–6914.

Liu, D., Vleugel, M., Backer, C.B., Hori, T., Fukagawa, T., Cheeseman, I.M. & Lampson, M.A., 2010. Regulated targeting of protein phosphatase 1 to the outer kinetochore by KNL1 opposes Aurora B kinase. *Journal of Cell Biology*, 188(6), pp.809–820.

Liu, D., Vleugel, M., Backer, C.B., Hori, T., Fukagawa, T., Cheeseman, I.M. & Lampson, M. a., 2010. Regulated targeting of protein phosphatase 1 to the outer kinetochore by KNL1 opposes Aurora B kinase. *Journal of Cell Biology*, 188(6), pp.809–820.

Liu, D. et al., 2009. Sensing Chromosome Bi-Orientation Kinase from Kinetochore Substrates. *Science (New York, N.Y.)*, 323(March), pp.1350–1353.

Liu, D., Davydenko, O. & Lampson, M. a., 2012. Polo-like kinase-1 regulates kinetochore-microtubule dynamics and spindle checkpoint silencing. *Journal of Cell Biology*, 198(4), pp.491–499.

London, N. et al., 2012. Phosphoregulation of Spc105 by Mps1 and PP1 Regulates Bub1 Localisation to Kinetochores. *Current Biology*, 22(22), pp.900–906.

Luo, X. & Yu, H., 2008. Protein Metamorphosis: The Two-State Behaviour of Mad2. *Structure2*, 16(11), pp.1616–1625.

Macek, B., Mann, M. & Olsen, J. V., 2009. Global and Site-Specific Quantitative Phosphoproteomics: Principles and Applications. *Annual Review of Pharmacology and Toxicology*, 49(1), pp.199–221.

Maciejowski, J. et al., 2017. Mps1 Regulates Kinetochore-Microtubule Attachment Stability via the Ska Complex to Ensure Error-Free Chromosome Segregation. *Developmental Cell*, 41(2), p.143–156.e6.

Magidson, V. et al., 2011. The spatial arrangements of chromosomes during prometaphase facilitates spindle assembly. *Cell*, 146(4), pp.555–567.

Malik, R. et al., 2009. Quantitative analysis of the human spindle phosphoproteome at distinct mitotic stages. *Journal of Proteome Research*, 8(10), pp.4553–4563.

Malvezzi, F. et al., 2013. A structural basis for kinetochore recruitment of the Ndc80 complex via two distinct centromere receptors. *EMBO Journal*, 32(3), pp.409–423.

Manning, A.L. et al., 2010. CLASP1, astrin and Kif2b form a molecular switch that regulates kinetochore-microtubule dynamics to promote mitotic progression and fidelity. *The EMBO journal*, 29(20), pp.3531–3543.

Manza, L.L. et al., 2005. Sample preparation and digestion for proteomic analyses using spin filters. *Proteomics*, 5(7), pp.1742–1745.

Maresca, T.J. & Salmon, E.D., 2009. Intrakinetochore stretch is associated with changes in kinetochore phosphorylation and spindle assembly checkpoint activity. *Journal of Cell Biology*, 184(3), pp.373–381.

Martin-Lluesma, S., Stucke, V.M. & Nigg, E.A., 2002. Role of Hec1 in spindle checkpoint signaling and kinetochore recruitment of Mad1/Mad2. *Science*, 297(5590), pp.2267–2270.

Mattison, C.P. et al., 2007. Mps1 activation loop autophosphorylation enhances kinase activity. *Journal of Biological Chemistry*, 282(42), pp.30553–30561.

Mayer, T.U. et al., 1999. Small Molecule Inhibitor of Mitotic Spindle Bipolarity Identified in a Phenotype-Based Screen. *October*, 286(October), pp.1997–2000.

McKinley, K.L. et al., 2015. The CENP-L-N Complex Forms a Critical Node in an Integrated Meshwork of Interactions at the Centromere-Kinetochore Interface. *Molecular Cell*, 60(6), pp.886–898.

Meraldi, P., Honda, R. & Nigg, E.A., 2004. Aurora kinases link chromosome segregation and cell division to cancer susceptibility. *Current Opinion in Genetics and Development*, 14(1), pp.29–36.

Mertins, P. et al., 2013. Integrated proteomic analysis of post-translational modifications by serial enrichment. *Nature Methods*, 10(7), pp.634–637.

Mitchison, T. & Kirschner, M., 1984. Dynamic instability of microtubule growth. *Nature*, 312, pp.237–242.

Mohammed, S. et al., 2007. Multiplexed Proteomics Mapping of Yeast RNA Polymerase II and III Allows Near-Complete Phosphorylation Sites. *Peptides*, xxx(xx), pp.2199–2204.

Montoya, A. et al., 2011. Characterization of a TiO2 enrichment method for label-free quantitative phosphoproteomics. *Methods*, 54(4), pp.370–378.

Mosalaganti, S. et al., 2017. Structure of the RZZ complex and molecular basis of its interaction with Spindly. *Journal of Cell Biology*, 216(4), pp.961–981.

Mundt, K.E. et al., 1997. On the regulation and function of human polo-like kinase 1 (PLK1): effects of overexpression on cell cycle progression. *Biochem Biophys Res Commun*, 239(2), pp.377–385.

Musacchio, A., 2015. The Molecular Biology of Spindle Assembly Checkpoint Signaling Dynamics. *Current Biology*, 25(20), pp.R1002–R1018.

Musacchio, A. & Desai, A., 2017. A Molecular View of Kinetochore Assembly and Function. *Biology*, 6(1), p.5.

Nakajima, H. et al., 2003. Identification of a Consensus Motif for Plk (Polo-like Kinase) Phosphorylation Reveals. , (41), pp.25277–25281.

Nicklas, R.B. & Koch, C.A., 1969. Chromosome micromanipulation. 3. Spindle fiber tension and the reorientation of mal-oriented chromosomes. *The Journal of cell biology*, 43(1), pp.40–50.

Nijenhuis, W. et al., 2014. Negative feedback at kinetochores underlies a responsive spindle checkpoint signal. *Nature Cell Biology*, 16(12), pp.1257–1264.

Nousiainen, M. et al., 2006. Phosphoproteome analysis of the human mitotic spindle. *Proc. Natl. Acad. Sci. USA*, 103(14), pp.5391–5396.

O'Connor, A. et al., 2016. Requirement for PLK1 kinase activity in the maintenance of a robust spindle assembly checkpoint. *Biology Open*, 5(1), pp.11–19.

Obuse, C. et al., 2004. Proteomics analysis of the centromere complex from HeLa interphase cells: UV-damaged DNA binding protein 1 (DDB-1) is a component of the CEN-complex, while BMI-1 is transiently co-localized with the centromeric region in interphase. *Genes to Cells*, 9(2), pp.105–120.

Ohta, S. et al., 2016. Identification of Mitosis-Specific Phosphorylation in Mitotic Chromosome-Associated Proteins. *Journal of Proteome Research*, 15(9), pp.3331–3341.

Okada, M. et al., 2006. The cenp-H–I complex is required for the efficient incorporation of newly synthesized CENP-A into centromeres. *Nature Cell Biology*, 8(5), pp.446–457.

Olsen, J. V. et al., 2010. Quantitative Phosphoproteomics Reveals Widespread Full Phosphorylation Site Occupancy During Mitosis. *Science Signaling*, 3(104), pp.ra3-ra3.

Ong, S.-E. et al., 2002. Stable Isotope Labeling by Amino Acids in Cell Culture, SILAC, as a Simple and Accurate Approach to Expression Proteomics. *Molecular & Cellular Proteomics*, 1(5), pp.376–386.

Overlack, K. et al., 2015. A molecular basis for the differential roles of Bub1 and BubR1 in the spindle assembly checkpoint. *eLife*, 4, pp.1–24.

Pachis, S.T. & Kops, G.J.P.L., 2018. Leader of the sac: molecular mechanisms of mps1/ttk regulation in mitosis. *Open Biology*, 8, p.180109.

Pagliuca, C. et al., 2009. Roles for the conserved Spc105p/Kre28p complex in kinetochore-microtubule binding and the spindle assembly checkpoint. *PLoS ONE*, 4(10).

Palozola, K.C. et al., 2017. Mitotic transcription and waves of gene reactivation during mitotic exit. *Science*, 358(6359), pp.119–122.

Park, J.-E., Erikson, R.L. & Lee, K.S., 2011. Feed-forward mechanism of converting biochemical cooperativity to mitotic processes at the kinetochore plate. *Proceedings of the National Academy of Sciences of the United States of America*, 108(20), pp.8200–8205.

Patel, V.J. et al., 2009. A comparison of labeling and label-free mass spectrometry-based proteomics approaches. *Journal of Proteome Research*, 8(7), pp.3752–3759.

Pentakota, S. et al., 2017. Decoding the centromeric nucleosome through CENP-N. *eLife*, 6, pp.1–25.

Petrovic, A. et al., 2014. Modular Assembly of RWD Domains on the Mis12 Complex Underlies Outer Kinetochore Organization. *Molecular Cell*, 53(4), pp.591–605.

Petrovic, A. et al., 2016. Structure of the MIS12 Complex and Molecular Basis of Its Interaction with CENP-C at Human Kinetochores. *Cell*, 167(4), p.1028–1040.e15.

Petrovic, A. et al., 2010. The MIS12 complex is a protein interaction hub for outer kinetochore assembly. *Journal of Cell Biology*, 190(5), pp.835–852.

Picard, A. et al., 1989. Involvement of protein phosphatases 1 and 2A in the control of M phase- promoting factor activity in starfish. *The Journal of cell biology*, 109(6), pp.3347–3354.

Pines, J. & Rieder, C.L., 2001. Re-staging mitosis: A contemporary view of mitotic progression. *Nature Cell Biology*, 3(1).

Pinkse, M.W.H. et al., 2004. Selective isolation at the femtomole level of phosphopeptides from proteolytic digests using 2D-NanoLC-ESI-MS/MS and titanium oxide precolumns. *Analytical Chemistry*, 76(14), pp.3935–3943.

Primorac, I. et al., 2013. Bub3 reads phosphorylated MELT repeats to promote spindle assembly checkpoint signaling. *eLife*, 2013(2), pp.1–20.

Qian, J. et al., 2017. An Attachment-Independent Biochemical Timer of the Spindle Assembly Checkpoint. *Molecular Cell*, 68(4), p.715–730.e5.

Rago, F., Gascoigne, K.E. & Cheeseman, I.M., 2015. Distinct organization and regulation of the outer kinetochore KMN network downstream of CENP-C and CENP-T. *Current Biology*, 25(5), pp.671–677.

Reyes-Lamothe, R., Wang, X. & Sherratt, D., 2008. Escherichia coli and its chromosome.

Trends in Microbiology, 16(5), pp.238–245.

Rieder, C. & Maiato, H., 2004. Stuck in Division or Passing through:\nWhat Happens When Cells Cannot\nSatisfy the Spindle Assembly Checkpoint. *Developmental Cell*, 7, pp.637–651.

Rieder, C.L. et al., 1995. The checkpoint delaying anaphase in response to chromosome monoorientation is mediated by an inhibitory signal produced by unattached kinetochores. *Journal of Cell Biology*, 130(4), pp.941–948.

Rieder, C.L. & Cole, R.W., 2002. Cold-Shock and the Mammalian Cell Cycle. *Cell Cycle*, 1(3), pp.168–174.

Sakurai, H. et al., 1999. The Rpb4 subunit of fission yeast Schizosaccharomyces pombe RNA polymerase II is essential for cell viability and similar in structure to the corresponding subunits of higher eukaryotes. *Molecular and cellular biology*, 19(11), pp.7511–8.

Santaguida, S. & Musacchio, A., 2009. The life and miracles of kinetochores. *The EMBO journal*, 28(17), pp.2511–2531.

Santamaria, A. et al., 2011. The Plk1-dependent Phosphoproteome of the Early Mitotic Spindle. *Molecular & Cellular Proteomics*, 10(1), p.M110.004457.

Sauer, G. et al., 2005. Proteome Analysis of the Human Mitotic Spindle. *Molecular & Cellular Proteomics*, 4(1), pp.35–43.

Saurin, A.T. et al., 2011. Aurora B potentiates Mps1 activation to ensure rapid checkpoint establishment at the onset of mitosis. *Nature Communications*, 2(1).

Schleiffer, A. et al., 2012. CENP-T proteins are conserved centromere receptors of the Ndc80 complex. *Nature Cell Biology*, 14(6), pp.604–613.

Schmidt, J.C. et al., 2010. Aurora B kinase controls the targeting of the Astrin-SKAP

complex to bioriented kinetochores. *Journal of Cell Biology*, 191(2), pp.269–280.

Schmidt, J.C. et al., 2012. The kinetochore-bound Ska1 complex tracks depolymerizing microtubules and binds to curved protofilaments. *Developmental Cell*, 23(5), pp.968–980.

von Schubert, C. et al., 2015. Plk1 and Mps1 Cooperatively Regulate the Spindle Assembly Checkpoint in Human Cells. *Cell Reports*, 12(1), pp.66–78.

Screpanti, E. et al., 2011. Direct binding of Cenp-C to the Mis12 complex joins the inner and outer kinetochore. *Current Biology*, 21(5), pp.391–398.

Sharma, K. et al., 2014. Ultradeep Human Phosphoproteome Reveals a Distinct Regulatory Nature of Tyr and Ser/Thr-Based Signaling. *Cell Reports*, 8(5), pp.1583–1594.

Shepperd, L.A. et al., 2012. Phosphodependent recruitment of Bub1 and Bub3 to Spc7/KNL1 by Mph1 kinase maintains the spindle checkpoint. *Current Biology*, 22(10), pp.891–899.

Shrestha, R.L. et al., 2017. Aurora-B kinase pathway controls the lateral to end-on conversion of kinetochore-microtubule attachments in human cells. *Nature Communications*, 8(1), pp.1–12.

Shrestha, R.L. & Draviam, V.M., 2013. Lateral to end-on conversion of chromosome-microtubule attachment requires kinesins cenp-e and MCAK. *Current Biology*, 23(16), pp.1514–1526.

Silió, V., McAinsh, A.D. & Millar, J.B., 2015. KNL1-Bubs and RZZ Provide Two Separable Pathways for Checkpoint Activation at Human Kinetochores. *Developmental Cell*, 35(5), pp.600–613.

Sironi, L. et al., 2002. Crystal structure of the tetrameric Mad1-Mad2 core complex: Implications of a “safety belt” binding mechanism for the spindle checkpoint. *EMBO Journal*, 21(10), pp.2496–2506.

Skoufias, D.A. et al., 2006. S-trityl-L-cysteine is a reversible, tight binding inhibitor of the human kinesin Eg5 that specifically blocks mitotic progression. *Journal of Biological Chemistry*, 281(26), pp.17559–17569.

Slevin, L.K. et al., 2012. The structure of the Plk4 cryptic polo box reveals two tandem polo boxes required for centriole duplication. *Structure*, 20(11), pp.1905–1917.

Storchova, Z. & Kuffer, C., 2008. The consequences of tetraploidy and aneuploidy. *Journal of Cell Science*, 121(23), pp.3859–3866.

Strebhardt, K., 2010. Multifaceted polo-like kinases: Drug targets and antitargets for cancer therapy. *Nature Reviews Drug Discovery*, 9(8), pp.643–660.

Strebhardt, K. & Ullrich, A., 2006. Targeting polo-like kinase 1 for cancer therapy. *Nature Reviews Cancer*, 6(4), pp.321–330.

Stucke, V.M. et al., 2002. Human Mps1 kinase is required for the spindle assembly checkpoint but not for centrosome duplication. *EMBO Journal*, 21(7), pp.1723–1732.

Suijkerbuijk, S.J.E., Vleugel, M., et al., 2012. Integration of Kinase and Phosphatase Activities by BUBR1 Ensures Formation of Stable Kinetochore-Microtubule Attachments. *Developmental Cell*, 23(4), pp.745–755.

Suijkerbuijk, S.J.E., van Dam, T.J.P., et al., 2012. The Vertebrate Mitotic Checkpoint Protein BUBR1 Is an Unusual Pseudokinase. *Developmental Cell*, 22(6), pp.1321–1329.

Sumara, I. et al., 2002. The dissociation of cohesin from chromosomes in prophase is regulated by polo-like kinase. *Molecular Cell*, 9(3), pp.515–525.

Sunkel, C.E. & Glover, D.M., 1988. polo, a mitotic mutant of Drosophila displaying abnormal spindle poles. *Journal of cell science*, 89 (Pt 1), pp.25–38.

Tamura, N. et al., 2015. A proteomic study of mitotic phase-specific interactors of EB1 reveals a role for SXIP-mediated protein interactions in anaphase onset. *Biology Open*,

4(2), pp.155–169.

Taylor, S.S. et al., 2001. Kinetochore localisation and phosphorylation of the mitotic checkpoint components Bub1 and BubR1 are differentially regulated by spindle events in human cells. *Journal of cell science*, 114(Pt 24), pp.4385–4395.

Taylor, S.S.S. & Kornev, A.A.P., 2011. Protein Kinases: Evolution of Dynamic Regulatory Proteins. *Trends in biochemical sciences*, 36(2), pp.65–77.

Thein, K.H. et al., 2007. Astrin is required for the maintenance of sister chromatid cohesion and centrosome integrity. *Journal of Cell Biology*, 178(3), pp.345–354.

Tien, J.F. et al., 2010. Cooperation of the Dam1 and Ndc80 kinetochore complexes enhances microtubule coupling and is regulated by aurora B. *Journal of Cell Biology*, 189(4), pp.713–723.

Tooley, J.G., Miller, S.A. & Stukenberg, P.T., 2011. The Ndc80 complex uses a tripartite attachment point to couple microtubule depolymerization to chromosome movement. *Molecular Biology of the Cell*, 22(8), pp.1217–1226.

Torres, E.M., Williams, B.R. & Amon, A., 2008. Aneuploidy: Cells losing their balance. *Genetics*, 179(2), pp.737–746.

Tsukahara, T., Tanno, Y. & Watanabe, Y., 2010. Phosphorylation of the CPC by Cdk1 promotes chromosome bi-orientation. *Nature*, 467(7316), pp.719–723.

Tyanova, S. et al., 2016. The Perseus computational platform for comprehensive analysis of (prote)omics data. *Nature Methods*, 13(9), pp.731–740.

Välk, K. et al., 2010. Gene Expression Profiles of Non-Small Cell Lung Cancer: Survival Prediction and New Biomarkers. *Oncology*, 79(3–4), pp.283–292.

Vleugel, M. et al., 2013. Arrayed BUB recruitment modules in the kinetochore scaffold KNL1 promote accurate chromosome segregation. *Journal of Cell Biology*, 203(6), pp.943–

955.

Vleugel, M. et al., 2015. Sequential Multisite Phospho-Regulation of KNL1-BUB3 Interfaces at Mitotic Kinetochores. *Molecular Cell*, 57(5), pp.824–835.

Waizenegger, I.C. et al., 2000. Two distinct pathways remove mammalian cohesin from chromosome arms in prophase and from centromeres in anaphase. *Cell*, 103, pp.399–410.

Wakula, P. et al., 2003. Degeneracy and function of the ubiquitous RVXF motif that mediates binding to protein phosphatase-1. *Journal of Biological Chemistry*, 278(21), pp.18817–18823.

Wan, X. et al., 2009. Protein Architecture of the Human Kinetochore Microtubule Attachment Site. *Cell*, 137(4), pp.672–684.

Wang, F. et al., 2010. Histone H3 Thr-3 Phosphorylation at Centromeres in Mitosis. *Science (New York, N.Y.)*, 330(October), pp.231–236.

Wang, H. et al., 2015. DNA damage checkpoint recovery and cancer development. *Experimental Cell Research*, 334(2), pp.350–358.

Wang, W. et al., 2009. Structural and mechanistic insights into Mps1 kinase activation. *Journal of Cellular and Molecular Medicine*, 13(8 B), pp.1679–1694.

Wang, X. et al., 2014. Dynamic autophosphorylation of mps1 kinase is required for faithful mitotic progression. *PLoS ONE*, 9(9), pp.1–10.

Wang, X. et al., 2012. Mitotic regulator SKAP forms a link between kinetochore core complex KMN and dynamic spindle microtubules. *Journal of Biological Chemistry*, 287(47), pp.39380–39390.

Wang, Z. & Cole, P.A., 2014. Catalytic Mechanisms and Regulation of Protein Kinases. *Methods Enzymol.*, 548, pp.1–21.

Weaver, B.A. & Cleveland, D.W., 2006. Does aneuploidy cause cancer? *Current Opinion in Cell Biology*, 18(6), pp.658–667.

Weir, J.R. et al., 2016. Insights from biochemical reconstitution into the architecture of human kinetochores. *Nature*, 537(7619), pp.249–253.

Weiss, E. & Winey, M., 1996. The Saccharomyces cerevisiae Spindle Pole Body Duplication Gene MPS1\nIs Part of a Mitotic Checkpoint. *The Journal of Cell Biology*, 132(January), pp.111–123.

Welburn, J.P.I. et al., 2010. Aurora B phosphorylates spatially distinct targets to differentially regulate the kinetochore-microtubule interface. , 38(3), pp.383–392.

Welburn, J.P.I. et al., 2010b. Aurora B phosphorylates spatially distinct targets to differentially regulate the kinetochore-microtubule interface. *Molecular Cell*, 38(3), pp.383–392.

Welburn, J.P.I. et al., 2009. The human kinetochore Ska1 complex facilitates microtubule depolymerization-coupled motility. *Developmental Cell*, 16(3), pp.374–385.

Westermann, S. et al., 2005. Formation of a dynamic kinetochore-microtubule interface through assembly of the Dam1 ring complex. *Molecular Cell*, 17(2), pp.277–290.

Westermann, S. et al., 2006. The Dam1 kinetochore ring complex moves processively on depolymerizing microtubule ends. *Nature*, 440(7083), pp.565–569.

Wiese, S. et al., 2007. Protein labeling by iTRAQ: A new tool for quantitative mass spectrometry in proteome research. *Proteomics*, 7(3), pp.340–350.

Williams, B.R. & Amon, A., 2009. Aneuploidy : Cancer ' s Fatal Flaw ? *Most*, 69(13), pp.5289–5291.

Wiśniewski, J.R. et al., 2009. Universal sample preparation method for proteome analysis. *Nature Methods*, 6(5), pp.359–362.

Wollman, R. et al., 2005. Efficient chromosome capture requires a bias in the “search-and-capture” process during mitotic-spindle assembly. *Current Biology*, 15, pp.828–832.

Wood, K.W. et al., 2010. Antitumor activity of an allosteric inhibitor of centromere-associated protein-E. *Proceedings of the National Academy of Sciences*, 107(13), pp.5839–5844.

Wu, H.-M., Chi, K.-H. & Lin, W.-W., 2002. Proteasome inhibitors stimulate activator protein-1 pathway via reactive oxygen species production. *FEBS letters*, 526(1–3), pp.101–105.

Xue, J. et al., 2002. Targeted Disruption of the Testicular SPAG5 / Deepest Protein Does Not Affect Spermatogenesis or Fertility. *Society*, 22(7), pp.1993–1997.

Yamagishi, Y. et al., 2012. MPS1/Mph1 phosphorylates the kinetochore protein KNL1/Spc7 to recruit SAC components. *Nature Cell Biology*, 14(7), pp.746–752.

Yamagishi, Y. et al., 2010. Two Histone Marks Establish the Inner Centromere and Chromosome Bi-Orientation. *Science*, 330, pp.239–243.

Yang, Y. et al., 2008. Phosphorylation of HsMis13 by Aurora B kinase is essential for assembly of functional kinetochore. *Journal of Biological Chemistry*, 283(39), pp.26726–26736.

Ye, A.A. et al., 2017. It ’ s all relative : Centromere- versus pole-based error correction It ’ s all relative : Centromere- versus pole-based error correction. , 4101(August), pp.78–80.

Ye, K. et al., 1998. Opium alkaloid noscapine is an antitumor agent that arrests metaphase and induces apoptosis in dividing cells. *Proceedings of the National Academy of Sciences of the United States of America*, 95(4), pp.1601–1606.

Yuan, L.J. et al., 2014. SPAG5 upregulation predicts poor prognosis in cervical cancer patients and alters sensitivity to taxol treatment via the mTOR signaling pathway. *Cell death & disease*, 5, pp.1–8.

Yue, X., Schunter, A. & Hummon, A.B., 2016. Comparing Multi-Step IMAC and Multi-Step

TiO2 Methods for Phosphopeptide Enrichment. *Anal Chem.*, 87(17), pp.8837–8844.

Zaytsev, A. V. et al., 2014. Accurate phosphoregulation of kinetochore-microtubule affinity requires unconstrained molecular interactions. *Journal of Cell Biology*, 206, pp.45–59.

Zhang, G. et al., 2017. Bub1 positions Mad1 close to KNL1 MELT repeats to promote checkpoint signalling. *Nature Communications*, 8(May).

Zhang, G. et al., 2015. Distinct domains in Bub1 localize RZZ and BubR1 to kinetochores to regulate the checkpoint. *Nature Communications*, 6, pp.1–14.

Zhang, G. et al., 2012. The Ndc80 internal loop is required for recruitment of the Ska complex to establish end-on microtubule attachment to kinetochores. *Journal of Cell Science*, 125(13), pp.3243–3253.

Zhang, G., Lischetti, T. & Nilsson, J., 2014. A minimal number of MELT repeats supports all the functions of KNL1 in chromosome segregation. *Journal of Cell Science*, 127(4), pp.871–884.

Zhang, H. et al., 2016. MIR-539 inhibits prostate cancer progression by directly targeting SPAG5. *Journal of Experimental and Clinical Cancer Research*, 35(1), pp.1–9.

Zhang, X. et al., 2007. Aurora B phosphorylates multiple sites on Mitotic Centromere-associated Kinesin to spatially and temporally regulate its function. *Molecular biology of the cell*, 18(1), pp.3264–3276.

Zhou, H. et al., 2013. Toward a comprehensive characterization of a human cancer cell phosphoproteome. *Journal of Proteome Research*, 12(1), pp.260–271.

Zhu, T. et al., 2013. Phosphorylation of microtubule-binding protein hec1 by mitotic kinase aurora b specifies spindle checkpoint kinase mps1 signaling at the kinetochore. *Journal of Biological Chemistry*, 288(50), pp.36149–36159.